International Journal of Thermophysics (2026) 47:195
https://doi.org/10.1007/s10765-026-03836-1

Wide-Ranging Measurements of the Viscosity and Density of Neon with a Combined Visco-Densimeter and Reevaluated Results of an Oscillating-Disk Viscometer

Ulrike Kochan-Eilers[1] · Ruben Harten[1] · Eckhard Vogel[2] · Karsten Meier[1]

Received: 14 August 2026 / Accepted: 26 August 2026
© The Author(s) 2026

Abstract
Accurate wide-ranging measurements of the viscosity and density of supercritical neon were performed with a combined vibrating-wire viscometer and single-sinker densimeter. They cover the temperature range between 300 K and 450 K with pressures up to 30 MPa. The viscosity measurements are characterized by a relative expanded (coverage factor $k = 2$) uncertainty of 0.25 %, while the relative expanded ($k = 2$) uncertainty in the density measurements is 0.05 %, except in the low-density regime, where it increases up to 0.1 % at 5 kg/m^3. The vibrating-wire viscometer was calibrated with helium using a highly accurate theoretical value for the viscosity of helium in the limit of zero density at 293 K. To validate the calibration of the viscometer, measurements on nitrogen along the two isotherms 293 K and 423 K were carried out and compared with literature data, which confirmed the calibration. Our measurement results for the viscosity of neon agree with the most accurate literature data within their mutual uncertainties in the regions where they overlap but deviate by up to 1.1 % from the corresponding-states model of Huber [M. L. Huber, NIST Internal Report 8209, National Institute of Standards and Technology, 2018]. Our results for the density agree with the current reference equation of state for neon within the uncertainty of our data. Furthermore, measurements of the viscosity of dilute neon gas carried out by one of the authors with an oscillating-disk viscometer in 1984 were reevaluated by applying a highly accurate theoretical value for the viscosity of helium in the calibration of the viscometer. After the reevaluation, the relative expanded ($k = 2$) uncertainty in these measurements amounts to 0.2 % to 0.4 %. Moreover, we present new correlations for the viscosity and thermal conductivity of neon in the limit of zero density, which are based on recent accurate *ab initio* calculations.

Keywords Density · Helium · Neon · Nitrogen · Vibrating-wire viscometer · Viscosity

Extended author information available on the last page of the article

Published online: 20 November 2026

1 Introduction

Thermodynamic temperatures can be measured directly with different types of primary thermometers such as acoustic gas thermometers [1], dielectric constant gas thermometers [2], and refractive index gas thermometers [3, 4]. These primary thermometers are sophisticated scientific experiments, which utilize noble gases as the working medium. Up till now, almost exclusively helium and argon have been employed because their properties are known with high accuracy. The noble gas neon represents another promising candidate for use in future primary thermometers. Neon can also be applied as a component in refrigerant mixtures in hydrogen liquefaction processes. Employing multi-component mixtures of hydrogen, nitrogen, neon, helium, and hydrocarbons ranging from methane to butane as refrigerants can significantly improve the efficiency of liquefaction processes [5]. Neon is also a model substance for validating statistical-mechanical theories of fluids. Because of its monatomic structure and spherical symmetry, it is possible to apply almost exact statistical-mechanical theories in combination with accurate models for interatomic interactions for the calculation of its properties. For these applications, the properties of neon must be known with high accuracy.

Since neon is less well investigated than helium and argon, this work aims at improving the data situation for the properties of neon. The objectives of this work are threefold: First, we report new wide-ranging measurements of the viscosity and density of neon, which were carried out with a combined vibrating-wire viscometer and single-sinker densimeter. Furthermore, we report reevaluated reference data for the viscosity of neon and helium in the limit of zero density, which were measured by one of the authors (E. V.) with an all-quartz oscillating-disk viscometer at the Universität Rostock in 1984 [6]. Finally, we provide new correlations for the viscosity and thermal conductivity of neon in the zero-density limit, which are based on recent highly accurate theoretically calculated values by Hellmann et al. [7].

This article is structured as follows. Section 2 outlines the experimental setup of the combined vibrating-wire viscometer and single-sinker densimeter employed in this study. Section 3 details the calibration of the vibrating-wire sensors with helium and the uncertainty budget, and Sect. 4 presents the results of the validation measurements with nitrogen. Section 5 reports the experimental results for the viscosity and density of neon. Section 6 deals with the reevaluation of the oscillating-disk data for the viscosity of neon. In Sect. 7, new correlations for the zero-density viscosity and thermal conductivity of neon are proposed. In Sect. 8, our results for neon are discussed and compared to data of other authors from the literature. Conclusions are presented in Sect. 9.

2 Experimental Setup

The viscosity and density measurements were carried out with a combined vibrating-wire viscometer and single-sinker densimeter, which was originally developed for accurate measurements of gases in the former group of one of the authors (E. V.) at the Universität Rostock. The viscometer was transferred from the Universität Rostock to the Helmut-Schmidt-Universität in Hamburg, where it was rebuilt and modernized in several respects, e.g., the temperature measurement system was replaced by a more accurate one. The vibrating-wire sensor was initially designed by Wilhelm et al. [8, 9]. In the first arrangement of the sensor, the wire was tensioned by a freely suspended weight, which was very susceptible to mechanical disturbances. Wilhelm and Vogel measured the viscosity of argon, krypton, propane [10, 11], and Wilhelm et al. measured the viscosity of sulfur hexafluoride [12]. Seibt [13] advanced the design of the viscosity sensor by introducing a lever arm mechanism to tension the wire, which reduced the influence of external disturbances on the vibration of the wire greatly. Moreover, Seibt combined three vibrating-wire viscosity sensors and a single-sinker densimeter in a common pressure vessel, which enabled simultaneous measurements of the viscosity and density of a gas. At first, a sinker made of quartz glass was employed. Seibt and co-workers performed measurements on helium and nitrogen [14] as well as ethane and propane [15]. During these measurements, it turned out that helium, which was used to calibrate the viscometer, was absorbed into the quartz glass sinker. Subsequently, Herrmann [16] replaced the quartz glass sinker of the densimeter by a silicon sinker to avoid the absorption of helium into the sinker. Herrmann measured the viscosity of helium [16], nitrogen [16], normal butane [17], and isobutane [18].

The theory of the vibrating-wire viscometer was developed by Retsina et al. [19, 20]. It provides relations between the viscosity η and density ρ of the gas on the one hand and the resonant frequency f and logarithmic decrement Δ of the fundamental resonance of the wire in the gas and the logarithmic decrement of the fundamental resonance of the wire in vacuum Δ_0 on the other hand. Retsina et al. introduced the dimensionless frequency of the wire in the gas

$$\Omega = \frac{\rho \omega R^2}{\eta}, \tag{1}$$

where $\omega = 2\pi f$ is the angular resonant frequency of the wire in the gas, and R denotes the radius of the wire. The radius of the wire is determined by calibration measurements with helium as will be described in Sect. 3. To determine the viscosity of the gas, the resonant frequency of the wire in the gas and the logarithmic decrements of the free vibration of the wire in the gas and in vacuum must be measured. Moreover, the density of the wire material ρ_W must be known and the density of the gas must be measured or calculated with an accurate equation of state. The dimensionless frequency of the wire Ω is found by an iterative solution of the nonlinear system of equations

$$A = (i - \Delta)\left(1 + \frac{2K_1(\sqrt{(i-\Delta)\Omega})}{\sqrt{(i-\Delta)\Omega}K_0(\sqrt{(i-\Delta)\Omega})}\right)^{-1}, \tag{2}$$

$$k = -1 + 2\,\mathrm{Im}\,(A), \tag{3}$$

$$k' = 2\,\mathrm{Re}\,(A) + 2\Delta\,\mathrm{Im}\,(A), \tag{4}$$

$$\Delta = \frac{2\Delta_0 + (\rho/\rho_\mathrm{W})k'}{2\left[1 + (\rho/\rho_\mathrm{W})k'\right]}, \tag{5}$$

for the four unknowns A, k, k', and Ω, in which K_0 and K_1 denote the modified Bessel functions of the second kind of the zeroth and first order, respectively, and i is the imaginary unit. The quantities k and k' are constants, which are related to the mass added by the moving gas to the mass of the wire and the drag of the gas, respectively. A is an integration constant, which arises in the solution of the differential equation describing the vibration of the wire. Finally, the viscosity is calculated by Eq. 1. The derivation of Eqs. 2 to 5 is described in detail in the works of Retsina et al. [19, 20] and Wilhelm [8]. They are obtained from the solutions of the partial differential equation describing the vibration of the wire and the continuity and Navier–Stokes equations for the velocity field in the gas.

The experimental setup was described in detail by Seibt et al. [13]. Therefore, only a brief description is provided here. Three vibrating-wire sensors are arranged in a triangular layout vertically inside a pressure vessel, which is made of a copper-beryllium alloy and designed for pressures up to 30 MPa. The wires are made of Chromel® and have a nominal diameter of 25 μm. The density of the wire material is $\rho_\mathrm{W} = 8500$ kg/m^3 and has a relative expanded ($k = 2$) uncertainty of 0.3 %. The wires are mounted in the center of a magnetic field between two permanent samarium-cobalt magnets, which are housed in hermetically sealed containers made of thin stainless steel sheets to prevent direct contact with the gas. The magnets have a length of 60 mm, while the length of the wires is 90 mm. The length ratio of 1.5 ensures that the 3rd harmonic vibration mode and all even harmonic vibration modes of the wire can neither be excited nor detected. The thermal expansion of the wire is accounted for in two ways. First, the change of the wire radius with temperature is taken into account by

$$R(T) = R(T = 293.15\ \mathrm{K})[1 + \alpha(T - 293.15\ \mathrm{K})], \tag{6}$$

where α is the isobaric thermal expansion coefficient of the wire material, and, second, the change of the density of the wire material is calculated by

$$\rho_\mathrm{W}(T) = \rho_\mathrm{W}(T = 293.15\ \mathrm{K})[1 - 3\alpha(T - 293.15\ \mathrm{K})]. \tag{7}$$

The thermal expansion coefficient was taken from the data sheet for Chromel® of the manufacturer of the wire as 17.2×10^{-6} K^{-1}, and a relative expanded ($k = 2$) uncertainty of 10 % was assumed.

Measurements are performed in the time domain by recording the free decay of the vibration of the wire. The vibration of the wire is initiated by an alternating sinusoidal voltage with a frequency close to the resonant frequency of the wire. After switching off the excitation voltage, the free decay of the vibration is detected by amplifying the voltage induced in the wire and recording it as a function of time. The resonant frequency and logarithmic decrement are obtained from a Levenberg–Marquardt fit of the function describing the decaying oscillation to the recorded data. Since the theory of the vibrating-wire viscometer strictly applies only for vanishing relative vibration amplitude $\varepsilon = y_0/R$, where y_0 denotes the initial amplitude of the vibration, six runs with different relative initial amplitudes ε are carried out. The logarithmic decrement and resonant frequency of the oscillation are then obtained by extrapolation of the values Δ and ω for all measured values of ε as a function of the excitation voltage squared to the limit $\varepsilon \to 0$. To improve the signal-to-noise ratio of the received signals, the wire was excited 100 times with each excitation amplitude with an interval of 0.2 s to 0.5 s between successive excitations, and the recorded signals were averaged. The lengths of the intervals between successive excitations were chosen such that a vibration had completely decayed before the next excitation started. Since the resonant frequency of the wires was approximately 290 Hz and 3000 data points were recorded with a sampling rate of 20 kHz, about 43 periods of the decaying vibration were recorded during the recording time of 0.15 s. The first 300 data points and last 200 data points were discarded, and the remaining 36 periods were evaluated.

For measuring the density, a commercial single-sinker densimeter originally supplied by Rubotherm Präzisionstechnik in Bochum, Germany, was applied. It covers the density range between 1 kg·m^{-3} and 2000 kg·m^{-3}. The single-sinker method was developed by Brachthäuser et al. [21] at the Ruhr-University Bochum and is based on the principle of Archimedes. The sinker employed in this work is made of silicon and located in the pressure vessel in the center between the three vibrating-wire sensors. An electronically controlled magnetic suspension coupling enables a contactless transmission of the force on the sinker from within the pressure vessel to a microbalance, which is operated at ambient conditions. In this work, a new high-precision balance (Sartorius, BP211) with a measurement range from 0 g to 80 g and relative expanded ($k = 2$) uncertainty of 0.002 % was employed. In contrast to the balance used by Seibt [13] and Herrmann [16], a buoyancy-free correction of the fundamental load and calibration of the balance were no longer possible. According to the principle of Archimedes, the gravitational force on a body in a fluid is reduced by the buoyancy force on the body. Thus, the weight of the body is reduced by the weight of the volume of the displaced fluid. In vacuum, only the gravitational force acts on the body in the direction of the gravitational acceleration g. By weighing the sinker in the fluid, the buoyancy force is determined. It follows by subtracting the gravitational force of the sinker in the fluid from the one in vacuum as

$$\rho g V_{\mathrm{S}} = m_{\mathrm{S,V}} g - m_{\mathrm{S,F}} g, \tag{8}$$

where V_{S} is the volume of the sinker, $m_{\mathrm{S,V}}$ its mass in vacuum, and $m_{\mathrm{S,F}}$ its apparent mass measured in the fluid. Canceling the gravitational acceleration and solving for the fluid density yields

$$\rho = \frac{m_{\mathrm{S,V}} - m_{\mathrm{S,F}}}{V_{\mathrm{S}}}. \tag{9}$$

To enable a coupling between the sinker and the permanent magnet at the upper end of the pressure vessel, a suspension is employed. Thus, in vacuum and in the fluid not only the masses of the sinker but the sum of the masses of the sinker and its suspension $m_{\mathrm{SG,V}} = m_{\mathrm{S,V}} + m_{\mathrm{G,V}}$ in vacuum and $m_{\mathrm{SG,F}} = m_{\mathrm{S,F}} + m_{\mathrm{G,F}}$ in the fluid are measured. Moreover, the volume $V_{\mathrm{SG}} = V_{\mathrm{S}} + V_{\mathrm{G}}$ must also include the volume of the suspension V_{G}. With this modification, the working equation for the single-sinker densimeter reads

$$\rho = \frac{m_{\mathrm{SG,V}} - m_{\mathrm{SG,F}}}{V_{\mathrm{SG}}}. \tag{10}$$

The volume and the mass of the silicon sinker at $T_0 = 293.15$ K and $p_0 = 100$ kPa were determined at the Physikalisch-Technische Bundesanstalt (PTB) in Braunschweig to be 12.8556 cm^3 with an expanded ($k = 2$) uncertainty of 0.0008 cm^3, while the volume of the suspension was measured by Rubotherm to be 0.24246 cm^3 with a relative expanded ($k = 2$) uncertainty of 0.05 %.

When measurements are carried out at other temperatures and at higher pressures, the dependence of the volume of the sinker and its suspension must be accounted for. The correction of the calibrated volume of the silicon sinker is described by the equation

$$V_{\mathrm{S}}(T,p) = V_{\mathrm{S},0}(T_0,p_0)\left[1 + 3\alpha(T)\left(T - T_0\right) - \frac{p - p_0}{K(T)}\right], \tag{11}$$

where α denotes the thermal expansion coefficient and K the bulk modulus of silicon. The temperature dependence of the thermal expansion coefficient is described by the polynomial correlation of Watanabe et al. [22],

$$\alpha(T) = \sum_{i=1}^{6} a_i (T/\mathrm{K})^i \tag{12}$$

Table 1 Values of the coefficients a_i in Eq. 12 for the calculation of the linear thermal expansion coefficient of silicon

i	a_i / K^{-1}
1	-3.0451×10^{-6}
2	3.5705×10^{-8}
3	-7.9810×10^{-11}
4	9.5783×10^{-14}
5	-5.8919×10^{-17}
6	1.4614×10^{-20}

with the values for the coefficients a_i in Table 1. The bulk modulus of silicon is expressed by the components of the elastic tensor c_{11} and c_{12} as

$$K(T) = \frac{c_{11}(T) + 2c_{12}(T)}{3}. \tag{13}$$

The temperature dependence of c_{11} and c_{12} is assumed to be linear, while their dependence on pressure is neglected, so that

$$c_{11}(T) = c_{11}(T_{0,c}) + \Delta c_{11}(T - T_{0,c}), \tag{14}$$

$$c_{12}(T) = c_{12}(T_{0,c}) + \Delta c_{12}(T - T_{0,c}). \tag{15}$$

The most accurate values for the components of the elastic tensor were determined by Hall [23] at $T_{0,c} = 298.15$ K to be $c_{11} = 165.64$ GPa and $c_{12} = 63.94$ GPa, and the values for the coefficients $\Delta c_{11} = -1.557016 \times 10^{-2}$ GPa K^{-1} and $\Delta c_{12} = -6.26612 \times 10^{-3}$ GPa K^{-1} used by Schilling [24] were also used here.

The correction of the volume of the suspension V_G, which is made of the stainless steel X6CrNiTi18-10, is carried out analogously. Here, the average thermal expansion coefficient $\bar{\alpha} = 16.5 \times 10^{-6}$ K^{-1} in the operating range of our apparatus is taken from the standard DIN 10088-1 [25]. Since the stainless steel is an isotropic material, the bulk modulus

$$K(T) = \frac{E(T)}{3 - 6\nu(T)} \tag{16}$$

can be expressed by the elastic modulus $E(T)$ and the Poisson number $\nu(T)$. With the average values for the elastic modulus from DIN 10088-1 [25] and for the Poisson number from ref. [26], an average value for the bulk modulus $\bar{K} = 164$ GPa is obtained.

To regulate the temperature in the pressure vessel, a two-stage thermostat is employed. The outer stage is formed by a double-walled oil-filled thermostat with a vacuum vessel for insulation of the pressure vessel. The outer stage is controlled by a circulating oil thermostat (Julabo, Presto LH40) with a stability of 10 mK to 50 mK. A heating tape wrapped around the adapter between the pressure vessel and magnetic suspension coupling, which is controlled with a stability of 10 mK by a precise temperature controller (LakeShore, LS 331), acts as inner stage. With the two-stage thermostat, a temperature stability of 2 mK in the pressure vessel is achieved. The temperature was measured in the wall at the bottom of the pressure vessel with a 25.5 Ω glass capsule standard platinum resistance thermometer (Fluke, 5686-B), which was calibrated on the International Temperature Scale of 1990 (ITS-90) at the PTB in Berlin. The resistance of the thermometer was measured with a bridge system (Fluke, Superthermometer 1595A) using a 100 Ω resistor (ASL, RR 100) as reference. The resistor was also calibrated at the PTB in Braunschweig. The expanded ($k = 2$) uncertainty in the calibration of the thermometer is 1.5 mK, and the relative expanded ($k = 2$) uncertainty in the measurement of the ratio of the resistance of the thermometer to the reference resistance by the bridge system is

0.2×10^{-6} (equivalent to 0.05 mK). Considering additionally the temperature stability in the pressure vessel of 2 mK and the relative expanded ($k = 2$) uncertainty in the resistance of the reference resistor of 5×10^{-8} (equivalent to 0.014 mK), the total expanded ($k = 2$) uncertainty in the temperature measurement is 2.5 mK, where the contributions have been added in quadrature.

The valve system, which is used for filling and exhausting the pressure vessel with the gas as well as measuring the pressure of the gas, consists of two branches. One branch contains the measured gas, and the other one contains nitrogen. The pressure is measured in the nitrogen branch of the valve system with four absolute Paroscientific Digiquartz transmitters with measurement ranges of 0.689 MPa (1100A-01), 2.76 MPa (1400A-01), 13.8 MPa (1002K-01), and 41.4 MPa (1006K-01). The two branches are separated by a differential pressure transducer (Rosemount, 3051S-CD) to protect the pressure transmitters from the measured gas. Since only helium, neon, and nitrogen are measured in this work, it was short-cut during all measurements, so that the nitrogen branch was always filled with the measured gas. The transmitters were calibrated at the Deutscher Kalibrierdienst (DKD) and are characterized by expanded ($k = 2$) uncertainties of 0.01 % of full scale. Since the operating ranges of the transmitters partially overlap, the lower 20 % to 25 % of their measurement ranges were not used, but pressures in these ranges were measured by the transmitter with the next lower range. With this procedure, the relative expanded ($k = 2$) uncertainty of the pressure transmitters is between 0.01 % and 0.05 % of reading. Since the pressure transmitters are mounted at a different geodetic height than the vibrating-wire sensors and the sinker, a hydrostatic head correction is applied. Its relative expanded ($k = 2$) uncertainty relative to the measured pressure is estimated to be 0.001 %. The total uncertainty in the pressure measurement is formed by adding the uncertainties of the pressure transmitters and the contribution due to the uncertainty in the hydrostatic head correction in quadrature. It is essentially equal to the uncertainty of the pressure transmitters and amounts to 0.01 % at full scale to 0.05 % at 20 % of full scale for each transmitter.

Since a very low vacuum pressure is required for measurements of the logarithmic decrement of the vibration of the wire in vacuum, a vacuum pump system (Pfeiffer, HiCube ECO) with a turbomolecular pump and multi-stage membrane pump was employed to evacuate the valve system and the pressure vessel. With the vacuum pump system, pressures of 1×10^{-6} hPa in the valve system near the pump were achieved. This was found to be low enough to perform the measurements of the decaying vibration of the wires in vacuum.

3 Calibration and Uncertainty Budget

Since the vibrating-wire viscometers had been equipped with new wires before the measurements of this work were started, calibration measurements with helium were carried out to determine their radii. Details of the helium and all other samples used in this work are summarized in Table 2. Our helium sample had a volume purity of 99.999 % and was used without purification as delivered. For the calibration of

Table 2 Chemical sample description

Chemical name	CAS number	Manufacturer	Volume purity	Impurities[a]
Samples for measurements with the combined vibrating-wire viscometer and densimeter:				
Helium	7440-59-7	Linde	0.99999	Oxygen: $\leq 2 \times 10^{-6}$
				Nitrogen: $\leq 3 \times 10^{-6}$
				Water: $\leq 3 \times 10^{-6}$
				Hydrocarbons: $\leq 0.2 \times 10^{-6}$
Nitrogen	7727-37-9	Westfalen	0.99999	Oxygen: $\leq 3 \times 10^{-6}$
				Water: $\leq 5 \times 10^{-6}$
				Hydrocarbons: $\leq 1 \times 10^{-6}$
Neon	7440-01-9	Messer Austria	0.99999	Oxygen: $\leq 1 \times 10^{-6}$
				Nitrogen: $\leq 2 \times 10^{-6}$
				Water: $\leq 1 \times 10^{-6}$
				Helium: $\leq 6 \times 10^{-6}$
				Carbon dioxide: $\leq 0.5 \times 10^{-6}$
				Hydrocarbons: $\leq 0.1 \times 10^{-6}$
Samples for reevaluated measurements with the oscillating-disk viscometer:				
Helium	7440-59-7		0.99999	
Neon	7440-01-9		0.9995	

[a]According to the manufacturer's specification

the wire radii, the theoretically calculated value $\eta_{0,\mathrm{He}} = 19.5979$ μPa·s of Cencek et al. [27] for the viscosity of helium in the limit of zero density at 293.15 K was used as reference. It has an expanded ($k = 2$) uncertainty of 0.002 %. The calibration measurements were carried out along the 293.15 K isotherm at 14 pressures between 1.2 MPa and 21 MPa starting at 21 MPa in descending order. As densities calculated with the reference equation of state for helium of Ortiz Vega et al. [28] have an expanded ($k = 2$) uncertainty of 0.03 % and, thus, are more accurate than the densities measured in this work with the single-sinker densimeter as will be described below the densities required for the evaluation of the viscosity measurements were calculated with the equation of state.

Since the temperature of a measured state point usually deviated by a few millikelvin from the nominal temperature of the isotherm, the measured values of the viscosity and density were converted into values valid at the nominal temperature 293.15 K. The converted values of the density and viscosity were obtained from Taylor series expansions of the density and viscosity centered at the measured pressures along isobars with the pressures of the measured state points, which were truncated after the linear term. The derivative of the density with respect to temperature was calculated with the equation of state of Ortiz Vega et al. [28] and the corresponding derivative of the viscosity with the correlation of Arp et al. [29]. The converted experimental viscosities were fitted by a second-order polynomial in density, $\eta(\rho, T = 293.15\ \mathrm{K}) = a_0 + a_1\rho + a_2\rho^2$ with coefficients a_i, in which the coefficient a_0 corresponds to the viscosity in the limit of zero density. The wire radius was then determined such that a_0 equals the reference

value of Cencek et al. [27]. The results of the calibration measurements with sensors 1 and 2 after the adjustment of the wire radii are reported in Tables 11 and 12 in the appendix. Since the measurements with the third vibrating-wire sensor did not exhibit the correct dependence of the viscosity of helium on density, it was not used in the remainder of this work. This failure was probably due to an inappropriate mounting of the wire.

Figure 1 exemplarily shows the experimental results for the viscosity of helium measured with sensor 1 after the calibration as a function of density. It is evident that the isotherm has a negative slope below 12 kg·m^{-3}, exhibits a shallow minimum and then increases at higher densities. The calibration measurements of Seibt [13] and Herrmann [16] with helium also exhibit a shallow minimum at the 293.15 K isotherm. This behavior was theoretically explained by Rainwater and Friend [30–32] and by Bich and Vogel [33] using the theory of the initial density dependence of the viscosity. The data below 2 kg·m^{-3} were excluded from the analysis because they are affected by the slip effect, i.e., at such low densities the fluid does not adhere to the surface of the wire.

From here on, we consider all uncertainties as expanded ($k = 2$) uncertainties if not denoted otherwise. If a literature source does not report whether an uncertainty is a standard uncertainty or an expanded ($k = 2$) uncertainty, we assume an expanded ($k = 2$) uncertainty. The combined uncertainty in viscosity was estimated according to the Guide to the Expression of Uncertainty in Measurement (GUM) [34] as

$$U_c(\eta) = \sqrt{[U(\eta)]^2 + \left(\frac{\partial \eta}{\partial \rho}\right)_T^2 [U(\rho)]^2 + \left(\frac{\partial \eta}{\partial T}\right)_\rho^2 [U(T)]^2} \tag{17}$$

by adding the contributions due to the uncertainties in the viscosity measurement $U(\eta)$, density measurement $U(\rho)$, and temperature measurement $U(T)$ in quadrature. According to the theory of the vibrating-wire viscometer, the viscosity

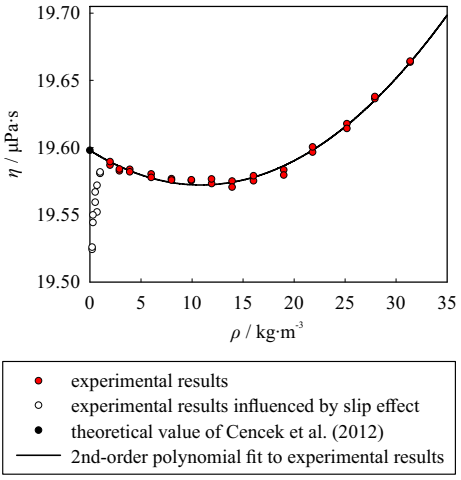

Fig. 1 Experimental results for the viscosity of helium at 293.15 K measured with sensor 1 as a function of density

$$\eta = f[\rho, R, \alpha, \omega, \Omega(\Delta, \Delta_0, \rho, \rho_W, \alpha)] \tag{18}$$

is a function of the density of the gas ρ, the wire radius R, the thermal expansion coefficient of the wire material α, the angular resonant frequency ω, and the quantity Ω, which depends on the logarithmic decrement in the gas Δ, the logarithmic decrement in vacuum Δ_0, the density of the gas ρ, the density of the wire material ρ_W, and the thermal expansion coefficient of the wire material. Adding all uncertainty contributions of the influencing quantities in Eq. 18 in quadrature yields for the relative uncertainty in viscosity

$$\begin{aligned} U_r(\eta) = \Bigg\{ & \left[\frac{\partial\eta}{\partial\rho}\frac{\rho}{\eta}U_r(\rho)\right]^2 + \left[\frac{\partial\eta}{\partial R}\frac{R}{\eta}U_r(R)\right]^2 + \left[\frac{\partial\eta}{\partial\alpha}\frac{\alpha}{\eta}U_r(\alpha)\right]^2 + \left[\frac{\partial\eta}{\partial\omega}\frac{\omega}{\eta}U_r(\omega)\right]^2 \\ & + \left[\frac{\partial\eta}{\partial\Delta_0}\frac{\Delta_0}{\eta}U_r(\Delta_0)\right]^2 + \left[\frac{\partial\eta}{\partial\rho_W}\frac{\rho_W}{\eta}U_r(\rho_W)\right]^2 + \left[\frac{\partial\eta}{\partial\Delta}\frac{\Delta}{\eta}U_r(\Delta)\right]^2 \\ & + 2\frac{\partial\eta}{\partial R}\frac{R}{\eta}\frac{\partial\eta}{\partial\rho_W}\frac{\rho_W}{\eta}U_r(R,\rho_W)\Bigg\}^{1/2} \end{aligned} \tag{19}$$

as an estimate for the relative uncertainty in viscosity, where $U_r(R, \rho_W) = U(R, \rho_W)/(R\rho_W)$ denotes the relative expanded ($k = 2$) covariance between the wire radius and density of the wire material. Since Ω must be determined iteratively, derivatives of the viscosity with respect to the influencing quantities cannot be calculated analytically or numerically in a simple way. The contributions of the influencing quantities in Eq. 19 were investigated in detail in the density range between 1 kg·m^{-3} and 1000 kg·m^{-3} by Seibt [13]. Seibt varied each influencing quantity by 0.5 % and calculated the change in viscosity. It turned out that the influencing factors of the wire radius $[(\partial\eta/\partial R)R/\eta = 2]$, and resonant frequency $[(\partial\eta/\partial\omega)\omega/\eta = 1]$ are independent of density, while the magnitudes of the influencing factors of the logarithmic decrement $[(\partial\eta/\partial\Delta)\Delta/\eta = 1 \ldots 2]$, fluid density $[(\partial\eta/\partial\rho)\rho/\eta = -0.2 \ldots -0.6]$, and density of the wire material $[(\partial\eta/\partial\rho_W)\rho_W/\eta = 1.1 \ldots 1.6]$ increase with density. The thermal expansion coefficient appears two times as an influencing quantity in Eq. 18. Its influence depends on temperature and is largest at the highest measured isotherms. It is described by the equation $(\partial\eta/\partial\alpha)\alpha/\eta\, U_r(\alpha) = 4.81 \times 10^{-6}\ \mathrm{K}^{-1}(T - 293.15\ \mathrm{K})$. At the highest measured temperature in this work 453.15 K, it amounts to 0.034 % at low density and increases to 0.077 % at the highest measured densities. The influencing factor of the logarithmic decrement in vacuum $(\partial\eta/\partial\Delta_0)\Delta_0/\eta$ depends on the magnitude of the logarithmic decrement in vacuum, decreases with density, and was found to be between −0.001314 and −0.001928 for sensor 1 and between −0.002521 and −0.003699 for sensor 2.

With the relative uncertainty in density of 0.05 % for densities larger than 10 kg·m^{-3} and an influencing factor of 0.5, a contribution of 0.025 % to the relative uncertainty in viscosity is obtained if the experimental densities measured by the single sinker are used in the evaluation of the viscosity measurements. As for helium, nitrogen, and neon accurate reference equations of state with relative

uncertainties in density of 0.03 %, 0.01 %, and 0.05 %, respectively, are available, we used densities calculated with the equations of state in the evaluation of our measurements. Their uncertainties contribute 0.015 %, 0.005 %, and 0.025 % to the uncertainty in viscosity. With a maximum influencing factor for the logarithmic decrement of 1.5 and its relative uncertainty of 0.05 %, a contribution of 0.075 % to the relative uncertainty in viscosity results. The relative uncertainty in the logarithmic decrement in vacuum is 39 % for sensor 1 and 27 % for sensor 2, which yields contributions of 0.075 % and 0.1 % to the uncertainty in viscosity, respectively. The uncertainty in the resonant frequency of the wire is 0.001 % with an influencing factor of unity and, hence, is negligible.

The uncertainty in the wire radius results from the calibration of the wire radius to the reference value of Cencek et al. [27]. In the calibration, the extrapolated value for the viscosity in the limit of zero density at the isotherm 293.15 K is treated as an experimental value, and its uncertainty is set equal to uncertainty $U_\mathrm{r}(\eta_{0,He}) = 20 \times 10^{-6}$ in the reference value for the viscosity of helium. Thus, the uncertainty in the wire radius is estimated by

$$U_\mathrm{r}(R) = \Bigg\{ [U_\mathrm{r}(\eta_{0,He})]^2 + \left[\frac{\partial \eta}{\partial \rho}\frac{\rho}{\eta} U_\mathrm{r}(\rho)\right]^2 + [U_\mathrm{r}(\omega)]^2 + \left[\frac{\partial \eta}{\partial \Delta}\frac{\Delta}{\eta} U_\mathrm{r}(\Delta)\right]^2 + \\ + \left[\frac{\partial \eta}{\partial \Delta_0}\frac{\Delta_0}{\eta} U_\mathrm{r}(\Delta_0)\right]^2 + \left[\frac{\partial \eta}{\partial \rho_\mathrm{W}}\frac{\rho_\mathrm{W}}{\eta} U_\mathrm{r}(\rho_\mathrm{W})\right]^2 \Bigg\}^{1/2} \frac{\partial R}{\partial \eta}\frac{\eta}{R}. \tag{20}$$

The uncertainty in the density of the wire material amounts to 0.3 % and, with the influencing factor of 1.1 at low density, yields a contribution of 0.33 % to the uncertainty in the viscosity. With Eq. 20, the influencing factors and uncertainties of the quantities described above, and $(\partial R/\partial \eta)\eta/R = 0.5$ a relative uncertainty in the wire radius of 0.18 % is obtained.

Since the uncertainty in the density of the wire material is rather high and yields the largest contribution to the uncertainty in the viscosity at high densities, the density of the wire material could in principle also be calibrated if a second very accurate reference value for the viscosity of helium at a high density were available. As no such reference presently exists, the radius and the density of the wire material are coupled by the calibration process, which is accounted for by the relative ($k = 2$) covariance between the wire radius and density of the wire material in Eq. 19. The covariance $U_\mathrm{r}(R, \rho_\mathrm{W})$ was estimated by examining the interdependence between R and ρ_W more closely. Holding all other influencing quantities constant, the extrapolated viscosity in the limit of zero density becomes a function of the wire radius and the density of the wire material, i.e., $\eta_\mathrm{extra}(R, \rho_\mathrm{W})$. By setting $\eta_\mathrm{extra}(R, \rho_\mathrm{W}) = \eta_{0,He}$, the coupling equation between R and ρ_W is obtained. This equation is fulfilled by infinitely many pairs of values of R and ρ_W, which reproduce the same reference value for the viscosity. Using the total differential of this relation

$$\mathrm{d}\,\eta_{\mathrm{extra}} = \frac{\partial \eta_{\mathrm{extra}}}{\partial R}\,\mathrm{d}\,R + \frac{\partial \eta_{\mathrm{extra}}}{\partial \rho_{\mathrm{W}}}\,\mathrm{d}\,\rho_{\mathrm{W}} = 0 \tag{21}$$

and introducing relative quantities

$$\frac{\partial \eta_{\mathrm{extra}}}{\partial R}\frac{R}{\eta_{\mathrm{extra}}}\frac{\mathrm{d}\,R}{R} + \frac{\eta_{\mathrm{extra}}}{\partial \rho_{\mathrm{W}}}\frac{\rho_{\mathrm{W}}}{\eta_{\mathrm{extra}}}\frac{\mathrm{d}\,\rho_{\mathrm{W}}}{\rho_{\mathrm{W}}} = 0, \tag{22}$$

a small relative change in the radius due to a change in density can be expressed as

$$\frac{\mathrm{d}\,R}{R} = -\frac{\dfrac{\partial \eta_{\mathrm{extra}}}{\partial \rho_{\mathrm{W}}}\dfrac{\rho_{\mathrm{W}}}{\eta_{\mathrm{extra}}}}{\dfrac{\partial \eta_{\mathrm{extra}}}{\partial R}\dfrac{R}{\eta_{\mathrm{extra}}}}\frac{\mathrm{d}\,\rho_{\mathrm{W}}}{\rho_{\mathrm{W}}}. \tag{23}$$

By simple mathematical transformations, it can be shown that the relative covariance between the wire radius and the density of the wire material is equal to the relative covariance of small changes in the wire radius and the density of the wire material, i.e., $U_{\mathrm{r}}(R, \rho_{\mathrm{W}}) = U_{\mathrm{r}}(\mathrm{d}\,R,\ \mathrm{d}\,\rho_{\mathrm{W}})$. Inserting Eq. 23 for $\mathrm{d}\,R$, yields

$$U_{\mathrm{r}}(R, \rho_{\mathrm{W}}) = -\frac{\dfrac{\partial \eta_{\mathrm{extra}}}{\partial \rho_{\mathrm{W}}}\dfrac{\rho_{\mathrm{W}}}{\eta_{\mathrm{extra}}}}{\dfrac{\partial \eta_{\mathrm{extra}}}{\partial R}\dfrac{R}{\eta_{\mathrm{extra}}}} U_{\mathrm{r}}(\mathrm{d}\,\rho_{\mathrm{W}},\ \mathrm{d}\,\rho_{\mathrm{W}}). \tag{24}$$

Since $U_{\mathrm{r}}(\mathrm{d}\,\rho_{\mathrm{W}},\ \mathrm{d}\,\rho_{\mathrm{W}})$ is the relative variance of $\mathrm{d}\,\rho_{\mathrm{W}}$, which can be replaced by $[U_{\mathrm{r}}(\rho_{\mathrm{W}})]^2$, the covariance between R and ρ_{W} can be estimated by

$$U_{\mathrm{r}}(R, \rho_{\mathrm{W}}) = -\frac{\dfrac{\partial \eta_{\mathrm{extra}}}{\partial \rho_{\mathrm{W}}}\dfrac{\rho_{\mathrm{W}}}{\eta_{\mathrm{extra}}}}{\dfrac{\partial \eta_{\mathrm{extra}}}{\partial R}\dfrac{R}{\eta_{\mathrm{extra}}}} \left[U_{\mathrm{r}}(\rho_{\mathrm{W}})\right]^2. \tag{25}$$

The negative sign shows that the coupling of the wire radius and the density of the wire material partially compensates the rather high uncertainty of the density of the wire material by the covariance between R and ρ_{W}. The sum of the contributions to the uncertainty in viscosity of the wire radius, the density of the wire material, and the covariance between them amounts to 0.13 % at low density and up to 0.20 % at high density.

Finally, the relative uncertainty in the viscosity measurement is obtained as between 0.18 % at low density and 0.25 % at high density. The calibration of the wire radius, the logarithmic decrement in the gas, the logarithmic decrement in vacuum, and the density of the wire material yield the dominating contributions, whereas the resonant frequency and density of the gas contribute only little.

The derivatives $(\partial\eta/\partial T)_{\rho}$ and $(\partial\eta/\partial\rho)_{T}$ in Eq. 17 were estimated by the viscosity correlation of Arp [29] for helium, the viscosity correlation of Huber et al. for nitrogen [35], and the extended corresponding-states model of Huber for neon [36].

With the low uncertainties of 2.5 mK in temperature and 0.03 %, 0.01 %, and 0.05% in the density of helium, nitrogen, and neon, respectively, their contributions to the combined relative uncertainty in viscosity are negligible. Thus, a combined relative uncertainty in viscosity of 0.25 % is finally obtained.

The combined uncertainty in the density measurement was also determined according to the GUM. Considering the uncertainties in the density, temperature, and pressure measurements $U(\rho)$, $U(T)$, and $U(p)$, respectively, the combined uncertainty in density is obtained as

$$U_c(\rho) = \sqrt{[U(\rho)]^2 + \left(\frac{\partial \rho}{\partial T}\right)_p^2 [U(T)]^2 + \left(\frac{\partial \rho}{\partial p}\right)_T^2 [U(p)]^2} \tag{26}$$

by adding the three contributions in quadrature. The uncertainty in the density measurement

$$U(\rho) = \sqrt{\left[\frac{\partial \rho}{\partial (m_{S,V} - m_{S,F})} U(m_{S,V} - m_{S,F})\right]^2 + \left[\frac{\partial \rho}{\partial V_S} U(V_S)\right]^2} \tag{27}$$

is obtained by adding the uncertainties in the weighing of the sinker and in the determination of its volume in quadrature. Evaluating the derivatives and forming an equation for the relative uncertainty results in

$$U_r(\rho) = \sqrt{\left[\frac{U(m_{S,V} - m_{S,F})}{(m_{S,V} - m_{S,F})}\right]^2 + \left[\frac{U(V_S)}{V_S}\right]^2}. \tag{28}$$

The uncertainty in the weighing consists of several contributions. First, the main contributions are the uncertainties in the weighings of the sinker in vacuum and in the fluid, which are estimated to be $U(m_{S,V}) = 35 \times 10^{-6}$ g and $U(m_{S,F}) = 55 \times 10^{-6}$ g [13], respectively. In the uncertainty in the weighings of the sinker in the fluid, a contribution of $20{\times}10^{-6}$ g for adsorption of the gas on the sinker surface is included [37]. Moreover, the relative uncertainties in the balance of $6{\times}10^{-6}$, in the sensitivity drift of the balance of $0.4{\times}10^{-6}$, and in the force transmission error of the magnetic suspension balance of 20 ppm must be considered. The force transmission error of the magnetic suspension balance is caused by the interaction between the permanent magnet and the coupling housing at different positions of the permanent magnet during the measurements [38, 39]. Adding all contributions in quadrature yields for the relative uncertainty in the mass determination

$$U_r(m_{S,V} - m_{S,F}) = \sqrt{0.0021\%^2 + \left(\frac{0.056 \text{ mg}}{m_{S,V} - m_{S,F}}\right)^2}. \tag{29}$$

Normalizing the uncertainty contribution of the mass determination to a weighing at the density 10 kg·m^{-3} leads to

$$U_{\mathrm{r}}(m_{\mathrm{S,V}} - m_{\mathrm{S,F}}) = \sqrt{0.0021\%^2 + \left(\frac{0.044\%}{\rho/10\ \mathrm{kg \cdot m^{-3}}}\right)^2}. \tag{30}$$

Taking the relative uncertainties in the determination of the volumes of the sinker of 0.0062 % and of the suspension of 0.05 % into account results in the relative uncertainty in the density measurement of

$$U_{\mathrm{r}}(\rho) = \sqrt{0.0065\%^2 + \left(\frac{0.044\%}{\rho/10\ \ \mathrm{kg}\ \cdot \mathrm{m^{-3}}}\right)^2}. \tag{31}$$

The derivatives $(\partial\rho/\partial T)_p$ and $(\partial\rho/\partial p)_T$ in the equation for the combined uncertainty, Eq. 26, were calculated by the equations of state of Ortiz Vega et al. for helium [28], of Span et al. for nitrogen [40], and of Thol et al. for neon [41] as implemented in REFPROP [42]. With the relative uncertainty in the pressure measurement of at most 0.05 % and the uncertainty in the temperature measurement of 2.5 mK, a relative combined uncertainty in the density measurement of 0.05 % is obtained, which increases strongly below 10 kg·m^{-3} and reaches 0.1 % at the lowest measured densities near 5 kg·m^{-3}.

Figure 2 compares our experimental results for the density of helium with values calculated with the equation of state by Ortiz Vega et al. [28] and with the experimental data of Seibt [13], Herrmann [16], Evers et al. [43], and McLinden and Lösch-Will [38]. The densities calculated with the equation of state are characterized by an uncertainty of 0.03 % in the temperature range between 200 K and 500 K and at pressures up to 40 MPa, which covers the range of our measurements. Above 6 kg·m^{-3}, our results agree with the equation of state and with the very accurate

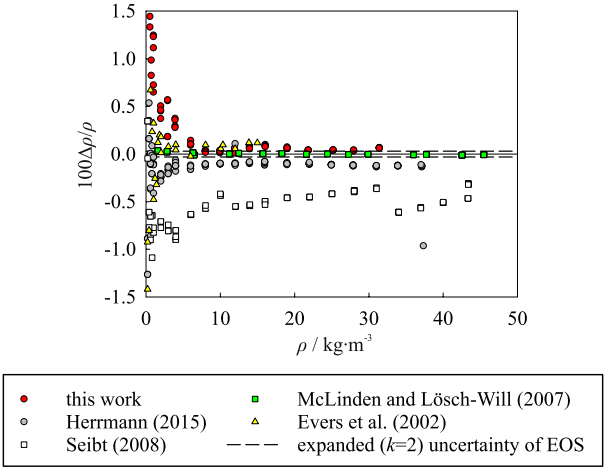

Fig. 2 Relative deviations of our experimental results for the density of helium and selected data of other authors from the literature from the values calculated with the equation of state of Ortiz Vega et al. [28] as a function of density

experimental data of McLinden and Lösch-Will, to which the equation of state was fitted, mostly within 0.05 %. Only the data at 13.9 kg·m^{-3}, 16.0 kg·m^{-3}, and 31.4 kg·m^{-3} show larger deviations up to 0.1 %. The data of Herrmann are about 0.1 % systematically lower than the equation of state, while the data of Seibt show systematic deviations of up to −0.7 % from the equation of state. These large deviations can be explained by the use of a quartz glass sinker in the single-sinker densimeter, which absorbed helium during the measurements [13]. The data of Evers et al. are somewhat higher than our results but also agree with the equation of state within 0.1 %. At densities below 6 kg·m^{-3}, our results and the data of Seibt and of Herrmann show larger systematic deviations from the equation of state, which is due to reduced sensitivity of our single-sinker densimeter at low pressure.

4 Validation Measurements

After the calibration, measurements with nitrogen were carried out along the two isotherms 293.15 K and 423.15 K to validate the calibration of the viscosity sensors. At both temperatures, the apparatus was filled with nitrogen at the highest measured pressure of 30 MPa, and the measurements were performed with both sensors in descending pressure steps. The results of these measurements are reported in the appendix in Tables 13 and 14. Figure 3 compares our results for the density of nitrogen and the experimental data of Seibt et al. [14], Herrmann [16], Evers et al. [43],

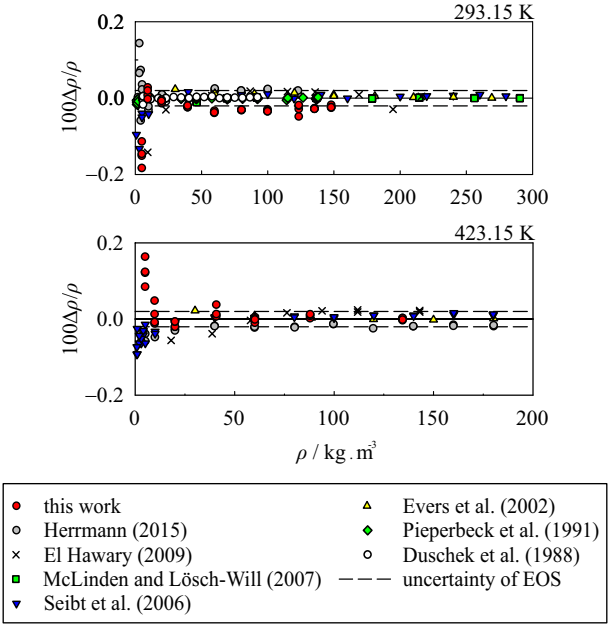

Fig. 3 Relative deviations of our experimental results for the density of nitrogen and selected data of other authors from the literature from the values calculated with the equation of state of Span et al. [40]

McLinden and Lösch-Will [38], El Hawary [44], Pieperbeck et al. [45], and Duschek et al. [46] with the reference equation of state of Span et al. [40] for nitrogen. The equation of state is characterized by an uncertainty in density of 0.02 % in the region of our measurements.

At the 293.15 K isotherm, our results above 5 kg·m^{-3} agree with the equation of state within 0.036 %. Their deviations from the equation of state are partly larger than its uncertainty but much lower than the uncertainty of our measurements. The data of Herrmann above 10 kg·m^{-3} also agree well with the equation of state and show a maximum deviation of 0.024 % at 100 kg·m^{-3}, while the data of Seibt et al. above 10 kg·m^{-3} agree with the equation of state within its uncertainty and show a maximum deviation of 0.016 % at 40 kg·m^{-3}. The data of Evers et al. also agree with the equation of state within its uncertainty with the exception of the value at 30 kg·m^{-3}, which deviates by +0.023 % from the equation of state. The data of El Hawary agree with the equation of state within its uncertainty with two exceptions at 23.1 kg·m^{-3} and 195 kg·m^{-3}, where the deviations amount to 0.03 %. McLinden and Lösch-Will performed very accurate measurements with a dual-sinker densimeter. Their data have relative uncertainties between 0.0025 % and 0.015 % and agree with the equation of state within 0.01 %. The data of Duschek et al. and Pieperbeck et al. were also measured with a dual-sinker densimeter and have relative uncertainties of 0.02 %. Both datasets were part of the data basis to which the equation of state was fitted and agree with it within 0.017 %.

At 423.15 K, our results above 5 kg·m^{-3} agree with the equation of state within its uncertainty with two exceptions at 9.74 kg·m^{-3} and 40 kg·m^{-3}, where the deviation is 0.048 % and 0.038 %, respectively. The data of Herrmann are 0.02 % systematically lower than the equation of state but mostly agree with it within its uncertainty, while the data of Seibt et al. and the data of Evers et al. with the exception of one value at 30 kg·m^{-3} agree with the equation of state within its uncertainty. The data of El Hawary deviate by between −0.05 % and +0.024 % from the equation of state. As for helium, our results at low densities show larger systematic deviations from the equation of state due to the lower sensitivity of the single-sinker densimeter at these conditions.

In Fig. 4, our results for the viscosity of nitrogen and data of Seibt et al. [14, 47], Herrmann [16], Evers et al. [43], El Hawary [44], Gracki et al. [48], and Kestin and Leidenfrost [49] are compared with the viscosity correlation of Huber et al. [35] for nitrogen. The uncertainty in viscosities calculated with the correlation amounts to 0.5 % in the dilute gas regime and 1 % in the temperature range between 270 K and 300 K up to pressures of 100 MPa. Outside this temperature range, the uncertainty in the correlation is 2 %. At 293.15 K, our results measured with sensors 1 and 2 agree with each other within 0.14 %, which is well within their uncertainty. They lie systematically up to 0.31 % below the correlation, which, however, is within its uncertainty. In 2006, Seibt et al. [47] performed measurements on nitrogen with a viscometer in which the wire of the viscosity sensor was tensioned with a freely suspended weight. These data agree with the correlation within 0.25 %, show a similar dependence on density as our results but are about 0.1 % higher. In 2009, Seibt et al. [14] measured the viscosity of nitrogen with the same experimental setup as employed in this work. These data, partially hidden behind the symbols for our

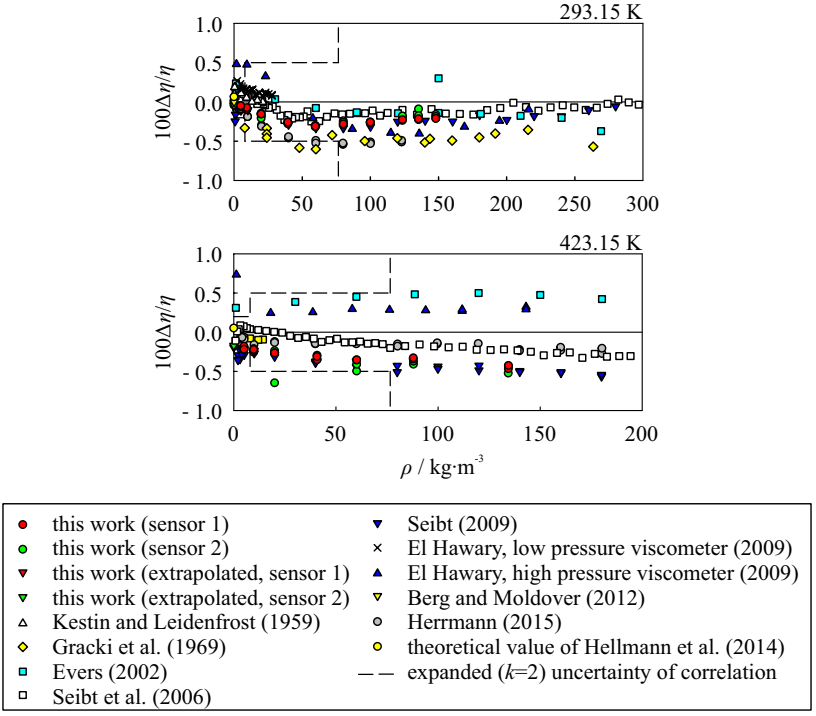

Fig. 4 Relative deviations of our experimental results for the viscosity of nitrogen and data of other authors from the literature from the values calculated with the correlation of Huber et al. [35]

results, agree better with our results but are about 0.2 % lower than the 2006 Seibt et al. data. The data of Herrmann [16] also show a similar density dependence as our results but are up to 0.25 % lower. They agree well with the data of Gracki et al. [48]. The data of Evers et al. are systematically higher than our results and mostly agree with the correlation within 0.2 %. Up to 210 kg·m^{-3}, they agree well with the 2006 Seibt et al. data. El Hawary [44] performed measurements with two rotating-body viscometers for different pressure ranges. The measurements carried out with the high-pressure viscometer at low densities are about 0.5 % higher than our results, but the data above 60 kg·m^{-3} agree with them within 0.2 %. The data measured with the low-pressure viscometer show the same trend as our data but are up to 0.25 % higher. Kestin and Leidenfrost [49] measured the viscosity at low densities up to 25 kg·m^{-3}. Their data are about 0.2 % higher than our results but agree well with the 2006 Seibt et al. data [47]. Our results for the viscosity in the zero-density limit are 0.024 % and 0.053 % lower than the correlation, which was constrained to the value recommended by Berg and Moldover [50], whereas the theoretical value of Hellmann et al. [51] is 0.064 % higher than the correlation.

At 423.15 K, our results obtained with sensors 1 and 2 agree within 0.15 % except for one value measured with sensor 2 at 20 kg·m^{-3}, which is an apparent outlier. They show systematic deviations between −0.18 % and −0.52 % from the correlation and agree best with the 2009 data of Seibt et al. [14]. The 2006 data

of Seibt et al. [47] are about 0.3 % higher than our data and deviate by −0.40 % to +0.09 % from the correlation. The data of Herrmann agree well with the 2006 data of Seibt et al. [47] and show similar deviations from the correlation. The data of Evers et al. [43] are systematically higher than our data and show deviations from +0.3 % to +0.5 % from the correlation. The data of El Hawary [44] are between 0.1 % and 0.2 % lower than the data of Evers et al. with the exception of the value at the lowest measured density, which is 0.4 % higher. Overall, this comparison shows that our combined vibrating-wire viscometer and single-sinker densimeter is capable of accurate viscosity and density measurements.

5 Experimental Results for Neon

The neon sample was purchased from Messer Austria and had a specified volume purity of better than 99.999 %. Details of the sample are provided in Table 2. We carried out measurements along ten isotherms in the supercritical region between 300 K and 450 K at pressures up to 30 MPa. Before and after measuring each isotherm, the pressure vessel was thoroughly evacuated, and the logarithmic decrement and the resonant frequency of the vibration of the wires in vacuum were determined. After the initial measurement in vacuum at an isotherm, the pressure vessel was filled with neon up to the highest pressure to be investigated of about 30 MPa. At completing each isotherm, measurements from 30 MPa down to between 0.15 MPa and 0.1 MPa were performed with both sensors. The results of these measurements are reported in the appendix in Tables 15 and 16.

The distribution of our measurements and data of other authors from the literature for the viscosity of neon is depicted in a pressure–temperature diagram in Fig. 5. Details of the datasets from the literature are summarized in Table 3. Most measurements [52–71] were carried out near ambient pressure. Besides our measurements, wider temperature and pressure ranges in the supercritical region are covered by the datasets of Trappeniers [72], Reynes and Thodos [73], Kestin and Whitelaw [74], Evers et al. [43], and Humberg and Richter [75]. Humberg [76] additionally carried out measurements at the two isotherms 298.15 K and 473.15 K. Only Slusar et al. [77] and Herreman and Grevendonk [78] reported data in the single-phase liquid region. Huth [79], Förster [80], Bewilogua et al. [81], and Bratby and Harris [82] measured the viscosity of saturated liquid neon. Huth [79], Bewilogua et al. [81], and Bratby and Harris [82] published their measurements only in graphical form. Bratby and Harris measured the neon isotopes ^{20}Ne and ^{22}Ne. Also shown in Fig. 5 are the state points of the measurements performed at the Universität Rostock with the oscillating-disk viscometer, whose reevaluation will be discussed in Sect. 6 below.

Figure 6 shows the distribution of our density measurements on neon and data of other authors from the literature for the density of supercritical neon in a pressure–temperature diagram. Table 4 summarizes details of literature datasets for the density of neon. Only the datasets of Michels and Gibson [85], Michels et al. [86], Rabinovich et al. [87], Vogl and Hall [88], and Evers et al. [43] overlap

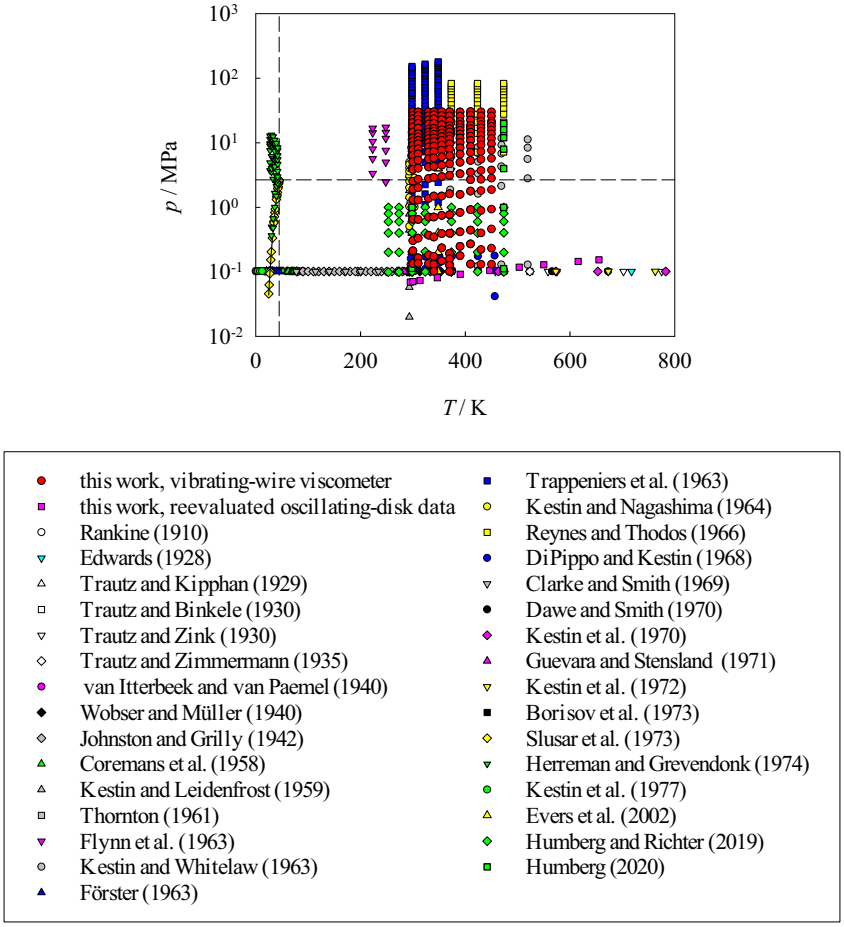

Fig. 5 Distribution of our measurements and data of other authors from the literature for the viscosity of neon in a pressure–temperature diagram

with the region of our measurements. Measurements in the liquid region or on saturated vapor were performed by Gladun [89], Scott [90], Gibbons [91], Lippold [92], and Onosovskii [93].

6 Reevaluated Data for the Viscosity of Helium and Neon

In the former group of one of the authors (E.V.) at the Universität Rostock, measurements of the viscosity of gaseous helium and neon at low pressure were carried out with an all-quartz oscillating-disk viscometer in 1984 [6]. As part of this work, we reevaluated these measurements using the Newell procedure [108], which was already applied in the reevaluation of many previous measurements performed at the

Table 3 Summary of selected experimental datasets for the viscosity of neon from the literature

Authors	Year	Method	Purity	Data	T/K	p/MPa	$U_r(c)$/%
Rankine [52]	1910	CV	n.r	1	283	0.1	n.r
Edwards [53]	1928	CV	0.98	6	195–718	0.1	n.r
Trautz [54]	1929	CV	0.99	3	293–473	0.1	n.r
Trautz [55]	1930	CV	0.99	7	286–1100	0.1	n.r
Trautz [56]	1930	CV	0.99, 0.995	4	293–523	0.1	n.r
Trautz [57]	1935	CV	n.r	11	90–523	0.1	n.r
van Itterbeek [58]	1940	OD	n.r	13	16.5–293	0.1	n.r
Wobser [59]	1941	FB	n.r	5	293–371	0.1	n.r
Johnston [60]	1942	OD	0.9975	27	80–300	0.045	0.3–0.5
Coremans [61]	1958	OD	n.r	30	20–78	0.0133	2.0–3.0
Kestin [49]	1959	OD	0.99959	10	293	0.02–3.1	0.05
Thornton [62]	1961	CV	n.r	1	291	0.933	1.0
Huth [79][a]	1962	OD	0.9993	7	24.8–27.1	SL	2.0
Flynn [83]	1963	CV	0.9997	23	223–373	2.42−17.1	0.1
Kestin [74]	1963	OD	0.99959	33	296–519	0.12−11.4	0.5
Förster [80]	1963	OD	0.9998	9	25–44	SL	2.0
Trappeniers [72]	1964	CV	0.999	87	298–348	0.69−174.6	0.1–0.3
Kestin [84]	1964	OD	0.99991	18	293–303	0.1−5.0	0.1
Reynes [73]	1966	CV	0.9999	36	373–473	7.1−83.0	n.r
Bewilogua [81][a]	1966	OD	n.r	52	24.7–28.7	SL	10.0
DiPippo [63]	1967	OD	n.r	12	293, 303	0.1–2.3	0.1
DiPippo [64]	1968	OD	n.r	17	296–347	0.04–0.17	n.r
Clarke[65]	1969	CV	0.999	10	77.5–374	0.1	0.5
Dawe [66]	1970	CV	0.9997	15	293–1600	0.01–0.13	1.0
Kestin [67]	1970	OD	0.99995	8	298–973	0.1	0.1
Guevara [70]	1971	CV	0.9998	21	1100–2100	0.1	n.r
Kestin [71]	1972	OD	0.99995	6	298–973	0.1	0.1–0.3
Bratby [82][a]	1972	OD	0.9995/0.996	66	25.4–32.8	SL	n.r
Borisov [68]	1973	CV	n.r	1	300	0.1	n.r
Slusar [77]	1973	FB	n.r	11	24–44	0.1–2.7	4.0
Herreman [78]	1974	TQ	n.r	48	27–42	0.4–11.0	3.0
Kestin [69]	1977	OD	0.99995	9	298–673	0.1	0.1–0.2
Evers [43]	2002	RB	0.99998	18	298, 348	0.1–15.8	0.15–0.40
Humberg [75]	2019	RB	0.99999	46	253–473	0.1–1.0	0.17–0.25
Humberg [76]	2020	RB	0.99999	14	298, 473	0.1–20.0	0.3–0.4

[a]Results are reported in graphical form only

CV capillary viscometer, *FB* falling-body viscometer, *n.r.* not reported, *OD* oscillating-disk viscometer, *RB* rotating-body viscometer, *SL* saturated liquid, *TQ* torsionally vibrating quartz crystal viscometer

Universität Rostock [109–112]. The reason for the reevaluation is that the viscometer used for the relative measurements was originally calibrated [113] with experimentally based reference values for the zero-density viscosity of the noble gases

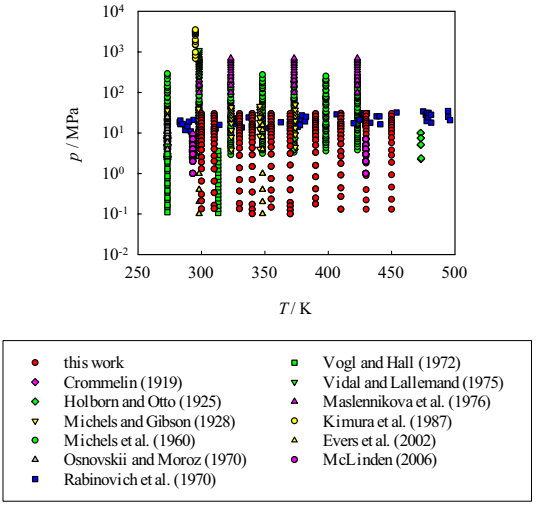

Fig. 6 Distribution of our measurements and data of other authors from the literature for the density of supercritical neon in a pressure–temperature diagram

and nitrogen at room temperature recommended by Kestin et al. [114, 115] in 1971 and 1972. These reference values are nowadays considered to be outdated. For the recalibration of the viscometer and the reevaluation of the measured data for helium and neon, a viscosity value for helium at room temperature theoretically calculated by Bich et al. [116] was used: $\eta_{0,298.15\mathrm{K,\,Bich}} = 19.826\ \mu$Pa·s. This value differs only marginally from the standard viscosity value for helium $\eta_{298.15K} = 19.8253\ \mu$Pa·s, which was obtained from an improved interatomic pair potential [27]. Additionally, we reevaluate in the same manner unpublished data from one series of measurements on helium by Strehlow performed for his Ph.D. thesis at the Universität Rostock in 1987 [117].

The theoretical calculations for the shear viscosity refer to the limit of zero density. In contrast, experiments in this limit are not feasible. Thus, the measurements were carried out somewhat below atmospheric pressure. To infer values at zero density, the experimental data have to be corrected using values of the initial density dependence of the viscosity. Unfortunately, the values of the density coefficient $\left[(\partial\eta/\partial\rho)/\eta\right]_T$, characterized by low uncertainty, are only available for noble gases at room temperature (see for example Table 6 in Ref. [118]). To perform the correction at any temperature, the Rainwater–Friend theory [31, 32] can be applied. For this purpose, we used the formalism based on the potential parameter ratios and the Lennard–Jones (12-6) length and energy parameters for helium and neon proposed by Bich and Vogel [119]. However, it must be considered that the Rainwater–Friend theory describes the initial density dependence only in an approximate manner due to the adopted Lennard–Jones potential, further physical simplifications, and the common corresponding-states treatment for several atomic and polyatomic gases. Thus, the standard uncertainty resulting from this correction could be of the order of 0.05 % to 0.3 % depending on the magnitude of the correction itself, which can amount to 2 % to 3 % near the normal boiling point decreasing down to 0.1 % to 0.2 % at higher temperatures. However, the correction is almost negligible for

Table 4 Summary of available literature data for the density of neon

Author	Year	Method	Purity	Data	T/K	p/MPa	$U(\rho)$/%
Ramsay [94]	1901	DW	n.r	26	284, 510	3.9–9.6	n.r
Crommelin [95]	1915	PM	n.r	44	55.7–293	2.2–9.5	n.r
Crommelin [96]	1919	PM	n.r	99	56–293	2.1–9.2	n.r
Holborn [97]	1925	PM	0.999	70	90.8–673	2.0–10.0	n.r
Baxter [98]	1928	DW	n.r	3	273.15	0.033–0.1	n.r
Michels [85]	1928	PM	n.r	45	273–374	3.2–48.7	0.05
Michels [86]	1960	PM	0.999987	316	273–423	2.4–285.6	n.r
Gladun [89]	1967	CVC	0.9999	114	26–43	0.49–98.7	n.r
Scott [90]	1967	FEM	0.99998	154	28–70	0.085–23.1	0.2
Sullivan [99]	1967	BM	0.999984	81	70–120	0.67–30.08	0.05–0.13
Streett [100]	1968	GE	n.r	8	100.78	6.71–53.69	0.5
Gibbons [91]	1969	CV	0.999967	309	27.1–70.1	0.24–20.6	0.13–0.15
Lippold [92]	1969	CV	0.9999	62	28.4–43.1	9.8–98.1	0.1–0.8
Onosovskii [101]	1970	PM	n.r	147	65–273	2–25.1	0.05–0.1
Rabinovich [87]	1970	PM	0.99888	92	283–727	11–50.6	0.12–0.21
Onosovskii [93]	1971	PM	0.9996	13	52	1.1–25.2	0.1–0.15
Streett [102]	1971	GE	0.9997	137	80–130	72.1–201.9	0.1
Vogl [88]	1972	BM	n.r	51	233–313	0.1–3.6	0.04–0.08
Vidal [103]	1975	DE	n.r	14	298	250–1100	0.5–1.0
Maslennikova [104]	1976	PM	0.9995	52	298–423	100–700	n.r
Kimura [105]	1987	VV	0.9999	13	295	683–3496	n.r
Evers[43]	2002	SS	0.99998	18	298–348	0.1–15.8	0.02–0.05
McLinden [106]	2006	TS	0.99999	60	293, 430	0.1–7.0	0.015
von Preetzmann [107]	2024	SS	0.99999	48	100–233	2.0–10.0	0.015–0.3

BM Burnett method, *CV* constant volume method, *CVC* constant volume calorimeter, *DW* direct weighing of a known volume of gas, *FEM* final expansion method, *GE* method of gas expansion, *n.r.* not reported, *PM* piezometer, *SS* single-sinker densimeter, *TS* two-sinker densimeter, *VV* variable volume method

helium and comparatively small for neon in the temperature range of the measurements. In principle, the experiments could be performed as isothermal series of measurements in terms of the density, so that zero-density data could be obtained by extrapolation to this limit. However, the measurements with the oscillating-disk viscometer were carried out isochorically. Therefore, the data were converted to nominal temperatures and rearranged in quasi-isotherms. In addition, all experimental temperatures were converted to the ITS-90, although the improvement in the uncertainty resulting from this correction is practically negligible.

The recalibration was performed employing the measurements closest to 298.15 K and reference viscosity values for helium calculated by

$$\eta(T,\rho) = \eta_{0,298.15\mathrm{K,\ Bich}} + (T - 298.15\ \mathrm{K})(\partial\eta/\partial T)_{\rho} + \rho(\partial\eta/\partial\rho)_{T}, \tag{32}$$

where $(\partial\eta/\partial T)_\rho = 0.0455\mu\text{Pa}\cdot\text{s}\cdot\text{K}^{-1}$ and $(\partial\eta/\partial\rho)_T = -10.644\text{nPa}\cdot\text{s}\cdot\text{m}^3\cdot\text{kg}^{-1}$ are the coefficients for the temperature and density dependencies of the viscosity, respectively. The first coefficient results from the temperature dependence of the viscosity values theoretically calculated [116], the second one was taken from Ref. [115]. The results for the reevaluated data of helium following from the two series of measurements in 1984 and those from the series in 1987 are given in Table 5. Besides the reevaluated data of the measurements themselves, the inferred viscosity values in the limit of zero density, η_0, are provided. In Table 6, the corresponding data for the series for neon from 1984 are presented.

For both helium and neon, the values in the limit of zero density were correlated by the fitting function presented in Ref. [6],

Table 5 Viscosity of helium at low density reevaluated with a recent theoretical reference value for the viscosity of helium in the zero-density limit at 298.15 K. The measurements were performed by Vogel [6] in 1984 and Strehlow [117] in 1987 with oscillating-disk viscometers at the Universität Rostock. η is the experimental viscosity, and η_0 denotes the inferred viscosity in the limit of zero density[a]

T/K	η/μPa·s	η_0/μPa·s	T/K	η/μPa·s	η_0/μPa·s
Ref. [6], Series 1, ρ=0.135 kg·m^{-3}			Ref. [6], Series 2, ρ=0.060 kg·m^{-3}		
294.45	19.667	19.668	298.24	19.824	19.824
319.17	20.780	20.781	321.38	20.866	20.866
350.67	22.170	22.170	352.98	22.248	22.249
395.74	24.097	24.098	392.36	23.942	23.942
454.62	26.512	26.513	444.48	26.096	26.096
509.43	28.706	28.707	502.53	28.426	28.426
561.05	30.714	30.716	548.23	30.210	30.210
609.26	32.549	32.550	627.54	33.227	33.227
647.88	34.008	34.009	641.36	33.769	33.770
300.11	19.910	19.910	297.75	19.805	19.806
Ref. [117], Series 1, ρ=0.126 kg·m^{-3}					
298.66	19.848	19.848	528.52	29.464	29.465
326.51	21.105	21.106	542.22	30.002	30.003
357.65	22.484	22.485	571.22	31.114	31.115
383.84	23.596	23.596	599.72	32.203	32.204
412.55	24.799	24.800	629.53	33.306	33.307
441.39	26.006	26.007	658.49	34.400	34.401
470.38	27.164	27.165	687.69	35.416	35.418
499.49	28.318	28.319	298.66	19.848	19.849

[a] The standard uncertainty in temperature is $u(T) = 50$ mK at $T = 295$ K increasing to $u(T) = 150$ mK at $T = 690$ K; the relative standard uncertainty in density is $u_r(\rho) = 1.0$ %. The relative combined expanded ($k = 2$) uncertainty in viscosity is $U_{c,r}(\eta) = 0.2$ % at temperatures between 295 K and 400 K and $U_{c,r}(\eta) = 0.4$ % at higher temperatures between 400 K and 690 K. The purity of the samples was $x_{He} \geq 0.99999$

Table 6 Viscosity of neon at low density (series 1: ρ=0.567 kg·m^{-3}) reevaluated with a recent theoretical reference value for the viscosity of helium in the zero-density limit. The measurements were performed by Vogel [6] in 1984 with an oscillating-disk viscometer at teh Universität Rostock. η is the experimental viscosity, and η_0 denotes the inferred viscosity in the limit of zero density[a]

T/K	η / μPa·s	η_0 / μPa·s
295.11	31.530	31.527
313.47	32.849	32.846
346.68	35.140	35.138
390.29	38.061	38.059
446.65	41.613	41.611
502.98	45.056	45.055
550.00	47.792	47.792
615.76	51.564	51.564
655.39	53.709	53.709
299.92	31.887	31.884

[a]The standard uncertainty in temperature is $u(T) = 50$ mK at 295 K, increasing to $u(T) = 150$ mK at 650 K; the relative standard uncertainty in density is $u_r(\rho) = 1.0$ %. The relative combined expanded ($k = 2$) uncertainty in viscosity is $U_{c,r}(\eta) = 0.2$ % at temperatures between 295 K and 400 K and $U_{c,r}(\eta) = 0.4$ % at higher temperatures between 400 K and 650 K. The purity of the samples was $x_{Ne} \geq 0.9995$

Table 7 Parameters of the fitting functions, Eq. 33, for helium and neon and standard deviations (s.d.) and root mean square deviations (r.m.s.) of the reevaluated experimental data from the fitting functions

Gas	S	A	B	C	D	s.d	r.m.s
	μPa·s					μPa·s	%
Helium	19.8253	0.741884	0.099832	−0.021820	−0.077956	0.0126	0.042
Neon	31.728	0.683586	0.065779	−0.029430	−0.035607	0.0165	0.028

$$\eta_0(T) = S \exp\left[A \ln(T_R) + \frac{B}{T_R} + \frac{C}{T_R^2} + D\right] \tag{33}$$

with $T_R = T/298.15$ K. The parameters A, B, C, and D were determined by a least squares fit to the reevaluated measurements. The parameter S was fixed to the theoretically calculated viscosity value at 298.15 K. The values of the parameters A, B, C, and D for helium and neon are given in Table 7, which also includes the standard deviation as well as the root mean square deviation of the reevaluated experimental data from Eq. 33. In the case of helium, the values of the deviations show an excellent consistency between the measurements with two completely different arrangements of the same viscometer type. For the measurements of Strehlow, a

Table 8 Values for the viscosity of helium and neon $\eta_{0,\mathrm{Eq.33}}$ calculated with the fitting function, Eq. 33, and $\eta_{0,\mathrm{th}}$ from theoretical calculations (for helium [116] and neon [7]) as a function of temperature T

T	Helium			Neon		
	$\eta_{0,\mathrm{Eq.33}}$	$\eta_{0,\mathrm{th}}$	dev	$\eta_{0,\mathrm{Eq.33}}$	$\eta_{0,\mathrm{th}}$	dev.
K	μPa·s	μPa·s	%	μPa·s	μPa·s	%
298.15	19.826	19.826	0.000	31.752	31.7254	0.084
300.00	19.911	19.910	0.005	31.885	31.8582	0.084
350.00	22.135	22.128	0.032	35.370		
400.00	24.272	24.261	0.045	38.674	38.6355	0.100
450.00	26.337	26.325	0.046	41.832		
500.00	28.342	28.331	0.039	44.870	44.8223	0.106
550.00	30.295			47.807	47.7532	0.113
600.00	32.203	32.196	0.022	50.656	50.5959	0.119
650.00	34.070			53.428	53.3615	0.125
700.00	35.901	35.905	−0.011	56.132	56.0585	0.131

new oscillating-disk viscometer, a new thermostat, and new equipment for determining the experimental quantities decrement and period of oscillation were constructed and built.

In Table 8, viscosity data in the limit of zero density calculated with Eq. 32 are compared with the viscosity values theoretically calculated by kinetic theory with the interatomic potentials for helium [116] and neon [120]. The deviations for helium do not exceed + 0.05 % in the complete temperature range, and those for neon are lower than + 0.13 %.

7 Correlations for the Viscosity and Thermal Conductivity of Neon in the Zero-Density Limit

Based on the recent theoretical calculations for the zero-density viscosity and thermal conductivity of neon by Hellmann et al. [7], correlations for the viscosity and thermal conductivity in the limit of zero density were developed. The theoretical calculations cover the temperature range between 4 K and 5000 K and have relative uncertainties between 0.014 % at 293 K and 0.5 % at 4 K. The linear structural optimization technique devised by Wagner [121] was used to establish the functional form of the correlations. Both viscosity and thermal conductivity are represented using the approach

$$X_0(T) = \frac{\sqrt{T}}{S_X(T)}, \tag{34}$$

where X stands for the viscosity η or thermal conductivity λ and $S_X(T)$ is an empirical function determined by the structural optimization. This functional form resembles the Chapman–Enskog solution to the Boltzmann equation [122]. The bank of terms for the structural optimization of $S_X(T)$ consisted of two types of terms, $a_i T^{n_i/6}$ with coefficients a_i and exponents $n_i/6$ with integers n_i between −30 and zero and $a_i T^{n_i/6} \exp(-T^{m_i/6})$ with coefficients a_i and exponents $n_i/6$ and $m_i/6$ with integers n_i and m_i between zero and 30. Terms of this type, in which the temperature occurs only in integer powers of $T^{1/6}$, were obtained using symbolic regression by Laesecke and Muzny in the development of a correlation for the zero-density viscosity of methane [123] and found suitable to accurately represent the data and to ensure a physically reasonable extrapolation behavior of the correlation to low and high temperatures. For both the viscosity and thermal conductivity, the structural optimization yielded eight terms for the function $S_X(T)$, i.e.,

$$S_\eta(T) = a_1 T^{n_1/6} + \sum_{i=2}^{8} a_i T^{n_i/6} \exp\left(-T^{m_i/6}\right) \tag{35}$$

and

$$S_\lambda(T) = a_1 + \sum_{i=2}^{8} a_i T^{n_i/6} \exp\left(-T^{m_i/6}\right). \tag{36}$$

The coefficients and parameters of these terms are reported in Table 9. The correlations yield η_0 in μPa·s and λ_0 in mW/(mK). For checking computer implementations of the correlations, the following values may be used: $T = 300$ K, $\eta_0 = 31.85836$ μPa·s, and $\lambda_0 = 49.40636$ mW/(m·K).

Figure 7 shows relative deviations of the theoretically calculated values for both properties from our correlations. The data for both properties are represented well within their uncertainties. In the temperature range of our measurements, i.e., between 300 K and 450 K, the theoretically calculated values for the viscosity are represented by our correlation within 22 parts per million. Also shown

Table 9 Values of the coefficients a_i and parameters n_i and m_i in Eqs. 35 and 36

i	a_i Viscosity ($X = \eta$)	n_i	m_i	a_i Thermal conductivity ($X = \lambda$)	n_i	m_i
1	$+0.76553090079\times10^{1}$	− 2		$+0.17458318341\times10^{0}$	0	
2	$-0.75409473882\times10^{1}$	0	1	$+0.50382627053\times10^{1}$	0	2
3	$-0.42089170026\times10^{1}$	5	4	$+0.88404800309\times10^{0}$	1	1
4	$-0.89052784924\times10^{-1}$	6	2	$+0.41801012690\times10^{1}$	2	3
5	$+0.52386001485\times10^{0}$	7	3	$-0.23521889815\times10^{1}$	7	4
6	$+0.63266779490\times10^{0}$	19	7	$-0.15416266259\times10^{-4}$	8	1
7	$+0.15782775955\times10^{-10}$	25	2	$+0.10166708819\times10^{-1}$	12	3
8	$+0.20667167207\times10^{-1}$	26	6	$+0.14197148158\times10^{0}$	13	6

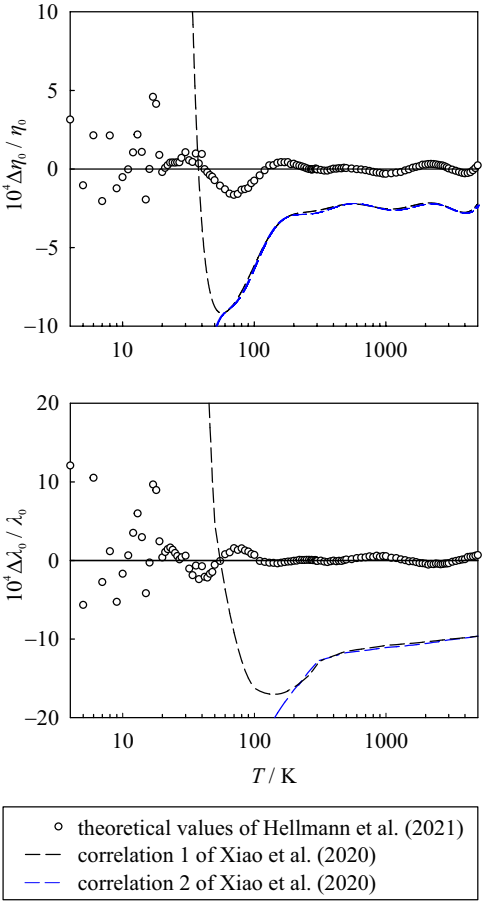

Fig. 7 Relative deviations of the theoretically calculated values for the viscosity η_0 and thermal conductivity λ_0 of neon in the zero-density limit by Hellmann et al. [7] and the correlations of Xiao et al. [124] from values calculated with our correlations, Eqs. 34 to 36, as a function of temperature T

are deviations of two different correlations published by Xiao et al. [124]. In the first correlation, denoted here as correlation 1, the temperature dependence of the viscosity is represented by an exponential of a tenth-order polynomial in $\ln T$. In the second correlation, denoted here as correlation 2, the temperature dependence of the viscosity is represented by the temperature dependence of the Chapman–Enskog solution to the Boltzmann equation for hard spheres, i.e., by $\sqrt{T}$ divided by a sum of four Gaussians in $T^{1/6}$. The correlations of Xiao et al. yield somewhat lower values than our correlations because they were fitted to the older theoretically calculated data of Bich et al. [120]. In Fig. 8, the values calculated with our correlations, the correlations of Xiao et al., and the corresponding-states model of Huber [36] for both properties are plotted versus temperature. As can be observed in Fig. 8, our correlations for both properties do not have any pole or inflection point up to at least 20,000 K, and the extrapolation behavior is physically reasonable down to 0 K and up to 20,000 K. Thus, our viscosity correlation provides a firm basis for a comparison of experimental data for the zero-density

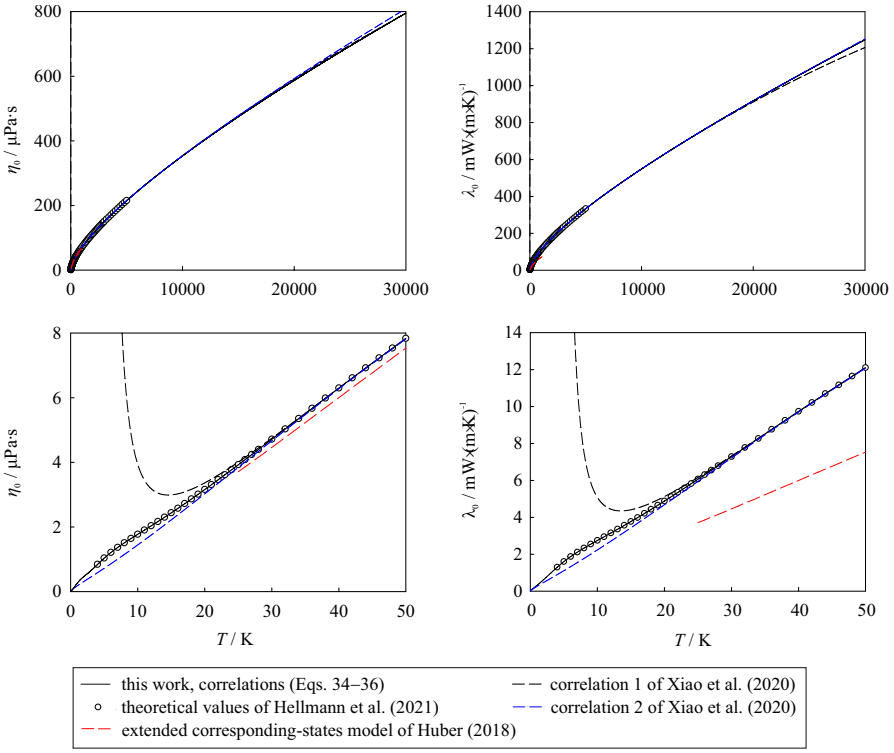

Fig. 8 Extrapolation behavior of our correlations for the viscosity and thermal conductivity of neon in the zero-density limit, Eqs. 34 to 36, the correlations of Xiao et al. [124], and the corresponding-states model of Huber [36]

viscosity of neon. The correlations of Xiao et al. also extrapolate well to high temperatures, but do not describe the recent theoretical values of Hellmann et al. [7] below 20 K correctly. The zero-density viscosity and especially thermal conductivity of the corresponding-states model of Huber show much larger deviations from our correlations than the correlations of Xiao et al. The viscosity and thermal conductivity in the limit of zero density in the corresponding-states model of Huber are described by a Chapman–Enskog solution to the Boltzmann equation with the correlations of the collision integrals for the Lennard–Jones potentials published by Neufeld et al. [125] and the Lennard–Jones parameters reported by Kestin et al. [115]. Since the Lennard–Jones potential can only be viewed as an effective potential to describe the interactions between two neon atoms, these correlations cannot describe the viscosity and thermal conductivity over a wide temperature range as accurately as the very accurate *ab initio* potential of Hellmann et al. [7].

We also derived values for the viscosity in the limit of zero density from our experimental data measured with the vibrating-wire viscometer. For this purpose, second-order polynomials were fitted to the isothermal data and extrapolated to

Table 10 Values for the viscosity of neon in the limit of zero density η_0 inferred from our isothermal measurement series with vibrating-wire sensors 1 and 2 and their relative deviations from our correlation given by Eqs. 34 and 35

T/K	η_0/μPa·s Sensor 1	Rel. dev./%	η_0/μPa·s Sensor 2	Rel. dev./%
300	31.851	−0.023	31.861	0.008
310	32.556	−0.045	32.565	−0.017
330	33.952	−0.052	33.981	0.034
340	34.646	−0.032	34.670	0.037
355	35.671	−0.009	35.693	0.053
370	36.663	−0.035	36.676	0.001
390	37.964	−0.064	37.948	−0.106
410	39.225	−0.132	39.246	−0.078
430	40.462	−0.200	40.522	−0.052
450	41.749	−0.095	41.718	−0.169

zero density. These inferred values for the zero-density viscosity and their relative deviations from our correlation are reported in Table 10. The uncertainty in the extrapolated values of 0.18 % is obtained by using Eq. 19 and assuming that the relative uncertainties in the wire radius and the wire density mostly cancel each other as described in Sect. 3.

Figure 9 depicts relative deviations of our results for the viscosity in the limit of zero density from values calculated with our correlation. Moreover, deviations of the theoretically calculated values of Hellmann et al. [7], the reevaluated data of this work measured with an oscillating-disk viscometer at the Universität Rostock, the experimental data of Humberg and Richter [75], Kestin and Whitelaw [74], Trappeniers et al. [72], and Flynn et al. [83] are shown. Also included are deviations of the recommended value of Berg and Moldover [50] at 298.15 K and values calculated with the correlations of Huber [36] and Xiao et al. [124] from our correlation. Our results inferred from the measurements with sensor 1 agree with the correlation within 0.065 % up to 390 K. Larger deviations up to 0.2 % are found at higher temperatures. The results inferred from the measurements with sensor 2 show a similar behavior. They agree with the correlation within 0.11 %, except for the value at 450 K, which lies 0.17 % below the correlation. Our reevaluated oscillating-disk data are between 0.065 % and 0.17 % higher than the correlation. Overall, all results for the viscosity in the zero density limit agree with the correlation and the theoretical values of Hellmann et al. [7] within their uncertainty. Our results obtained with both vibrating-wire sensors agree with the data of Trappeniers et al., Flynn et al., and Humberg and Richter within their uncertainty. The two data points of Evers et al. at 298 K and 348 K deviate from the correlation by −0.12 % and 0.20 %, respectively. The two data points

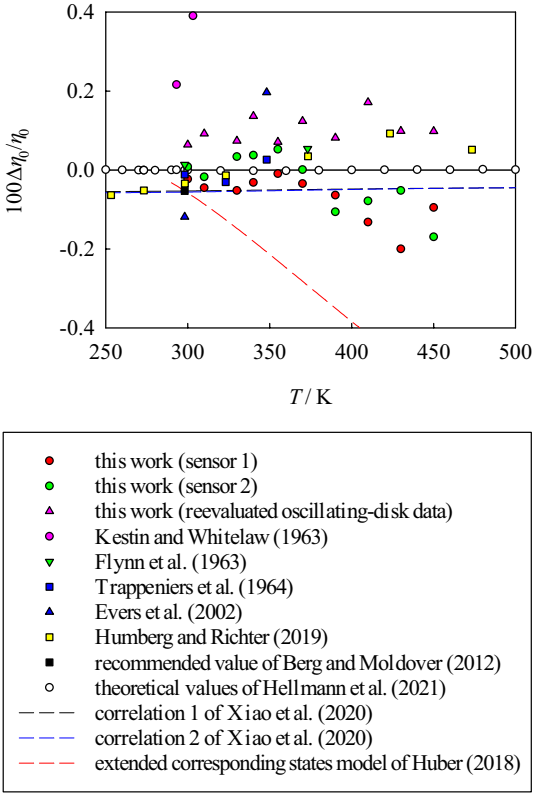

Fig. 9 Relative deviations of our results for the zero-density viscosity of neon, selected experimental data of other authors from the literature, theoretical *ab initio* calculations of Hellmann et al. [7], and correlations of other authors from the literature for the viscosity of neon in the limit of zero density from values calculated with our correlation

of Kestin and Whitelaw at 293 K and 303 K lie 0.22 % and 0.39 %, respectively, above the correlation. The corresponding-states model of Huber [36] exhibits a different temperature dependence than our correlation and data. It agrees well with our data near 300 K but shows negative deviations at higher temperatures that increase up to about −0.55 % at 450 K. Both correlations of Xiao et al. [124] yield values for the zero-density viscosity, which are up to 0.06 % lower than values calculated with our correlation because they were fitted to the theoretically calculated values of Bich et al. [120], which are 0.06 % lower than the more recent values of Hellmann et al. [7].

8 Discussion

8.1 Density

In the following, we compare the results of our density measurements on neon with the equation of state by Thol et al. [42] (TEOS) implemented in the NIST reference database REFPROP [42] and with the experimental data of McLinden [106], Evers et al. [43], Michels et al. [86], Michels and Gibson [85], and Rabinovich et al. [87]. The TEOS is valid from the triple-point temperature to 700 K and pressures up to

70 MPa, which covers the range of our measurements. Figure 10 depicts relative deviations of our results for the density and the literature data from values calculated with the TEOS. Our results are mostly systematically lower than the TEOS but agree with it within 0.05 % above 10 kg·m^{-3} at most measured isotherms, which is within the relative uncertainty of 0.05 % of our measurements. Somewhat larger deviations up to − 0.1 % from the TEOS are found at 310 K and the highest measured isotherm 450 K. Below 10 kg·m^{-3}, the deviations are larger due to the reduced sensitivity of our single-sinker sensor at low density. The higher deviations of up to 0.09 % at low density at 430 K are probably due to the fact that the pressure measurement system was not switched to the sensor with the next lower measuring range before the measurements were taken. At 300 K and 355 K, our results agree well with the data of Evers et al. [43] with the exception of one value at the state point (298 K, 62.7 kg·m^{-3}) and the value at (348 K, 1.39 kg·m^{-3}), which is an outlier. Our results agree with the data of McLinden [106] at 293 K and 430 K, which among all literature data shown in Fig. 10 agree best with the TEOS, mostly within 0.04 %. Our results also agree mostly within 0.05 % with the data of Michels et al. [86], but their data are at most isotherms somewhat higher than our data and agree better with the TEOS, except at the isotherm 430 K, where they are on average 0.03 % lower than our data. The data of Michels and Gibson [85] at 300 K, 330 K, 340 K, and 370 K are systematically higher than our results and the Michels et al. data. At low density, they deviate by up to + 0.1 % from our results. The deviations increase with density, and at high density, the symbols lie partially outside the scale of the plots. The data of Rabinovich et al. [87] scatter more than all other data, show larger deviations from our results and the data of the other authors, and mostly lie outside the scale of the plots. Overall, the comparison shows that our results above 10 kg·m^{-3} agree with the most accurate data from the literature and the TEOS mostly within much less than their uncertainty.

8.2 Viscosity

In this section, we compare our experimental results for the viscosity of neon with the corresponding-states model of Huber [36], the recent reference correlation for the viscosity of neon of Sotiriadou et al. [126], and selected experimental data of other authors from the literature. The corresponding-states model represents the viscosity as a sum of the viscosity in the limit of zero density and a residual viscosity. As already mentioned in Sect. 7, the viscosity in the limit of zero density is described by the Chapman–Enskog solution to the Boltzmann equation for the Lennard–Jones model fluid. The residual viscosity is modeled by an extended corresponding-states model, which is based on the viscosity of nitrogen as reference. The parameters of the residual contribution were fitted to the experimental viscosity data for neon of Förster [80], Kestin et al. [115], Reynes and Thodos [73], Slusar et al. [77], and Vogel [6]. In the temperature range of our measurements, the relative uncertainty of the corresponding-states model amounts to 2 % at atmospheric pressure and increases up to 4 % at 80 MPa. The correlation of Sotiriadou et al. [126]

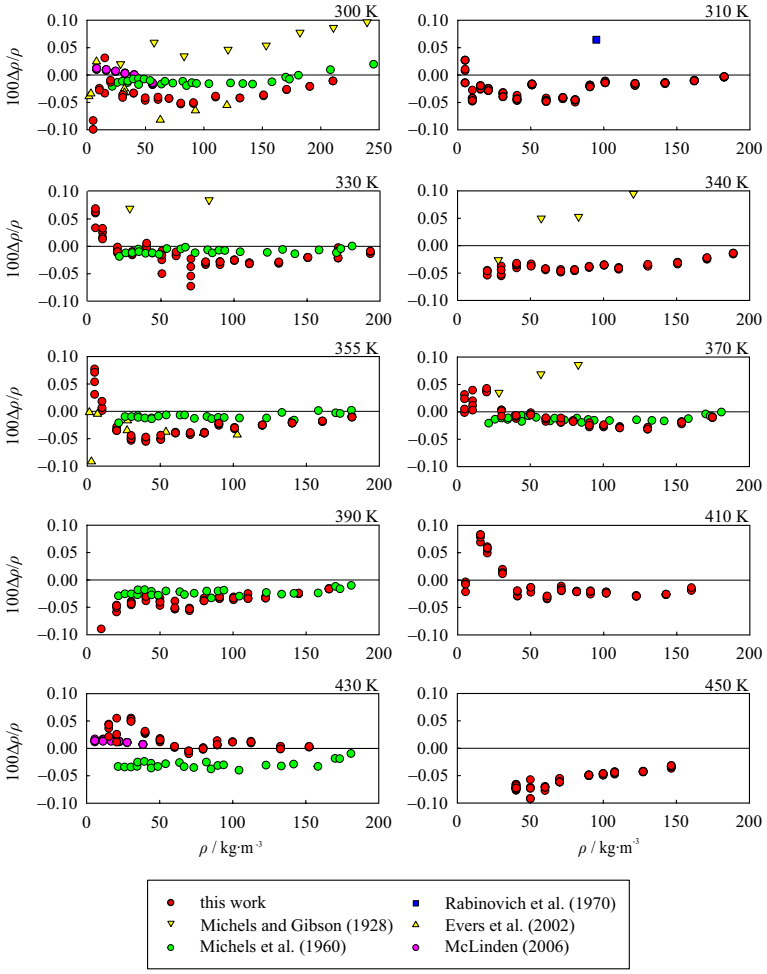

Fig. 10 Relative deviations of our experimental results for the densities of neon and data of other authors from the literature from values calculated with the equation of state of Thol et al. [42]

was developed after the measurements of this work were completed. Our results were used as part of the database to which the correlation was fitted. In the limit of zero density, it is based on our correlation for the zero-density viscosity, Eqs. 34 and 35. In the range of our measurements, it has a ($k = 2$) uncertainty of 0.016 % in the limit of zero density, 0.2 % at pressures below 1 MPa, 0.4 % at pressures between 1 MPa and 20 MPa, and 2 % at higher pressures.

Figure 11 shows relative deviations of our experimental results from values calculated with the corresponding-states model as a function of density. Also shown are deviations of values calculated with the correlation of Sotiriadou et al. [126] and of the data of Trappeniers et al. [72], Evers et al. [43], Kestin and Nagashima [84], Kestin and Whitelaw [74], Flynn et al. [83], Reynes and Thodos [73], Humberg and

Richter [75], and Humberg [76]. Data in the limit of zero density that were already discussed in Sect. 7 are also shown in Fig. 11 but are not discussed here again in detail. Experimental pressures were converted into densities with the TEOS. Our results obtained with sensors 1 and 2 agree mostly within 0.2 %, which is well within their combined ($k = 2$) uncertainty of 0.24 %. Larger differences exceeding 0.24 % up to 0.25 % are found at 13 state points at the isotherms 330 K, 430 K, and 450 K. Since this number of measurements outside the uncertainty is less than 5 % of the total number of measurements, it is consistent with our uncertainty estimation. Small systematic differences between results obtained with the two sensors along whole isotherms, as for example at 330 K and 430 K, are due to small differences in the results for the logarithmic decrements of the vibration of the wires in vacuum. In the dilute gas regime, our results agree with the corresponding-states model between within 0.1 % at 300 K and 0.4 % at 430 K and 450 K. With increasing density, the deviations become negative and increase up to − 1.1 % at the highest measured densities. The data of Trappeniers et al. [72] at 300 K and 355 K, the data of Evers et al. [43] at 300 K and 355 K, the data of Kestin and Nagashima [84] at 300 K, the data of Flynn et al. [83] at 370 K, the data of Reynes and Thodos [73], the data of Humberg and Richter [75], and the data of Humberg [76] exhibit a similar dependence on density as our results and agree with them mostly within the expanded ($k = 2$) uncertainty of our results. The data of Evers et al. at 355 K are about 0.2 % to 0.35 % higher than our results, while the data of Reynes and Thodos are up to 0.5 % lower than our results. The data of Kestin and Whitelaw at 300 K and 370 K show a different dependence on density than all other datasets. They are probably subject to a systematic error because their deviations increase strongly with density. The correlation of Sotiriadou et al. [126] represents our results up to 100 kg·m^3 within their uncertainty of up to 0.25 %. At higher densities, its deviations from our results become larger and reach about 1 % near 200 kg·m^3.

9 Concluding Remarks

A combined vibrating-wire viscometer and single-sinker densimeter, which was originally developed in the group of one of the authors at the Universität Rostock, was transferred to the Helmut-Schmidt-Universität in Hamburg, rebuilt in the laboratory of the Institute of Thermodynamics, and used to perform measurements of the density and viscosity of neon in the temperature range between 300 K and 450 K at pressures up to 30 MPa. Before the neon measurements, the vibrating-wire sensors were calibrated with helium using an accurate theoretically calculated value for the viscosity of helium in the zero density limit at 293.15 K as reference. Density measurements on helium obtained with the single sinker as a byproduct of the calibration measurements agree with the reference equation of state for helium of Ortiz Vega et al. [28] within 0.1 %. To validate the calibration of the vibrating-wire sensors, measurements on nitrogen at the two isotherms 293.15 K and 423.15 K were carried out. The results for the density agree with the reference equation of state of Span et al. [40] and the most accurate experimental data for the density of nitrogen from the literature within 0.04 %. Our results for the viscosity agree with the

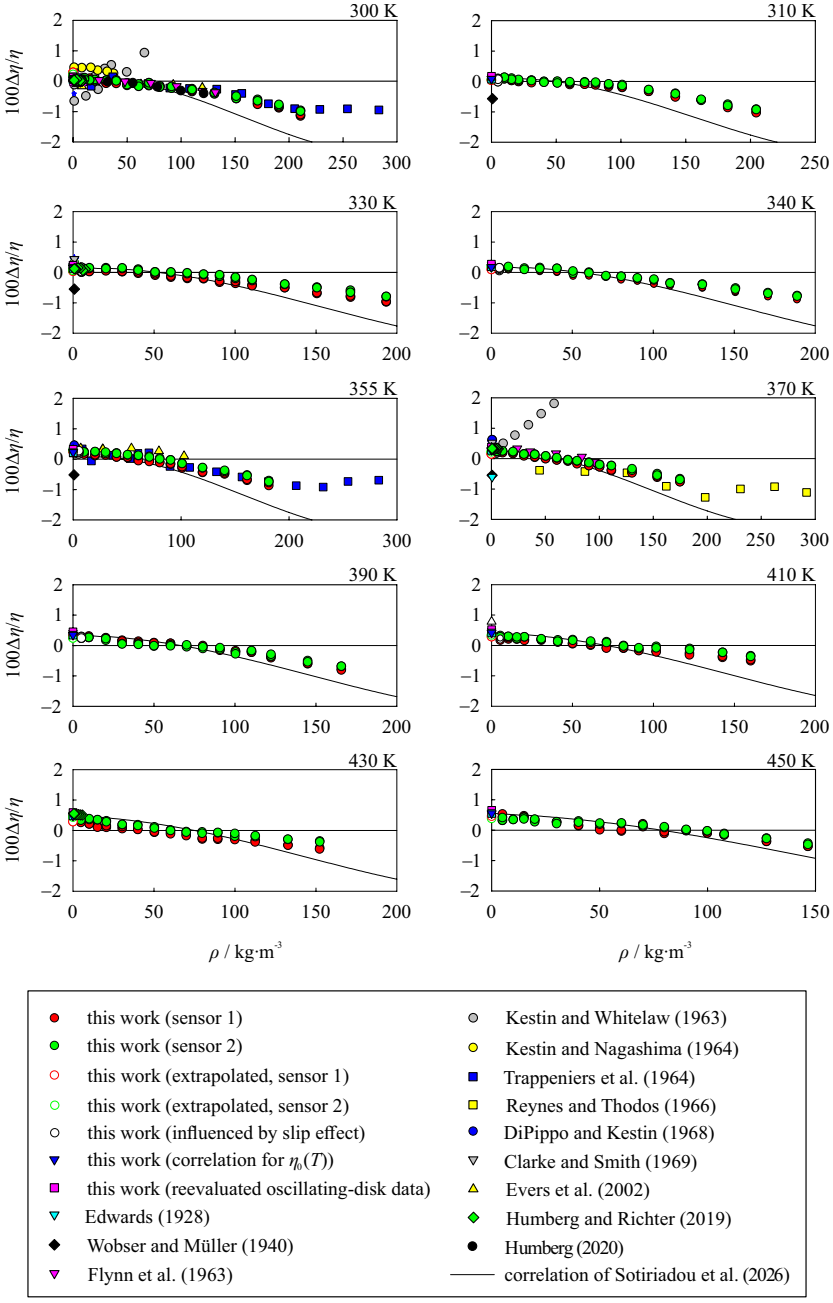

Fig. 11 Relative deviations of our experimental results for the viscosity of neon, selected data of other authors from the literature, and values calculated with the correlation of Sotiriadou et al. [126] from values calculated with the corresponding-states model of Huber [36]

most accurate literature data within their relative uncertainty of 0.25 % and with the correlation of Huber et al. [35] within 0.3 % at 298.15 K and within 1.0 % at 423.15 K, which is within the uncertainty of the correlation. This confirms that the single-sinker densimeter and vibrating-wire viscometer operate within the estimated relative expanded ($k = 2$) uncertainties of 0.05 % and 0.24 %, respectively.

After the validation of the instrument, measurements on neon at ten isotherms between 300 K and 450 K at 156 state points were performed. Our results for the density agree with the TEOS and the accurate data of Michels et al. mostly within 0.05 %. Our results for the viscosity agree with the data of Trappeniers et al. [72], Flynn et al. [83], Reynes and Thodos [73], and Humberg and Richter [75] within the expanded ($k = 2$) uncertainty of our results, while we observe larger deviations up to 1.1 % from the extended corresponding-states model of Huber [36]. Values for the viscosity in the limit of zero density inferred from our measurements agree within 0.18 % with the very accurate recent theoretically calculated values for the viscosity in the zero-density limit of Hellmann et al. [7].

Moreover, measurements of the viscosity of neon carried out in 1984 and 1987 at the Universität Rostock with an all-quartz oscillating-disk viscometer were reevaluated using a recent accurate theoretically calculated value for the viscosity of helium as a reference for the calibration. Values for the viscosity in the limit of zero density derived from these data agree with recent theoretically calculated values for the viscosity within 0.17 %. As a side product of this work, we provide new correlations for the zero-density viscosity and thermal conductivity of neon, which represent the theoretically calculated values in the temperature range between 4 K and 5000 K within 0.05 %.

Our measurements extend the database for the density and viscosity of neon. The results for the viscosity were already used as part of the database for the development of a new reference correlation for the viscosity of neon [126]. We note that, closely related to this work, we also carried out comprehensive speed-of-sound measurements in supercritical neon in our laboratory [127].

Appendix: Experimental Results

See Tables 11, 12, 13, 14, 15, and 16.

Table 11 Results of our $\eta\rho pT$ measurements for helium measured with sensor 1, where T is the measured temperature, T_n is the nominal temperature of the measured isotherm, p is the measured pressure, ρ_{exp} is the measured density at T and p, ρ_{exp,T_n} is the experimental density at T_n and p, ρ_{eos} is the density calculated with the equation of state of Ortiz Vega et al. [28] at T and p, ρ_{eos,T_n} is the density calculated with the equation of state of Ortiz Vega et al. [28] at T_n and p, η is the measured viscosity at T and p, and η_{T_n} is the experimental viscosity at T_n and p[a]

T	T_n	p	ρ_{exp}	ρ_{exp,T_n}	ρ_{eos}	ρ_{eos,T_n}	η	η_{T_n}
K	K	MPa	kg·m^{-3}	kg·m^{-3}	kg·m^{-3}	kg·m^{-3}	μPa·s	μPa·s
293.149	293.150	21.023	31.408	31.408	31.387	31.387	19.663	19.663
293.150	293.150	21.022	31.405	31.405	31.386	31.386	19.664	19.664
293.138	293.150	18.508	27.940	27.939	27.931	27.930	19.636	19.636
293.138	293.150	18.506	27.940	27.939	27.928	27.927	19.637	19.638
293.142	293.150	16.542	25.186	25.186	25.176	25.175	19.617	19.618
293.145	293.150	16.541	25.185	25.184	25.174	25.174	19.614	19.614
293.144	293.150	14.186	21.823	21.823	21.814	21.814	19.596	19.597
293.145	293.150	14.184	21.821	21.820	21.812	21.811	19.600	19.600
293.143	293.150	12.240	18.999	18.998	18.985	18.985	19.583	19.583
293.143	293.150	12.240	18.997	18.997	18.985	18.985	19.579	19.579
293.148	293.150	10.240	16.041	16.040	16.027	16.027	19.575	19.575
293.146	293.150	10.241	16.040	16.040	16.027	16.027	19.579	19.579
293.144	293.150	8.8434	13.938	13.937	13.929	13.929	19.575	19.575
293.144	293.150	8.8434	13.937	13.937	13.929	13.929	19.570	19.570
293.137	293.150	7.5210	11.926	11.926	11.919	11.918	19.573	19.573
293.144	293.150	7.5124	11.906	11.906	11.905	11.905	19.576	19.577
293.146	293.150	6.2338	9.9402	9.9401	9.9377	9.9376	19.575	19.575
293.145	293.150	6.2334	9.9402	9.9400	9.9372	9.9370	19.576	19.576
293.144	293.150	4.9803	7.9885	7.9884	7.9861	7.9860	19.576	19.577
293.144	293.150	4.9800	7.9870	7.9869	7.9857	7.9855	19.575	19.576
293.145	293.150	3.7187	6.0049	6.0048	5.9987	5.9986	19.580	19.580
293.145	293.150	3.7187	6.0049	6.0048	5.9987	5.9986	19.577	19.578
293.140	293.150	2.4006	3.9083	3.9081	3.8968	3.8967	19.583	19.584
293.148	293.150	2.4006	3.9075	3.9075	3.8967	3.8967	19.582	19.582
293.140	293.150	1.7773	2.8989	2.8988	2.8937	2.8936	19.582	19.583
293.139	293.150	1.7772	2.8989	2.8988	2.8936	2.8935	19.583	19.584
293.152	293.150	1.2071	1.9797	1.9797	1.9706	1.9706	19.587	19.587
293.151	293.150	1.2072	1.9782	1.9782	1.9708	1.9708	19.590	19.589

[a] Expanded uncertainty ($k = 2$) in temperature: $U(T) = 2.5$ mK, expanded relative ($k = 2$) uncertainty in pressure: $U_r(p) = 0.01$ % (at full scale of pressure transducers) to 0.05 % (at lower limit of pressure transducers), expanded relative ($k = 2$) uncertainty in density: $U_r(\rho) = 0.05$ %, and expanded relative uncertainty ($k = 2$) in viscosity: $U_r(\eta) = 0.20$ %

Table 12 Results of our $\eta\rho pT$ measurements for helium with sensor 2, where T is the measured temperature, T_n is the nominal temperature of the measured isotherm, p is the measured pressure, ρ_{exp} is the measured density at T and p, ρ_{exp,T_n} is the experimental density at T_n and p, ρ_{eos} is the density calculated with the equation of state of Ortiz Vega et al. [28] at T and p, ρ_{eos,T_n} is the density calculated with the equation of state of Ortiz Vega et al. [28] at T_n and p, η is the measured viscosity at T and p, and η_{T_n} is the experimental viscosity at T_n and p[a]

T	T_n	p	ρ_{exp}	ρ_{exp,T_n}	ρ_{eos}	ρ_{eos,T_n}	η	η_{T_n}
K	K	MPa	kg·m^{-3}	kg·m^{-3}	kg·m^{-3}	kg·m^{-3}	μPa·s	μPa·s
293.151	293.150	21.019	31.402	31.402	31.381	31.381	19.671	19.671
293.150	293.150	21.018	31.400	31.400	31.380	31.380	19.675	19.675
293.137	293.150	18.516	27.952	27.951	27.942	27.941	19.644	19.644
293.138	293.150	18.514	27.950	27.949	27.939	27.938	19.649	19.650
293.135	293.150	16.546	25.192	25.191	25.183	25.182	19.625	19.626
293.136	293.150	16.546	25.191	25.190	25.182	25.181	19.625	19.626
293.139	293.150	14.194	21.834	21.834	21.826	21.825	19.604	19.605
293.139	293.150	14.193	21.834	21.833	21.825	21.824	19.607	19.608
293.141	293.150	12.240	18.997	18.996	18.985	18.984	19.585	19.585
293.140	293.150	12.240	18.996	18.995	18.985	18.985	19.588	19.588
293.154	293.150	10.241	16.043	16.043	16.027	16.027	19.584	19.583
293.153	293.150	10.240	16.040	16.040	16.026	16.026	19.585	19.585
293.144	293.150	8.8429	13.939	13.939	13.928	13.928	19.580	19.580
293.144	293.150	8.8424	13.939	13.939	13.928	13.927	19.583	19.584
293.144	293.150	7.5146	11.911	11.911	11.909	11.908	19.580	19.580
293.144	293.150	7.5139	11.911	11.911	11.908	11.907	19.578	19.578
293.144	293.150	6.2354	9.9440	9.9438	9.9402	9.9400	19.578	19.578
293.145	293.150	6.2351	9.9409	9.9408	9.9397	9.9396	19.581	19.581
293.144	293.150	4.9804	7.9893	7.9891	7.9864	7.9862	19.582	19.582
293.144	293.150	4.9800	7.9885	7.9884	7.9856	7.9855	19.578	19.578
293.146	293.150	3.7186	6.0041	6.0040	5.9986	5.9985	19.585	19.585
293.161	293.150	3.7140	5.9995	5.9997	5.9910	5.9913	19.584	19.583
293.142	293.150	2.4029	3.9151	3.9150	3.9006	3.9005	19.585	19.585
293.142	293.150	2.4028	3.9144	3.9143	3.9005	3.9004	19.581	19.582
293.145	293.150	1.7781	2.9111	2.9111	2.8949	2.8949	19.588	19.588
293.153	293.150	1.7770	2.9096	2.9097	2.8932	2.8932	19.584	19.584
293.157	293.150	1.2065	1.9797	1.9797	1.9697	1.9698	19.590	19.589
293.160	293.150	1.2063	1.9782	1.9782	1.9693	1.9694	19.588	19.587

[a] Expanded uncertainty ($k = 2$) in temperature: $U(T) = 2.5$ mK, expanded relative ($k = 2$) uncertainty in pressure: $U_r(p) = 0.01$ % (at full scale of pressure transducers) to 0.05 % (at lower limit of pressure transducers), expanded relative ($k = 2$) uncertainty in density: $U_r(\rho) = 0.05$ %, and expanded relative uncertainty ($k = 2$) in viscosity: $U_r(\eta) = 0.20$ %

Table 13 Results of our $\eta\rho pT$ measurements for nitrogen measured with sensor 1, where T is the measured temperature, T_n is the nominal temperature of the measured isotherm, p is the measured pressure, ρ_{exp} is the measured density at T and p, ρ_{exp,T_n} is the experimental density at T_n and p, ρ_{eos} is the density calculated with the equation of state of Span et al. [40] at T and p, ρ_{eos,T_n} is the density calculated with the equation of state of Span et al. [40] at T_n and p, η is the measured viscosity at T and p, and η_{T_n} is the experimental viscosity at T_n and p^a

T K	T_n K	p MPa	ρ_{exp} kg·m^{-3}	ρ_{exp,T_n} kg·m^{-3}	ρ_{eos} kg·m^{-3}	ρ_{eos,T_n} kg·m^{-3}	η μPa·s	η_{T_n} μPa·s
293.149	293.150	13.022	147.96	147.96	148.00	148.00	20.635	20.635
293.149	293.150	13.020	147.96	147.96	147.98	147.98	20.635	20.635
293.149	293.150	11.853	135.29	135.29	135.33	135.33	20.259	20.259
293.149	293.150	11.853	135.29	135.29	135.33	135.33	20.262	20.262
293.149	293.150	10.777	123.43	123.43	123.49	123.49	19.927	19.927
293.149	293.150	10.776	123.44	123.44	123.47	123.47	19.928	19.928
293.148	293.150	8.6751	99.901	99.900	99.935	99.935	19.315	19.315
293.150	293.150	8.6739	99.891	99.892	99.921	99.921	19.316	19.316
293.155	293.150	6.9361	80.087	80.089	80.112	80.114	18.854	18.854
293.152	293.150	6.9354	80.082	80.082	80.106	80.107	18.855	18.855
293.143	293.150	5.1602	59.644	59.643	59.668	59.666	18.428	18.428
293.143	293.150	5.1601	59.645	59.643	59.666	59.665	18.426	18.426
293.146	293.150	3.4122	39.425	39.425	39.433	39.432	18.061	18.061
293.146	293.150	3.4121	39.423	39.422	39.432	39.432	18.064	18.064
293.155	293.150	1.7185	19.818	19.818	19.819	19.819	17.769	17.769
293.157	293.150	1.7183	19.814	19.814	19.817	19.817	17.767	17.767
293.140	293.150	0.80580	9.2808	9.2804	9.2782	9.2779	17.625	17.625
293.140	293.150	0.80576	9.2785	9.2781	9.2778	9.2774	17.629	17.629
293.141	293.150	0.42621	4.8961	4.8960	4.9036	4.9034	17.572	17.572
293.141	293.150	0.42609	4.8931	4.8929	4.9021	4.9019	17.574	17.574
423.238	423.150	18.332	134.47	134.50	134.46	134.49	25.541	25.538
423.238	423.150	18.330	134.46	134.49	134.45	134.48	25.551	25.548
423.076	423.150	11.572	87.929	87.913	87.927	87.911	24.389	24.392
423.076	423.150	11.568	87.906	87.890	87.899	87.883	24.393	24.396
423.114	423.150	7.7810	60.158	60.153	60.155	60.150	23.825	23.827
423.114	423.150	7.7805	60.152	60.146	60.151	60.146	23.825	23.826
423.081	423.150	5.2111	40.741	40.735	40.726	40.719	23.491	23.493
423.083	423.150	5.2089	40.713	40.707	40.709	40.702	23.500	23.503
423.101	423.150	2.5272	19.948	19.946	19.952	19.950	23.210	23.212
423.103	423.150	2.5269	19.946	19.944	19.950	19.948	23.209	23.211
423.109	423.150	1.2287	9.7437	9.7427	9.7449	9.7439	23.087	23.088
423.109	423.150	1.2283	9.7406	9.7397	9.7414	9.7405	23.091	23.093
423.111	423.150	0.62691	4.9862	4.9857	4.9820	4.9815	23.046	23.048
423.111	423.150	0.62689	4.9900	4.9895	4.9818	4.9814	23.037	23.039

[a] Expanded uncertainty ($k = 2$) in temperature: $U(T) = 2.5$ mK, expanded relative ($k = 2$) uncertainty in pressure: $U_r(p) = 0.01$ % (at full scale of pressure transducers) to 0.05 % (at lower limit of pressure transducers), expanded relative ($k = 2$) uncertainty in density: $U_r(\rho) = 0.05$ %, and expanded relative uncertainty ($k = 2$) in viscosity: $U_r(\eta) = 0.24$ %

Table 14 Results of our $\eta\rho pT$ measurements for nitrogen measured with sensor 2, where T is the measured temperature, T_n is the nominal temperature of the measured isotherm, p is the measured pressure, ρ_{exp} is the measured density at T and p, ρ_{exp,T_n} is the experimental density at T_n and p, ρ_{eos} is the density calculated with the equation of state of Span et al. [40] at T and p, ρ_{eos,T_n} is the density calculated with the equation of state of Span et al. [40] at T_n and p, η is the measured viscosity at T and p, and η_{T_n} is the experimental viscosity at T_n and p[a]

T K	T_n K	p MPa	ρ_{exp} kg·m^{-3}	ρ_{exp,T_n} kg·m^{-3}	ρ_{eos} kg·m^{-3}	ρ_{eos,T_n} kg·m^{-3}	η μPa·s	η_{T_n} μPa·s
293.149	293.150	13.025	148.00	148.00	148.03	148.03	20.646	20.646
293.149	293.150	13.023	147.98	147.98	148.02	148.02	20.640	20.640
293.148	293.150	11.853	135.29	135.29	135.33	135.33	20.287	20.287
293.148	293.150	11.853	135.29	135.29	135.33	135.33	20.269	20.269
293.161	293.150	10.782	123.51	123.52	123.54	123.55	19.937	19.937
293.155	293.150	10.779	123.48	123.49	123.51	123.51	19.938	19.938
293.147	293.150	8.6776	99.932	99.931	99.964	99.963	19.317	19.317
293.148	293.150	8.6764	99.916	99.915	99.951	99.950	19.316	19.316
293.158	293.150	6.9390	80.121	80.124	80.146	80.148	18.863	18.863
293.158	293.150	6.9375	80.104	80.106	80.129	80.131	18.859	18.858
293.141	293.150	5.1607	59.654	59.652	59.674	59.672	18.425	18.426
293.142	293.150	5.1605	59.649	59.647	59.672	59.670	18.424	18.425
293.146	293.150	3.4123	39.424	39.424	39.434	39.433	18.063	18.064
293.146	293.150	3.4122	39.425	39.425	39.433	39.432	18.065	18.065
293.159	293.150	1.7179	19.812	19.812	19.812	19.813	17.758	17.758
293.159	293.150	1.7175	19.806	19.807	19.808	19.808	17.768	17.768
293.141	293.150	0.80571	9.2769	9.2767	9.2772	9.2769	17.627	17.628
293.142	293.150	0.80567	9.2785	9.2782	9.2766	9.2764	17.625	17.625
293.141	293.150	0.42619	4.8977	4.8975	4.9032	4.9031	17.568	17.569
293.143	293.150	0.42613	4.8954	4.8952	4.9025	4.9024	17.567	17.567
423.235	423.150	18.328	134.43	134.46	134.44	134.47	25.549	25.546
423.234	423.150	18.324	134.41	134.44	134.42	134.44	25.526	25.523
423.085	423.150	11.581	87.998	87.984	87.988	87.974	24.374	24.376
423.081	423.150	11.576	87.962	87.947	87.952	87.937	24.382	24.385
423.112	423.150	7.7838	60.170	60.164	60.176	60.170	23.791	23.792
423.115	423.150	7.7820	60.161	60.156	60.162	60.156	23.812	23.813
423.087	423.150	5.2172	40.775	40.769	40.772	40.766	23.504	23.507
423.081	423.150	5.2146	40.758	40.751	40.753	40.746	23.492	23.494
423.101	423.150	2.5272	19.951	19.949	19.953	19.950	23.216	23.218
423.103	423.150	2.5270	19.950	19.947	19.951	19.949	23.121	23.122
423.108	423.150	1.2285	9.7444	9.7435	9.7432	9.7422	23.084	23.085
423.110	423.150	1.2282	9.7452	9.7443	9.7405	9.7396	23.094	23.096
423.110	423.150	0.62696	4.9885	4.9880	4.9824	4.9819	23.039	23.040
423.111	423.150	0.62695	4.9885	4.9880	4.9823	4.9818	23.035	23.036

[a] Expanded uncertainty ($k = 2$) in temperature: $U(T) = 2.5$ mK, expanded relative ($k = 2$) uncertainty in pressure: $U_r(p) = 0.01$ % (at full scale of pressure transducers) to 0.05 % (at lower limit of pressure transducers), expanded relative ($k = 2$) uncertainty in density: $U_r(\rho) = 0.05$ %, and expanded relative uncertainty ($k = 2$) in viscosity: $U_r(\eta) = 0.24$ %

Table 15 Results of our $\eta\rho pT$ measurements for neon obtained with sensor 1, where T is the measured temperature, T_n is the nominal temperature of the measured isotherm, p is the measured pressure, ρ_{exp} is the measured density at T and p, ρ_{exp,T_n} is the experimental density at T_n and p, ρ_{eos} is the density calculated with the TEOS at T and p, ρ_{eos,T_n} is the density calculated with the TEOS at T_n and p, η is the measured viscosity at T and p, and η_{T_n} is the experimental viscosity at T_n and p^a

T	T_n	p	ρ_{exp}	ρ_{exp,T_n}	ρ_{eos}	ρ_{eos,T_n}	η	η_{T_n}
K	K	MPa	kg·m^{-3}	kg·m^{-3}	kg·m^{-3}	kg·m^{-3}	μPa·s	μPa·s
299.999	300.000	29.857	210.52	210.52	210.54	210.54	33.972	33.972
299.999	300.000	29.856	210.51	210.51	210.54	210.54	33.985	33.985
300.003	300.000	26.642	190.58	190.58	190.62	190.62	33.709	33.709
300.003	300.000	26.641	190.58	190.58	190.62	190.62	33.718	33.717
300.000	300.000	23.545	170.81	170.81	170.86	170.86	33.432	33.432
300.000	300.000	23.544	170.81	170.81	170.85	170.85	33.412	33.412
300.003	300.000	20.536	151.03	151.04	151.09	151.09	33.174	33.173
300.003	300.000	20.535	151.03	151.03	151.09	151.09	33.162	33.162
300.003	300.000	17.540	130.79	130.79	130.84	130.84	32.922	32.921
300.003	300.000	17.539	130.78	130.78	130.84	130.84	32.925	32.924
300.003	300.000	14.551	110.01	110.01	110.05	110.05	32.662	32.661
300.003	300.000	14.551	110.01	110.01	110.05	110.05	32.671	32.671
300.001	300.000	11.898	91.051	91.052	91.099	91.099	32.477	32.477
300.001	300.000	11.898	91.047	91.048	91.093	91.094	32.483	32.483
299.998	300.000	10.406	80.182	80.182	80.225	80.224	32.376	32.376
299.997	300.000	10.405	80.178	80.177	80.219	80.218	32.366	32.366
300.000	300.000	9.0395	70.101	70.101	70.131	70.131	32.284	32.284
300.000	300.000	9.0388	70.096	70.096	70.126	70.126	32.315	32.315
299.998	300.000	7.7798	60.684	60.683	60.711	60.711	32.207	32.207
299.998	300.000	7.7795	60.684	60.683	60.708	60.708	32.194	32.194
299.996	300.000	6.3426	49.803	49.802	49.826	49.825	32.135	32.135
299.996	300.000	6.3422	49.802	49.801	49.823	49.822	32.108	32.108
299.997	300.000	5.0435	39.846	39.845	39.859	39.859	32.076	32.076
299.997	300.000	5.0430	39.843	39.842	39.856	39.855	32.053	32.053
299.997	300.000	3.8350	30.468	30.467	30.479	30.479	31.995	31.995
299.997	300.000	3.8347	30.463	30.463	30.476	30.475	31.990	31.990
299.994	300.000	2.5181	20.133	20.132	20.135	20.135	31.966	31.966
299.993	300.000	2.5177	20.130	20.130	20.132	20.132	31.959	31.959
299.997	300.000	1.9023	15.250	15.249	15.255	15.255	31.927	31.928
299.997	300.000	1.9011	15.250	15.249	15.245	15.245	31.955	31.955
299.995	300.000	1.3086	10.520	10.520	10.523	10.522	31.915	31.916
299.994	300.000	1.3084	10.518	10.518	10.521	10.521	31.919	31.920
299.997	300.000	0.65015	5.2386	5.2386	5.2438	5.2438	31.872	31.872
299.997	300.000	0.64994	5.2379	5.2378	5.2422	5.2422	31.873	31.873
309.995	310.000	29.867	204.42	204.42	204.42	204.42	34.601	34.602
309.995	310.000	29.866	204.42	204.41	204.41	204.41	34.589	34.590
309.994	310.000	26.237	182.47	182.47	182.48	182.48	34.281	34.282
309.994	310.000	26.237	182.47	182.47	182.48	182.47	34.266	34.266

Table 15 (continued)

T K	T_n K	p MPa	ρ_{exp} kg·m^{-3}	ρ_{exp,T_n} kg·m^{-3}	ρ_{eos} kg·m^{-3}	ρ_{eos,T_n} kg·m^{-3}	η μPa·s	η_{T_n} μPa·s
309.996	310.000	22.952	161.97	161.96	161.98	161.98	34.015	34.015
309.996	310.000	22.951	161.96	161.96	161.98	161.97	34.016	34.016
309.996	310.000	19.837	141.94	141.94	141.97	141.96	33.745	33.746
309.996	310.000	19.836	141.94	141.94	141.96	141.96	33.739	33.739
310.001	310.000	16.733	121.41	121.41	121.43	121.43	33.512	33.512
310.001	310.000	16.731	121.40	121.40	121.42	121.42	33.511	33.511
310.000	310.000	13.718	100.91	100.91	100.92	100.92	33.294	33.294
310.001	310.000	13.718	100.91	100.91	100.92	100.92	33.298	33.298
309.998	310.000	12.223	90.514	90.513	90.532	90.531	33.184	33.184
309.999	310.000	12.223	90.511	90.510	90.530	90.529	33.202	33.202
310.001	310.000	10.786	80.370	80.370	80.407	80.407	33.114	33.114
310.001	310.000	10.786	80.365	80.365	80.405	80.405	33.094	33.093
309.998	310.000	9.6116	72.003	72.003	72.034	72.033	33.018	33.018
309.998	310.000	9.6116	72.002	72.001	72.033	72.033	33.018	33.018
309.995	310.000	8.0166	60.489	60.488	60.516	60.515	32.908	32.909
309.995	310.000	8.0165	60.490	60.489	60.515	60.515	32.921	32.922
309.995	310.000	6.6955	50.837	50.837	50.847	50.846	32.860	32.860
309.995	310.000	6.6952	50.836	50.835	50.844	50.844	32.846	32.846
309.999	310.000	5.3095	40.559	40.559	40.575	40.575	32.774	32.774
309.999	310.000	5.3094	40.559	40.559	40.574	40.574	32.782	32.782
309.997	310.000	4.0275	30.948	30.947	30.958	30.958	32.726	32.726
309.997	310.000	4.0275	30.948	30.947	30.958	30.958	32.703	32.703
309.999	310.000	2.7057	20.917	20.917	20.923	20.923	32.663	32.663
309.999	310.000	2.7056	20.917	20.917	20.922	20.922	32.660	32.660
309.996	310.000	2.0038	15.541	15.541	15.546	15.545	32.638	32.639
309.995	310.000	2.0038	15.541	15.541	15.545	15.545	32.638	32.638
310.002	310.000	1.2909	10.042	10.042	10.047	10.047	32.639	32.639
310.002	310.000	1.2908	10.044	10.044	10.046	10.046	32.623	32.623
309.997	310.000	0.64557	5.0397	5.0396	5.0393	5.0393	32.583	32.584
309.997	310.000	0.64555	5.0397	5.0396	5.0392	5.0391	32.564	32.565
330.035	330.000	29.917	193.36	193.38	193.39	193.41	35.771	35.769
330.035	330.000	29.914	193.35	193.36	193.37	193.39	35.776	35.774
330.047	330.000	26.077	171.30	171.33	171.31	171.33	35.456	35.452
330.048	330.000	26.068	171.24	171.26	171.25	171.28	35.467	35.464
330.034	330.000	22.577	150.51	150.53	150.54	150.56	35.166	35.164
330.035	330.000	22.575	150.50	150.51	150.53	150.55	35.177	35.175
330.010	330.000	19.325	130.63	130.64	130.67	130.68	34.942	34.941
330.011	330.000	19.325	130.63	130.63	130.67	130.67	34.940	34.939
330.000	330.000	16.124	110.50	110.50	110.54	110.54	34.705	34.705
329.999	330.000	16.123	110.50	110.50	110.53	110.53	34.694	34.694
330.016	330.000	14.526	100.24	100.25	100.27	100.27	34.597	34.596

Table 15 (continued)

T K	T_n K	p MPa	ρ_{exp} kg·m^{-3}	ρ_{exp,T_n} kg·m^{-3}	ρ_{eos} kg·m^{-3}	ρ_{eos,T_n} kg·m^{-3}	η μPa·s	η_{T_n} μPa·s
330.016	330.000	14.525	100.24	100.24	100.26	100.27	34.618	34.617
330.009	330.000	13.015	90.402	90.405	90.428	90.431	34.498	34.497
330.009	330.000	13.014	90.402	90.404	90.427	90.429	34.511	34.510
330.004	330.000	11.518	80.524	80.525	80.551	80.552	34.432	34.431
330.005	330.000	11.518	80.527	80.528	80.551	80.552	34.436	34.435
329.997	330.000	10.014	70.477	70.477	70.493	70.493	34.335	34.335
329.998	330.000	10.012	70.428	70.427	70.479	70.479	34.344	34.344
329.998	330.000	8.5231	60.377	60.377	60.387	60.387	34.258	34.258
329.998	330.000	8.5230	60.378	60.378	60.386	60.386	34.271	34.271
330.000	330.000	7.1074	50.664	50.664	50.668	50.668	34.199	34.199
330.000	330.000	7.1057	50.631	50.631	50.656	50.656	34.214	34.214
329.999	330.000	5.6017	40.197	40.197	40.197	40.197	34.143	34.143
329.998	330.000	5.6017	40.197	40.197	40.197	40.197	34.157	34.157
330.006	330.000	4.1909	30.254	30.255	30.259	30.259	34.093	34.092
330.006	330.000	4.1908	30.254	30.255	30.259	30.259	34.096	34.095
330.000	330.000	2.7873	20.248	20.248	20.249	20.249	34.071	34.071
330.002	330.000	2.7872	20.246	20.246	20.249	20.249	34.049	34.049
330.003	330.000	1.3690	10.010	10.010	10.008	10.008	33.985	33.985
330.003	330.000	1.3689	10.010	10.010	10.007	10.007	33.980	33.980
330.007	330.000	0.69995	5.1349	5.1350	5.1318	5.1319	33.948	33.947
330.008	330.000	0.69994	5.1349	5.1350	5.1317	5.1318	33.955	33.954
340.022	340.000	30.023	188.78	188.79	188.80	188.81	36.391	36.389
340.021	340.000	30.021	188.76	188.77	188.79	188.80	36.382	36.380
340.021	340.000	26.805	170.77	170.78	170.81	170.82	36.119	36.118
340.021	340.000	26.804	170.76	170.77	170.80	170.81	36.114	36.113
340.012	340.000	23.317	150.70	150.70	150.75	150.75	35.847	35.846
340.012	340.000	23.315	150.69	150.70	150.74	150.74	35.857	35.856
340.012	340.000	19.872	130.29	130.29	130.34	130.34	35.601	35.600
340.013	340.000	19.872	130.29	130.30	130.34	130.34	35.605	35.604
339.997	340.000	16.604	110.37	110.37	110.42	110.42	35.362	35.362
339.997	340.000	16.603	110.36	110.36	110.41	110.41	35.361	35.361
340.009	340.000	15.002	100.40	100.40	100.43	100.44	35.263	35.263
340.010	340.000	15.001	100.39	100.40	100.43	100.43	35.260	35.259
339.999	340.000	13.384	90.185	90.184	90.220	90.220	35.180	35.181
339.999	340.000	13.383	90.182	90.182	90.216	90.216	35.178	35.178
340.005	340.000	11.817	80.153	80.154	80.190	80.191	35.096	35.096
340.005	340.000	11.817	80.154	80.155	80.189	80.190	35.086	35.085
339.994	340.000	10.360	70.709	70.708	70.740	70.739	35.026	35.026
339.993	340.000	10.360	70.702	70.701	70.736	70.735	35.031	35.031
339.999	340.000	8.7767	60.306	60.306	60.332	60.332	34.951	34.951
339.999	340.000	8.7766	60.306	60.306	60.331	60.331	34.942	34.942

Table 15 (continued)

T K	T_n K	p MPa	ρ_{exp} kg·m^{-3}	ρ_{exp,T_n} kg·m^{-3}	ρ_{eos} kg·m^{-3}	ρ_{eos,T_n} kg·m^{-3}	η μPa·s	η_{T_n} μPa·s
339.993	340.000	7.2954	50.450	50.449	50.468	50.467	34.859	34.859
339.993	340.000	7.2946	50.446	50.445	50.463	50.462	34.880	34.880
339.995	340.000	5.8197	40.498	40.497	40.514	40.514	34.828	34.828
339.996	340.000	5.8194	40.498	40.497	40.512	40.512	34.834	34.834
339.989	340.000	4.2785	29.972	29.971	29.983	29.982	34.766	34.767
339.988	340.000	4.2779	29.963	29.962	29.979	29.978	34.775	34.775
339.992	340.000	2.8926	20.383	20.383	20.392	20.392	34.723	34.724
339.992	340.000	2.8926	20.382	20.382	20.392	20.392	34.726	34.726
339.990	340.000	1.4853	10.520	10.520	10.535	10.534	34.679	34.679
339.989	340.000	1.4852	10.518	10.517	10.534	10.534	34.681	34.682
339.999	340.000	0.70279	4.9863	4.9863	5.0014	5.0014	34.640	34.640
339.999	340.000	0.70278	4.9871	4.9871	5.0014	5.0013	34.653	34.653
355.001	355.000	29.962	181.20	181.20	181.22	181.22	37.243	37.243
355.002	355.000	29.962	181.20	181.20	181.22	181.22	37.279	37.279
355.002	355.000	26.229	160.98	160.98	161.01	161.01	36.976	36.976
355.002	355.000	26.228	160.98	160.98	161.01	161.01	36.988	36.988
355.001	355.000	22.515	140.26	140.26	140.29	140.29	36.737	36.737
355.001	355.000	22.514	140.25	140.25	140.28	140.28	36.749	36.749
354.995	355.000	18.965	119.85	119.85	119.88	119.88	36.471	36.471
354.995	355.000	18.964	119.85	119.84	119.88	119.87	36.476	36.476
355.008	355.000	15.746	100.81	100.82	100.85	100.85	36.287	36.286
355.008	355.000	15.746	100.81	100.81	100.84	100.84	36.301	36.301
355.000	355.000	13.974	90.130	90.130	90.151	90.151	36.209	36.209
355.000	355.000	13.973	90.125	90.125	90.145	90.145	36.216	36.216
355.005	355.000	12.351	80.178	80.179	80.210	80.211	36.126	36.126
355.004	355.000	12.350	80.174	80.175	80.206	80.207	36.122	36.122
355.005	355.000	10.786	70.466	70.467	70.496	70.497	36.051	36.051
355.006	355.000	10.784	70.461	70.462	70.488	70.490	36.040	36.039
355.004	355.000	9.1852	60.409	60.410	60.433	60.434	35.971	35.971
354.996	355.000	9.1819	60.389	60.389	60.413	60.413	35.960	35.960
355.005	355.000	7.6028	50.324	50.325	50.350	50.351	35.912	35.912
355.005	355.000	7.6022	50.324	50.325	50.347	50.347	35.918	35.917
355.000	355.000	6.0122	40.059	40.059	40.081	40.081	35.843	35.843
354.999	355.000	6.0121	40.061	40.061	40.080	40.080	35.843	35.843
355.004	355.000	4.4718	29.988	29.989	30.004	30.004	35.808	35.808
355.006	355.000	4.4711	29.985	29.986	29.999	29.999	35.800	35.800
354.998	355.000	2.9899	20.178	20.178	20.185	20.185	35.734	35.734
354.998	355.000	2.9898	20.178	20.178	20.185	20.185	35.744	35.744
354.996	355.000	1.4896	10.121	10.121	10.120	10.120	35.706	35.706
354.995	355.000	1.4895	10.121	10.121	10.120	10.120	35.703	35.703
354.998	355.000	0.74743	5.0954	5.0954	5.0938	5.0938	35.678	35.678

Table 15 (continued)

T K	T_n K	p MPa	ρ_{exp} kg·m^{-3}	ρ_{exp,T_n} kg·m^{-3}	ρ_{eos} kg·m^{-3}	ρ_{eos,T_n} kg·m^{-3}	η μPa·s	η_{T_n} μPa·s
354.997	355.000	0.74736	5.0969	5.0969	5.0933	5.0933	35.694	35.694
370.017	370.000	30.012	174.75	174.76	174.77	174.78	38.146	38.145
370.016	370.000	30.010	174.74	174.75	174.76	174.76	38.143	38.142
370.023	370.000	25.972	153.58	153.59	153.61	153.62	37.863	37.861
370.021	370.000	25.970	153.57	153.58	153.60	153.61	37.875	37.874
369.997	370.000	21.683	130.37	130.37	130.41	130.41	37.583	37.583
369.997	370.000	21.681	130.36	130.36	130.40	130.40	37.572	37.572
370.003	370.000	18.256	111.26	111.26	111.29	111.29	37.347	37.347
370.004	370.000	18.256	111.25	111.25	111.29	111.29	37.355	37.355
370.006	370.000	16.326	100.25	100.26	100.28	100.28	37.261	37.260
370.006	370.000	16.326	100.25	100.25	100.28	100.28	37.260	37.259
369.986	370.000	14.623	90.406	90.403	90.431	90.428	37.163	37.164
369.986	370.000	14.621	90.395	90.392	90.418	90.414	37.161	37.162
370.007	370.000	12.737	79.344	79.345	79.358	79.359	37.085	37.084
370.006	370.000	12.735	79.333	79.335	79.346	79.348	37.068	37.068
370.000	370.000	11.321	70.922	70.922	70.936	70.936	37.018	37.018
370.000	370.000	11.319	70.912	70.912	70.926	70.926	37.024	37.024
370.017	370.000	9.6193	60.670	60.673	60.681	60.684	36.942	36.941
370.016	370.000	9.6186	60.670	60.672	60.677	60.680	36.940	36.939
370.005	370.000	7.9231	50.322	50.323	50.324	50.325	36.875	36.874
370.004	370.000	7.9228	50.322	50.322	50.323	50.323	36.871	36.870
369.993	370.000	6.2960	40.249	40.249	40.254	40.254	36.813	36.813
369.993	370.000	6.2954	40.247	40.246	40.250	40.250	36.818	36.819
370.005	370.000	4.7062	30.283	30.284	30.282	30.283	36.778	36.778
370.005	370.000	4.7059	30.282	30.282	30.281	30.281	36.764	36.764
370.003	370.000	3.1083	20.138	20.139	20.131	20.131	36.736	36.736
370.003	370.000	3.1082	20.138	20.139	20.131	20.131	36.732	36.732
370.004	370.000	1.6120	10.508	10.508	10.504	10.504	36.703	36.703
370.004	370.000	1.6115	10.503	10.503	10.501	10.501	36.696	36.696
370.004	370.000	0.76571	5.0084	5.0084	5.0068	5.0068	36.667	36.666
370.004	370.000	0.76565	5.0076	5.0077	5.0064	5.0065	36.666	36.666
389.998	390.000	29.835	165.69	165.69	165.72	165.72	39.256	39.256
389.998	390.000	29.835	165.69	165.69	165.72	165.72	39.243	39.243
390.008	390.000	25.690	144.85	144.86	144.89	144.89	39.001	39.001
390.007	390.000	25.689	144.85	144.85	144.89	144.89	39.005	39.005
389.995	390.000	21.335	122.27	122.26	122.30	122.30	38.758	38.758
389.999	390.000	21.315	122.16	122.16	122.20	122.20	38.771	38.771
390.008	390.000	19.064	110.18	110.19	110.22	110.22	38.671	38.671
390.007	390.000	19.062	110.18	110.18	110.21	110.21	38.674	38.673
389.996	390.000	17.235	100.30	100.30	100.34	100.34	38.559	38.560
389.997	390.000	17.234	100.30	100.30	100.33	100.33	38.570	38.570

Table 15 (continued)

T K	T_n K	p MPa	ρ_{exp} kg·m^{-3}	ρ_{exp,T_n} kg·m^{-3}	ρ_{eos} kg·m^{-3}	ρ_{eos,T_n} kg·m^{-3}	η μPa·s	η_{T_n} μPa·s
389.997	390.000	15.480	90.691	90.691	90.723	90.722	38.486	38.486
389.999	390.000	15.480	90.691	90.691	90.722	90.722	38.466	38.467
390.000	390.000	13.581	80.144	80.144	80.174	80.174	38.404	38.404
389.999	390.000	13.580	80.142	80.142	80.169	80.169	38.416	38.416
390.001	390.000	11.811	70.162	70.163	70.200	70.200	38.310	38.310
390.000	390.000	11.811	70.158	70.158	70.197	70.198	38.313	38.313
390.008	390.000	10.066	60.198	60.199	60.230	60.231	38.258	38.258
390.008	390.000	10.065	60.196	60.197	60.220	60.221	38.257	38.257
389.996	390.000	8.2981	49.968	49.967	49.991	49.991	38.183	38.183
389.993	390.000	8.2968	49.967	49.966	49.984	49.983	38.178	38.178
390.009	390.000	6.6568	40.346	40.347	40.358	40.359	38.132	38.131
390.009	390.000	6.6566	40.343	40.344	40.357	40.357	38.116	38.116
389.997	390.000	4.9578	30.244	30.243	30.258	30.257	38.077	38.078
389.995	390.000	4.9575	30.244	30.244	30.256	30.256	38.066	38.067
390.007	390.000	3.2926	20.214	20.214	20.226	20.226	38.050	38.050
390.007	390.000	3.2925	20.216	20.216	20.225	20.225	38.044	38.044
390.000	390.000	1.5797	9.7606	9.7605	9.7693	9.7693	38.020	38.020
389.998	390.000	1.5795	9.7575	9.7575	9.7683	9.7682	38.001	38.001
389.995	390.000	0.83032	5.1384	5.1384	5.1502	5.1502	37.971	37.971
389.994	390.000	0.83009	5.1399	5.1399	5.1488	5.1488	37.990	37.990
409.999	410.000	30.209	160.06	160.06	160.09	160.09	40.517	40.517
409.998	410.000	30.208	160.06	160.06	160.09	160.09	40.531	40.532
409.999	410.000	26.583	142.66	142.66	142.70	142.70	40.295	40.295
409.997	410.000	26.583	142.66	142.66	142.70	142.70	40.311	40.311
410.006	410.000	22.453	122.28	122.28	122.32	122.32	40.068	40.068
410.007	410.000	22.452	122.28	122.28	122.31	122.31	40.041	40.041
410.000	410.000	18.410	101.74	101.74	101.77	101.77	39.836	39.836
409.999	410.000	18.409	101.74	101.74	101.77	101.77	39.820	39.820
409.998	410.000	16.339	90.987	90.987	91.005	91.004	39.721	39.721
409.996	410.000	16.339	90.982	90.981	91.005	91.004	39.714	39.714
409.997	410.000	14.543	81.518	81.517	81.535	81.535	39.645	39.645
409.995	410.000	14.542	81.513	81.512	81.530	81.529	39.650	39.650
410.004	410.000	12.569	70.972	70.973	70.980	70.981	39.552	39.551
410.004	410.000	12.566	70.951	70.952	70.962	70.963	39.545	39.545
409.995	410.000	10.777	61.244	61.243	61.265	61.264	39.494	39.494
409.994	410.000	10.777	61.245	61.244	61.263	61.262	39.504	39.504
410.000	410.000	8.7458	50.087	50.087	50.094	50.094	39.423	39.423
409.999	410.000	8.7423	50.067	50.067	50.075	50.074	39.428	39.428
410.003	410.000	7.1050	40.932	40.933	40.945	40.945	39.379	39.378
410.003	410.000	7.1041	40.928	40.928	40.940	40.940	39.384	39.384
410.006	410.000	5.3031	30.772	30.772	30.767	30.768	39.337	39.337

Table 15 (continued)

T K	T_n K	p MPa	ρ_{exp} kg·m^{-3}	ρ_{exp,T_n} kg·m^{-3}	ρ_{eos} kg·m^{-3}	ρ_{eos,T_n} kg·m^{-3}	η μPa·s	η_{T_n} μPa·s
410.007	410.000	5.3030	30.773	30.773	30.767	30.767	39.348	39.348
410.010	410.000	3.4871	20.382	20.383	20.370	20.370	39.285	39.284
410.010	410.000	3.4854	20.370	20.371	20.360	20.361	39.274	39.273
410.006	410.000	2.6639	15.621	15.621	15.610	15.610	39.286	39.286
410.007	410.000	2.6630	15.617	15.617	15.605	15.605	39.273	39.272
410.008	410.000	1.7712	10.428	10.428	10.414	10.414	39.245	39.244
410.008	410.000	1.7700	10.419	10.420	10.407	10.407	39.263	39.262
410.000	410.000	0.91489	5.3965	5.3965	5.3968	5.3968	39.204	39.204
410.000	410.000	0.91408	5.3919	5.3919	5.3921	5.3921	39.232	39.232
430.003	430.000	29.999	152.32	152.32	152.32	152.32	41.591	41.591
430.005	430.000	29.997	152.31	152.32	152.31	152.31	41.574	41.574
430.002	430.000	25.769	132.75	132.75	132.74	132.74	41.342	41.342
430.002	430.000	25.768	132.74	132.74	132.73	132.73	41.338	41.338
430.004	430.000	21.531	112.55	112.55	112.54	112.54	41.133	41.133
430.005	430.000	21.527	112.54	112.54	112.52	112.52	41.111	41.111
430.008	430.000	18.945	99.929	99.930	99.917	99.918	40.991	40.990
429.999	430.000	16.824	89.398	89.398	89.393	89.393	40.875	40.876
430.002	430.000	16.821	89.392	89.393	89.380	89.380	40.891	40.891
430.004	430.000	14.912	79.771	79.771	79.770	79.771	40.778	40.778
430.004	430.000	14.911	79.766	79.767	79.765	79.766	40.792	40.792
430.001	430.000	12.985	69.931	69.931	69.935	69.935	40.749	40.749
430.001	430.000	12.984	69.927	69.928	69.932	69.932	40.730	40.730
429.998	430.000	11.104	60.207	60.207	60.206	60.206	40.688	40.688
429.997	430.000	11.104	60.205	60.205	60.204	60.204	40.669	40.669
429.994	430.000	9.2000	50.229	50.228	50.223	50.222	40.609	40.609
429.994	430.000	9.1995	50.229	50.229	50.220	50.220	40.615	40.615
430.005	430.000	7.2786	40.018	40.019	40.008	40.008	40.577	40.576
430.005	430.000	7.2782	40.017	40.017	40.005	40.006	40.573	40.573
430.008	430.000	5.4898	30.386	30.386	30.370	30.371	40.522	40.521
430.007	430.000	5.4889	30.383	30.383	30.366	30.366	40.551	40.551
430.005	430.000	3.6952	20.579	20.579	20.576	20.576	40.484	40.484
430.004	430.000	3.6935	20.578	20.578	20.567	20.567	40.505	40.505
430.002	430.000	2.7141	15.170	15.170	15.167	15.167	40.481	40.481
430.002	430.000	2.7139	15.173	15.173	15.166	15.166	40.463	40.463
430.002	430.000	1.7809	10.010	10.011	9.9861	9.9861	40.480	40.480
430.002	430.000	1.7808	10.012	10.012	9.9855	9.9855	40.479	40.479
430.001	430.000	0.85013	4.8058	4.8059	4.7833	4.7833	40.481	40.481
430.004	430.000	0.84999	4.8058	4.8059	4.7825	4.7825	40.473	40.473
449.998	450.000	30.099	146.50	146.50	146.55	146.55	42.721	42.721
449.998	450.000	30.097	146.50	146.50	146.54	146.54	42.722	42.722
450.001	450.000	25.782	127.27	127.27	127.32	127.32	42.514	42.513

Table 15 (continued)

T K	T_n K	p MPa	ρ_{exp} kg·m^{-3}	ρ_{exp,T_n} kg·m^{-3}	ρ_{eos} kg·m^{-3}	ρ_{eos,T_n} kg·m^{-3}	η μPa·s	η_{T_n} μPa·s
450.004	450.000	25.781	127.26	127.27	127.31	127.31	42.515	42.515
450.004	450.000	21.521	107.74	107.74	107.79	107.79	42.349	42.349
450.004	450.000	21.520	107.74	107.74	107.78	107.79	42.351	42.351
450.003	450.000	19.839	99.883	99.884	99.929	99.929	42.282	42.282
450.003	450.000	19.839	99.882	99.883	99.928	99.929	42.285	42.285
450.000	450.000	17.769	90.086	90.086	90.126	90.126	42.202	42.202
450.008	450.000	17.769	90.081	90.082	90.123	90.125	42.216	42.215
450.005	450.000	15.665			80.020	80.021	42.061	42.061
450.006	450.000	15.664			80.015	80.016	42.085	42.085
450.007	450.000	13.627	70.056	70.057	70.094	70.095	42.058	42.058
450.008	450.000	13.626	70.051	70.052	70.088	70.089	42.099	42.099
449.997	450.000	11.615	60.117	60.117	60.158	60.157	41.911	41.911
450.001	450.000	11.610	60.085	60.085	60.130	60.130	41.924	41.924
449.995	450.000	9.6040	50.052	50.052	50.087	50.087	41.869	41.869
449.999	450.000	9.6027	50.052	50.052	50.080	50.080	41.848	41.849
450.005	450.000	7.6693	40.235	40.236	40.265	40.265	41.833	41.833
450.006	450.000	7.6688	40.232	40.232	40.262	40.263	41.840	41.840
450.001	450.000	5.6959	30.076	30.076	30.110	30.110	41.821	41.821
450.001	450.000	5.6956	30.074	30.074	30.109	30.109	41.818	41.818
450.008	450.000	3.7581	19.975	19.976	20.001	20.001	41.787	41.787
450.007	450.000	3.7578	19.972	19.972	19.999	20.000	41.796	41.796
450.005	450.000	2.8096	14.980	14.981	15.003	15.004	41.830	41.829
450.005	450.000	2.8095	14.979	14.979	15.003	15.003	41.814	41.814
449.998	450.000	0.93706			5.0371	5.0371	41.715	41.715
449.998	450.000	0.93696			5.0366	5.0365	41.760	41.760
449.997	450.000	0.93687			5.0361	5.0360	41.803	41.804

[a] Expanded uncertainty ($k = 2$) in temperature: $U(T) = 2.5$ mK, expanded relative ($k = 2$) uncertainty in pressure: $U_r(p) = 0.01$ % (at full scale of pressure transducers) to 0.05 % (at lower limit of pressure transducers), expanded relative ($k = 2$) uncertainty in density: $U_r(\rho) = 0.05$ %, and expanded relative uncertainty ($k = 2$) in viscosity: $U_r(\eta) = 0.24$ %

Table 16 Results of our $\eta\rho pT$ measurements for neon measured with sensor 2, where T is the measured temperature, T_n is the nominal temperature of the measured isotherm, p is the measured pressure, ρ_{exp} is the measured density at T and p, ρ_{exp,T_n} is the experimental density at T_n and p, ρ_{eos} is the density calculated with the TEOS at T and p, ρ_{eos,T_n} is the density calculated with the TEOS at T_n and p, η is the measured viscosity at T and p, and η_{T_n} is the experimental viscosity at T_n and p^a

T	T_n	p	ρ_{exp}	ρ_{exp,T_n}	ρ_{eos}	ρ_{eos,T_n}	η	η_{T_n}
K	K	MPa	kg·m^{-3}	kg·m^{-3}	kg·m^{-3}	kg·m^{-3}	μPa·s	μPa·s
299.999	300.000	29.859	210.53	210.52	210.55	210.55	34.035	34.035
299.999	300.000	29.857	210.52	210.52	210.54	210.54	34.025	34.025
300.003	300.000	26.643	190.59	190.59	190.63	190.63	33.730	33.730
300.003	300.000	26.643	190.58	190.59	190.63	190.63	33.747	33.747
300.000	300.000	23.543	170.80	170.80	170.85	170.85	33.467	33.467
300.000	300.000	23.542	170.80	170.80	170.84	170.84	33.452	33.452
300.003	300.000	20.537	151.04	151.05	151.10	151.10	33.164	33.164
300.003	300.000	20.536	151.04	151.04	151.10	151.10	33.187	33.187
300.003	300.000	17.539	130.78	130.78	130.83	130.83	32.914	32.914
300.003	300.000	17.538	130.78	130.78	130.83	130.83	32.929	32.929
300.003	300.000	14.553	110.02	110.02	110.06	110.07	32.693	32.693
300.003	300.000	14.552	110.02	110.02	110.06	110.06	32.684	32.684
300.001	300.000	11.897	91.041	91.042	91.087	91.087	32.473	32.473
300.001	300.000	11.896	91.033	91.033	91.081	91.081	32.491	32.491
299.999	300.000	10.408	80.193	80.193	80.237	80.237	32.382	32.382
299.999	300.000	10.407	80.190	80.189	80.231	80.231	32.368	32.369
300.000	300.000	9.0381	70.090	70.090	70.121	70.121	32.289	32.289
300.000	300.000	9.0374	70.086	70.086	70.116	70.116	32.312	32.312
299.998	300.000	7.7805	60.690	60.689	60.716	60.716	32.215	32.215
299.998	300.000	7.7802	60.687	60.686	60.714	60.713	32.189	32.190
299.995	300.000	6.3417	49.798	49.797	49.820	49.819	32.120	32.120
299.995	300.000	6.3413	49.796	49.795	49.816	49.815	32.115	32.115
299.997	300.000	5.0445	39.853	39.853	39.867	39.866	32.090	32.090
299.997	300.000	5.0440	39.850	39.849	39.863	39.862	32.079	32.079
299.997	300.000	3.8343	30.461	30.461	30.473	30.473	32.021	32.021
299.997	300.000	3.8340	30.459	30.458	30.470	30.470	32.021	32.021
299.994	300.000	2.5187	20.138	20.138	20.140	20.140	31.958	31.959
299.994	300.000	2.5184	20.136	20.135	20.138	20.137	31.972	31.972
299.997	300.000	1.9011	15.244	15.244	15.245	15.245	31.935	31.935
299.997	300.000	1.9000	15.247	15.246	15.236	15.236	31.936	31.936
299.995	300.000	1.3091	10.523	10.523	10.526	10.526	31.932	31.932
299.995	300.000	1.3088	10.522	10.521	10.525	10.524	31.914	31.914
299.997	300.000	0.64973	5.2363	5.2363	5.2405	5.2405	31.873	31.874
299.997	300.000	0.64953	5.2363	5.2363	5.2389	5.2388	31.881	31.881
309.996	310.000	29.864	204.41	204.41	204.40	204.40	34.629	34.629
309.996	310.000	29.863	204.40	204.40	204.40	204.39	34.623	34.623
309.994	310.000	26.239	182.48	182.48	182.49	182.49	34.301	34.301
309.994	310.000	26.238	182.48	182.48	182.49	182.48	34.286	34.287

Table 16 (continued)

T K	T_n K	p MPa	ρ_{exp} kg·m^{-3}	ρ_{exp,T_n} kg·m^{-3}	ρ_{eos} kg·m^{-3}	ρ_{eos,T_n} kg·m^{-3}	η μPa·s	η_{T_n} μPa·s
309.996	310.000	22.950	161.95	161.95	161.97	161.97	34.005	34.005
309.996	310.000	22.949	161.95	161.94	161.96	161.96	34.017	34.017
309.996	310.000	19.839	141.96	141.95	141.98	141.97	33.778	33.778
309.996	310.000	19.838	141.95	141.95	141.97	141.97	33.770	33.771
310.001	310.000	16.730	121.39	121.39	121.41	121.41	33.526	33.526
310.001	310.000	16.729	121.39	121.39	121.41	121.41	33.527	33.527
310.000	310.000	13.720	100.92	100.92	100.93	100.93	33.322	33.322
310.000	310.000	13.719	100.91	100.91	100.92	100.92	33.312	33.312
309.997	310.000	12.225	90.524	90.523	90.540	90.540	33.205	33.205
309.997	310.000	12.224	90.517	90.516	90.536	90.535	33.211	33.211
310.000	310.000	10.788	80.385	80.385	80.422	80.422	33.110	33.110
310.000	310.000	10.787	80.377	80.377	80.413	80.413	33.121	33.121
309.998	310.000	9.6114	72.001	72.001	72.032	72.032	33.040	33.040
309.997	310.000	9.6112	72.001	72.001	72.031	72.030	33.035	33.035
309.994	310.000	8.0165	60.487	60.486	60.515	60.514	32.924	32.924
309.994	310.000	8.0163	60.485	60.484	60.514	60.513	32.935	32.936
309.995	310.000	6.6948	50.833	50.832	50.842	50.841	32.859	32.860
309.995	310.000	6.6946	50.832	50.831	50.840	50.840	32.840	32.840
309.999	310.000	5.3100	40.560	40.560	40.579	40.579	32.781	32.781
309.999	310.000	5.3097	40.559	40.559	40.577	40.577	32.770	32.770
309.996	310.000	4.0276	30.949	30.949	30.959	30.959	32.728	32.728
309.996	310.000	4.0275	30.946	30.946	30.958	30.958	32.790	32.790
309.998	310.000	2.7059	20.920	20.919	20.925	20.925	32.667	32.667
309.998	310.000	2.7058	20.918	20.918	20.924	20.924	32.678	32.679
309.994	310.000	2.0038	15.542	15.542	15.545	15.545	32.659	32.660
309.994	310.000	2.0002	15.544	15.544	15.518	15.517	32.646	32.647
310.001	310.000	1.2910	10.044	10.044	10.048	10.048	32.623	32.623
310.001	310.000	1.2910	10.043	10.043	10.047	10.048	32.637	32.636
309.995	310.000	0.64554	5.0405	5.0404	5.0391	5.0390	32.597	32.597
309.995	310.000	0.64551	5.0382	5.0381	5.0389	5.0388	32.590	32.590
330.037	330.000	29.914	193.35	193.37	193.37	193.39	35.833	35.830
330.037	330.000	29.914	193.35	193.37	193.37	193.39	35.836	35.834
330.049	330.000	26.066	171.21	171.23	171.24	171.27	35.535	35.531
330.049	330.000	26.064	171.19	171.22	171.23	171.25	35.509	35.506
330.031	330.000	22.581	150.54	150.55	150.57	150.58	35.241	35.239
330.033	330.000	22.579	150.53	150.54	150.56	150.57	35.234	35.232
330.011	330.000	19.325	130.63	130.63	130.67	130.67	34.979	34.978
330.011	330.000	19.324	130.63	130.63	130.67	130.67	34.982	34.981
330.001	330.000	16.125	110.52	110.52	110.55	110.55	34.754	34.754
330.001	330.000	16.124	110.51	110.51	110.54	110.54	34.766	34.766
330.015	330.000	14.524	100.23	100.24	100.26	100.26	34.653	34.652

Table 16 (continued)

T K	T_n K	p MPa	ρ_{exp} kg·m^{-3}	ρ_{exp,T_n} kg·m^{-3}	ρ_{eos} kg·m^{-3}	ρ_{eos,T_n} kg·m^{-3}	η μPa·s	η_{T_n} μPa·s
330.015	330.000	14.524	100.23	100.23	100.26	100.26	34.668	34.667
330.009	330.000	13.016	90.409	90.411	90.439	90.441	34.564	34.563
330.009	330.000	13.016	90.409	90.411	90.434	90.437	34.582	34.581
330.001	330.000	11.518	80.524	80.524	80.549	80.549	34.477	34.477
329.999	330.000	11.518	80.526	80.526	80.549	80.549	34.483	34.483
330.002	330.000	10.006	70.397	70.397	70.435	70.436	34.388	34.388
330.009	330.000	10.003	70.389	70.391	70.416	70.417	34.399	34.399
329.997	330.000	8.5230	60.376	60.375	60.386	60.386	34.311	34.311
329.996	330.000	8.5227	60.379	60.378	60.385	60.384	34.316	34.317
330.003	330.000	7.1015	50.614	50.615	50.627	50.627	34.236	34.236
330.005	330.000	7.1005	50.611	50.612	50.619	50.620	34.235	34.235
329.997	330.000	5.6017	40.197	40.196	40.198	40.197	34.188	34.188
329.996	330.000	5.6017	40.200	40.199	40.197	40.197	34.177	34.177
330.008	330.000	4.1909	30.256	30.256	30.259	30.259	34.129	34.128
330.008	330.000	4.1909	30.256	30.256	30.259	30.259	34.135	34.135
329.999	330.000	2.7872	20.248	20.248	20.249	20.249	34.084	34.084
329.997	330.000	2.7871	20.246	20.246	20.248	20.248	34.074	34.074
330.002	330.000	1.3694	10.012	10.012	10.010	10.010	34.015	34.015
330.002	330.000	1.3692	10.010	10.010	10.009	10.009	34.023	34.023
330.007	330.000	0.69993	5.1334	5.1335	5.1316	5.1318	34.002	34.002
330.006	330.000	0.69989	5.1349	5.1350	5.1314	5.1315	33.986	33.986
340.021	340.000	30.026	188.79	188.80	188.82	188.83	36.432	36.431
340.021	340.000	30.025	188.79	188.80	188.81	188.82	36.425	36.424
340.021	340.000	26.803	170.76	170.77	170.80	170.81	36.163	36.162
340.021	340.000	26.800	170.75	170.75	170.78	170.79	36.156	36.154
340.012	340.000	23.318	150.71	150.72	150.76	150.76	35.899	35.898
340.011	340.000	23.317	150.71	150.71	150.75	150.76	35.886	35.885
340.013	340.000	19.871	130.29	130.29	130.34	130.34	35.647	35.646
340.013	340.000	19.871	130.29	130.29	130.33	130.34	35.642	35.641
339.997	340.000	16.606	110.38	110.38	110.43	110.43	35.396	35.396
339.997	340.000	16.606	110.38	110.38	110.43	110.43	35.390	35.391
340.007	340.000	15.002	100.40	100.40	100.44	100.44	35.307	35.306
340.009	340.000	15.002	100.40	100.40	100.44	100.44	35.316	35.315
339.999	340.000	13.386	90.195	90.195	90.231	90.231	35.209	35.209
339.999	340.000	13.385	90.191	90.191	90.226	90.226	35.214	35.214
340.004	340.000	11.818	80.154	80.155	80.191	80.192	35.127	35.127
340.005	340.000	11.818	80.154	80.155	80.190	80.191	35.125	35.125
339.994	340.000	10.361	70.711	70.710	70.745	70.744	35.034	35.034
339.994	340.000	10.361	70.710	70.709	70.743	70.741	35.041	35.041
340.001	340.000	8.7766	60.304	60.304	60.331	60.331	34.987	34.987
340.002	340.000	8.7765	60.305	60.305	60.330	60.331	34.979	34.979

Table 16 (continued)

T K	T_n K	p MPa	ρ_{exp} kg·m^{-3}	ρ_{exp,T_n} kg·m^{-3}	ρ_{eos} kg·m^{-3}	ρ_{eos,T_n} kg·m^{-3}	η μPa·s	η_{T_n} μPa·s
339.991	340.000	7.2943	50.395	50.394	50.461	50.459	34.892	34.893
339.996	340.000	7.2882	50.400	50.400	50.419	50.419	34.917	34.918
339.996	340.000	5.8191	40.496	40.496	40.510	40.510	34.874	34.874
339.996	340.000	5.8189	40.496	40.495	40.509	40.508	34.874	34.875
339.988	340.000	4.2768	29.956	29.955	29.971	29.970	34.811	34.812
339.989	340.000	4.2767	29.957	29.956	29.971	29.970	34.801	34.802
339.991	340.000	2.8927	20.382	20.381	20.393	20.392	34.748	34.748
339.991	340.000	2.8927	20.383	20.383	20.393	20.392	34.732	34.732
339.990	340.000	1.4853	10.518	10.518	10.535	10.534	34.702	34.703
339.990	340.000	1.4853	10.518	10.518	10.535	10.534	34.716	34.716
339.998	340.000	0.70278	4.9886	4.9886	5.0014	5.0014	34.665	34.665
339.998	340.000	0.70278	4.9856	4.9855	5.0014	5.0013	34.671	34.671
355.000	355.000	29.962	181.20	181.20	181.22	181.22	37.304	37.304
355.000	355.000	29.961	181.20	181.20	181.21	181.21	37.292	37.292
355.002	355.000	26.230	160.99	160.99	161.02	161.02	37.043	37.043
355.002	355.000	26.230	160.99	160.99	161.02	161.02	37.035	37.035
355.001	355.000	22.513	140.25	140.25	140.28	140.28	36.768	36.768
355.002	355.000	22.512	140.25	140.25	140.27	140.27	36.781	36.781
354.999	355.000	18.967	119.86	119.86	119.89	119.89	36.526	36.526
354.997	355.000	18.966	119.86	119.86	119.89	119.89	36.530	36.530
355.007	355.000	15.745	100.81	100.81	100.84	100.84	36.341	36.340
355.007	355.000	15.744	100.80	100.80	100.83	100.83	36.341	36.340
355.000	355.000	13.977	90.143	90.143	90.164	90.164	36.262	36.262
355.000	355.000	13.976	90.135	90.135	90.158	90.158	36.260	36.260
355.004	355.000	12.350	80.171	80.172	80.202	80.203	36.176	36.176
354.999	355.000	12.347	80.151	80.151	80.184	80.183	36.165	36.165
355.003	355.000	10.787	70.476	70.476	70.505	70.506	36.102	36.102
355.004	355.000	10.786	70.471	70.472	70.501	70.502	36.093	36.093
354.995	355.000	9.1811	60.385	60.384	60.409	60.408	36.018	36.019
354.994	355.000	9.1803	60.381	60.380	60.404	60.403	36.022	36.022
355.006	355.000	7.6038	50.331	50.332	50.357	50.358	35.944	35.943
355.006	355.000	7.6033	50.328	50.329	50.353	50.354	35.949	35.949
354.995	355.000	6.0119	40.058	40.058	40.079	40.079	35.891	35.891
354.995	355.000	6.0115	40.057	40.056	40.077	40.077	35.886	35.887
355.004	355.000	4.4722	29.990	29.990	30.006	30.006	35.818	35.817
355.004	355.000	4.4720	29.990	29.990	30.004	30.005	35.834	35.834
354.998	355.000	2.9897	20.178	20.178	20.184	20.184	35.779	35.779
354.998	355.000	2.9895	20.176	20.176	20.183	20.183	35.782	35.782
354.997	355.000	1.4897	10.121	10.121	10.121	10.121	35.731	35.731
354.996	355.000	1.4897	10.121	10.121	10.121	10.120	35.727	35.727
354.996	355.000	0.74726	5.0954	5.0954	5.0927	5.0926	35.702	35.703

Table 16 (continued)

T K	T_n K	p MPa	ρ_{exp} kg·m^{-3}	ρ_{exp,T_n} kg·m^{-3}	ρ_{eos} kg·m^{-3}	ρ_{eos,T_n} kg·m^{-3}	η μPa·s	η_{T_n} μPa·s
354.994	355.000	0.74708	5.0954	5.0953	5.0915	5.0914	35.714	35.715
370.012	370.000	30.007	174.73	174.73	174.75	174.75	38.183	38.182
370.012	370.000	30.005	174.72	174.72	174.74	174.74	38.171	38.170
370.016	370.000	25.976	153.60	153.61	153.64	153.64	37.909	37.907
370.016	370.000	25.974	153.60	153.60	153.63	153.63	37.889	37.888
369.996	370.000	21.673	130.31	130.31	130.36	130.35	37.604	37.604
369.996	370.000	21.672	130.31	130.31	130.35	130.35	37.624	37.624
370.004	370.000	18.257	111.26	111.26	111.29	111.29	37.411	37.410
370.007	370.000	18.257	111.25	111.26	111.29	111.29	37.409	37.409
370.003	370.000	16.326	100.26	100.26	100.28	100.28	37.291	37.290
370.001	370.000	16.326	100.26	100.26	100.28	100.28	37.286	37.286
369.991	370.000	14.629	90.447	90.445	90.465	90.463	37.204	37.205
369.986	370.000	14.626	90.428	90.425	90.450	90.447	37.198	37.199
370.001	370.000	12.733	79.320	79.321	79.333	79.333	37.103	37.102
370.000	370.000	12.731	79.311	79.311	79.325	79.325	37.105	37.105
370.003	370.000	11.328	70.964	70.965	70.977	70.978	37.038	37.038
370.002	370.000	11.325	70.951	70.951	70.959	70.960	37.033	37.033
370.014	370.000	9.6178	60.664	60.667	60.673	60.675	36.964	36.963
370.011	370.000	9.6175	60.664	60.666	60.671	60.673	36.969	36.968
370.007	370.000	7.9233	50.323	50.324	50.326	50.327	36.905	36.905
370.009	370.000	7.9233	50.322	50.324	50.325	50.327	36.905	36.904
369.994	370.000	6.2947	40.242	40.242	40.246	40.245	36.851	36.851
369.994	370.000	6.2942	40.240	40.240	40.243	40.242	36.848	36.848
370.004	370.000	4.7055	30.279	30.279	30.278	30.279	36.790	36.790
370.004	370.000	4.7051	30.273	30.274	30.276	30.276	36.787	36.786
370.002	370.000	3.1081	20.137	20.137	20.130	20.130	36.749	36.749
370.001	370.000	3.1079	20.137	20.137	20.128	20.128	36.756	36.756
370.003	370.000	1.6126	10.509	10.509	10.508	10.508	36.717	36.717
370.004	370.000	1.6123	10.507	10.507	10.506	10.506	36.719	36.718
370.004	370.000	0.76549	5.0053	5.0054	5.0054	5.0055	36.681	36.681
370.004	370.000	0.76544	5.0053	5.0054	5.0051	5.0051	36.685	36.684
390.003	390.000	29.836	165.69	165.70	165.72	165.72	39.291	39.291
389.999	390.000	29.836	165.69	165.69	165.72	165.72	39.291	39.291
390.004	390.000	25.687	144.84	144.84	144.88	144.88	39.041	39.041
390.004	390.000	25.686	144.84	144.84	144.87	144.87	39.025	39.024
389.999	390.000	21.337	122.27	122.27	122.31	122.31	38.779	38.780
389.997	390.000	21.336	122.27	122.27	122.31	122.31	38.802	38.802
390.002	390.000	19.061	110.17	110.17	110.20	110.20	38.690	38.690
389.999	390.000	19.059	110.16	110.16	110.20	110.20	38.691	38.691
389.994	390.000	17.235	100.31	100.31	100.34	100.34	38.554	38.554
389.996	390.000	17.235	100.31	100.30	100.34	100.34	38.530	38.531

Table 16 (continued)

T K	T_n K	p MPa	ρ_{exp} kg·m^{-3}	ρ_{exp,T_n} kg·m^{-3}	ρ_{eos} kg·m^{-3}	ρ_{eos,T_n} kg·m^{-3}	η μPa·s	η_{T_n} μPa·s
389.995	390.000	15.479	90.692	90.691	90.720	90.719	38.480	38.480
389.993	390.000	15.478	90.688	90.687	90.717	90.715	38.500	38.501
390.002	390.000	13.583	80.151	80.152	80.181	80.182	38.378	38.378
390.001	390.000	13.582	80.146	80.146	80.177	80.177	38.400	38.400
390.001	390.000	11.812	70.166	70.166	70.202	70.202	38.303	38.303
389.999	390.000	11.811	70.158	70.158	70.195	70.195	38.327	38.327
390.003	390.000	10.066	60.194	60.194	60.226	60.226	38.239	38.239
390.002	390.000	10.065	60.193	60.193	60.224	60.224	38.225	38.225
390.012	390.000	8.3022	49.994	49.995	50.013	50.015	38.141	38.140
390.013	390.000	8.3015	49.988	49.990	50.009	50.010	38.147	38.146
390.007	390.000	6.6563	40.339	40.340	40.355	40.356	38.097	38.097
390.004	390.000	6.6555	40.339	40.339	40.351	40.351	38.090	38.090
390.007	390.000	4.9583	30.248	30.248	30.260	30.261	38.034	38.034
390.001	390.000	4.9580	30.245	30.245	30.258	30.259	38.029	38.029
390.006	390.000	3.2922	20.213	20.214	20.224	20.224	38.018	38.018
390.005	390.000	3.2920	20.212	20.213	20.222	20.222	38.037	38.036
389.995	390.000	1.5791	9.7560	9.7559	9.7659	9.7658	38.004	38.004
389.993	390.000	1.5789	9.7545	9.7543	9.7644	9.7642	38.002	38.002
390.001	390.000	0.83058	5.1407	5.1407	5.1518	5.1518	37.984	37.984
389.998	390.000	0.83046	5.1415	5.1414	5.1511	5.1511	37.971	37.971
409.997	410.000	30.208	160.06	160.05	160.09	160.08	40.584	40.584
409.996	410.000	30.207	160.06	160.06	160.09	160.08	40.574	40.574
410.004	410.000	26.584	142.66	142.66	142.70	142.70	40.363	40.362
410.003	410.000	26.584	142.66	142.66	142.70	142.70	40.363	40.363
410.003	410.000	22.455	122.29	122.29	122.33	122.33	40.128	40.128
410.003	410.000	22.454	122.29	122.29	122.32	122.33	40.112	40.112
410.005	410.000	18.411	101.75	101.75	101.77	101.77	39.895	39.894
410.004	410.000	18.410	101.75	101.75	101.77	101.77	39.875	39.875
410.000	410.000	16.340	90.991	90.991	91.010	91.010	39.742	39.742
409.999	410.000	16.340	90.990	90.990	91.009	91.009	39.753	39.753
409.994	410.000	14.540	81.505	81.504	81.521	81.520	39.681	39.681
409.994	410.000	14.539	81.498	81.497	81.515	81.514	39.677	39.677
409.994	410.000	14.538	81.494	81.492	81.511	81.510	39.674	39.674
410.005	410.000	12.576	71.004	71.004	71.018	71.019	39.629	39.629
410.005	410.000	12.573	70.990	70.991	71.003	71.004	39.617	39.617
409.994	410.000	10.776	61.240	61.239	61.260	61.259	39.531	39.531
409.994	410.000	10.776	61.240	61.239	61.258	61.257	39.548	39.549
410.003	410.000	8.7523	50.118	50.118	50.129	50.129	39.478	39.478
410.001	410.000	8.7489	50.104	50.104	50.111	50.111	39.469	39.469
410.006	410.000	7.1014	40.916	40.916	40.924	40.925	39.407	39.407
410.006	410.000	7.1003	40.910	40.911	40.918	40.919	39.389	39.389

Table 16 (continued)

T K	T_n K	p MPa	ρ_{exp} kg·m^{-3}	ρ_{exp,T_n} kg·m^{-3}	ρ_{eos} kg·m^{-3}	ρ_{eos,T_n} kg·m^{-3}	η μPa·s	η_{T_n} μPa·s
410.006	410.000	5.3032	30.772	30.772	30.768	30.768	39.348	39.347
410.006	410.000	5.3031	30.771	30.772	30.768	30.768	39.355	39.355
410.009	410.000	3.4835	20.361	20.361	20.350	20.350	39.320	39.319
410.006	410.000	3.4817	20.351	20.351	20.339	20.339	39.321	39.321
410.005	410.000	2.6663	15.637	15.637	15.624	15.624	39.279	39.279
410.005	410.000	2.6647	15.628	15.628	15.615	15.615	39.301	39.300
410.006	410.000	1.7687	10.413	10.413	10.399	10.400	39.278	39.278
410.004	410.000	1.7676	10.409	10.409	10.393	10.393	39.279	39.279
410.001	410.000	0.91724	5.4102	5.4102	5.4106	5.4106	39.264	39.264
410.001	410.000	0.91646	5.4049	5.4049	5.4060	5.4060	39.248	39.248
430.000	430.000	30.002	152.34	152.34	152.33	152.33	41.685	41.685
429.996	430.000	30.001	152.34	152.33	152.33	152.33	41.673	41.673
430.003	430.000	25.757	132.68	132.68	132.68	132.69	41.415	41.415
430.006	430.000	25.756	132.68	132.68	132.68	132.68	41.420	41.419
430.005	430.000	21.536	112.58	112.58	112.57	112.57	41.184	41.184
430.005	430.000	21.534	112.57	112.57	112.56	112.56	41.198	41.198
430.007	430.000	18.943	99.920	99.922	99.909	99.910	41.037	41.036
430.006	430.000	18.942	99.914	99.915	99.903	99.905	41.074	41.073
429.997	430.000	16.830	89.428	89.427	89.423	89.422	40.964	40.964
429.998	430.000	16.827	89.418	89.418	89.412	89.411	40.969	40.969
430.005	430.000	14.910	79.754	79.755	79.756	79.757	40.875	40.875
430.005	430.000	14.909	79.754	79.755	79.754	79.755	40.857	40.857
430.002	430.000	12.987	69.940	69.941	69.947	69.948	40.784	40.783
430.001	430.000	12.986	69.939	69.939	69.942	69.942	40.777	40.777
429.996	430.000	11.103	60.200	60.200	60.199	60.198	40.721	40.721
429.996	430.000	11.102	60.199	60.198	60.197	60.196	40.713	40.713
429.995	430.000	9.2005	50.232	50.232	50.225	50.225	40.682	40.683
429.995	430.000	9.2002	50.232	50.231	50.224	50.223	40.666	40.666
430.007	430.000	7.2769	40.010	40.010	39.998	39.999	40.637	40.636
430.007	430.000	7.2766	40.009	40.010	39.997	39.997	40.625	40.625
430.009	430.000	5.4899	30.387	30.388	30.371	30.372	40.575	40.574
430.008	430.000	5.4899	30.386	30.386	30.371	30.371	40.578	40.577
430.003	430.000	3.6950	20.577	20.577	20.575	20.575	40.570	40.570
430.003	430.000	3.6944	20.577	20.577	20.572	20.572	40.559	40.558
430.001	430.000	2.7142	15.173	15.173	15.168	15.168	40.563	40.563
430.002	430.000	2.7142	15.174	15.174	15.168	15.168	40.565	40.564
429.993	430.000	1.7803	10.004	10.004	9.9832	9.9831	40.538	40.538
429.995	430.000	1.7803	10.005	10.005	9.9830	9.9829	40.550	40.551
429.999	430.000	0.85026	4.8081	4.8081	4.7840	4.7840	40.510	40.510
429.999	430.000	0.85018	4.8066	4.8066	4.7836	4.7836	40.503	40.503
449.996	450.000	30.096	146.50	146.49	146.54	146.54	42.766	42.766

Table 16 (continued)

T K	T_n K	p MPa	ρ_{exp} kg·m^{-3}	ρ_{exp,T_n} kg·m^{-3}	ρ_{eos} kg·m^{-3}	ρ_{eos,T_n} kg·m^{-3}	η μPa·s	η_{T_n} μPa·s
449.995	450.000	30.095	146.49	146.49	146.53	146.53	42.749	42.749
449.994	450.000	25.784	127.28	127.28	127.33	127.33	42.561	42.562
449.997	450.000	25.783	127.28	127.28	127.33	127.33	42.555	42.556
450.004	450.000	21.518	107.73	107.73	107.78	107.78	42.371	42.370
450.006	450.000	21.516	107.73	107.73	107.77	107.77	42.361	42.361
450.003	450.000	19.839	99.881	99.882	99.925	99.926	42.310	42.310
450.005	450.000	19.835	99.867	99.868	99.910	99.911	42.315	42.314
450.011	450.000	17.769	90.079	90.082	90.122	90.124	42.211	42.211
450.013	450.000	17.768	90.077	90.080	90.119	90.121	42.223	42.222
449.998	450.000	15.669			80.040	80.039	42.142	42.142
449.999	450.000	15.668			80.036	80.035	42.154	42.154
450.006	450.000	13.630	70.067	70.068	70.109	70.110	42.070	42.070
450.006	450.000	13.630	70.066	70.067	70.108	70.109	42.085	42.084
450.004	450.000	11.615	60.096	60.096	60.158	60.159	42.013	42.012
450.005	450.000	11.615	60.115	60.115	60.157	60.157	42.022	42.022
450.005	450.000	9.6029	50.035	50.036	50.081	50.081	41.924	41.924
450.002	450.000	9.6004	50.032	50.033	50.068	50.068	41.940	41.940
450.003	450.000	7.6681	40.230	40.230	40.259	40.259	41.899	41.899
449.998	450.000	7.6661	40.219	40.219	40.249	40.249	41.881	41.881
450.003	450.000	5.6973	30.083	30.083	30.117	30.118	41.824	41.824
450.000	450.000	5.6963	30.079	30.079	30.113	30.113	41.797	41.797
450.006	450.000	3.7576	19.968	19.969	19.999	19.999	41.766	41.765
450.003	450.000	3.7575	19.970	19.970	19.998	19.998	41.801	41.801
450.001	450.000	2.8098			15.005	15.005	41.807	41.807
450.004	450.000	2.8094			15.002	15.002	41.785	41.785
450.004	450.000	1.8754			10.047	10.047	41.753	41.753
450.002	450.000	1.8753			10.047	10.047	41.752	41.752
450.000	450.000	0.93723			5.0380	5.0380	41.717	41.717
449.999	450.000	0.93717			5.0377	5.0377	41.754	41.754

[a] Expanded uncertainty ($k = 2$) in temperature: $U(T) = 2.5$ mK, expanded relative ($k = 2$) uncertainty in pressure: $U_r(p) = 0.01$ % (at full scale of pressure transducers) to 0.05 % (at lower limit of pressure transducers), expanded relative ($k = 2$) uncertainty in density: $U_r(\rho) = 0.05$ %, and expanded relative uncertainty ($k = 2$) in viscosity: $U_r(\eta) = 0.24$ %

Acknowledgements We thank Dr. Arno Laesecke for his support in translating Russian literature sources and for more than three decades of collaboration. Dr. Marcia Huber and Prof. Marc Assael read preliminary versions of the manuscript and made valuable suggestions.

Author Contributions Ulrike Kochan-Eilers: data curation, formal analysis, investigation, visualization, writing—original draft. Ruben Harten: formal analysis, investigation. Eckhard Vogel: data curation, formal analysis, investigation, writing—original draft, editing and reviewing. Karsten Meier: data curation, supervision, visualization, writing—original draft, editing and reviewing.

Funding Open Access funding enabled and organized by Projekt DEAL. This research was partially funded by dtec.bw—Digitalization and Technology Research Center of the Bundeswehr in the project H2MIXPROP. dtec.bw is funded by the European Union—NextGenerationEU.

Data Availability The authors declare that the data supporting the findings of this study are available within the paper.

Declarations

Conflict of interest The authors have no conflict of interest to declare that are relevant to the content of this article.

Open Access This article is licensed under a Creative Commons Attribution 4.0 International License, which permits use, sharing, adaptation, distribution and reproduction in any medium or format, as long as you give appropriate credit to the original author(s) and the source, provide a link to the Creative Commons licence, and indicate if changes were made. The images or other third party material in this article are included in the article's Creative Commons licence, unless indicated otherwise in a credit line to the material. If material is not included in the article's Creative Commons licence and your intended use is not permitted by statutory regulation or exceeds the permitted use, you will need to obtain permission directly from the copyright holder. To view a copy of this licence, visit http://creativecommons.org/licenses/by/4.0/.

References

1. M.R. Moldover, R.M. Gavioso, J.B. Mehl, L. Pitre, M. de Podesta, J.T. Zhang, Acoustic gas thermometry. Metrologia **51**, R1–R19 (2014). https://doi.org/10.1088/0026-1394/51/1/R1
2. C. Gaiser, T. Zandt, B. Fellmuth, Dielectric-constant gas thermometry. Metrologia **52**, S217–S226 (2015). https://doi.org/10.1088/0026-1394/52/5/S217
3. P.M.C. Rourke, C. Gaiser, B. Gao, D. Madonna Ripa, M.R. Moldover, L. Pitre, R.J. Underwood, Refractive-index gas thermometry. Metrologia **56**, 032001 (2019). https://doi.org/10.1088/1681-7575/ab0dbe
4. P.M.C. Rourke, Perspective on the refractive-index gas metrology data landscape. J. Phys. Chem. Ref. Data **50**, 033104 (2021). https://doi.org/10.1063/5.0055412
5. S.Z.S. Al Ghafri, S. Munro, U. Cardella, T. Funke, W. Notardonato, J.P.M. Trusler, J. Leachman, R. Span, S. Kamiya, G. Pearce, A. Swanger, E. Dorador Rodriguez, P. Bajada, F. Jiao, K. Peng, A. Siahvashi, M.L. Johns, E.F. May, Hydrogen liquefaction: a review of the fundamental physics, engineering practice and future opportunities. Energy Environ. Sci. **15**, 2690–2731 (2022). https://doi.org/10.1039/d2ee00099g
6. E. Vogel, Präzisionsmessungen des Viskositätskoeffizienten von Stickstoff und den Edelgasen zwischen Raumtemperatur und 650 K. Ber. Bunsenges. Phys. Chem. **88**, 997–1002 (1984). https://doi.org/10.1002/bbpc.19840881014
7. R. Hellmann, C. Gaiser, B. Fellmuth, T. Vasyltsova, E. Bich, Thermophysical properties of low-density neon gas from highly accurate first-principles calculations and dielectric constant gas thermometry measurements. J. Chem. Phys. **154**, 164304 (2021). https://doi.org/10.1063/5.0047999
8. J. Wilhelm, Entwicklung eines Viskosimeters mit schwingendem Draht für Untersuchungen an Gasen in größeren Temperatur- und Dichtebereichen—Messungen an Argon, Krypton und Propan. Dissertation, Universität Rostock, Rostock (1998)
9. J. Wilhelm, E. Vogel, J.K. Lehmann, W.A. Wakeham, A vibrating-wire viscometer for dilute and dense gases. Int. J. Thermophys. **19**, 391–401 (1998). https://doi.org/10.1023/A:1022505209226
10. J. Wilhelm, E. Vogel, Viscosity measurements on gaseous argon, krypton, and propane. Int. J. Thermophys. **21**, 301–318 (2000). https://doi.org/10.1023/A:1006667125801
11. J. Wilhelm, E. Vogel, Viscosity measurements on gaseous propane. J. Chem. Eng. Data **46**, 1467–1471 (2001). https://doi.org/10.1021/je010062k

12. J. Wilhelm, D. Seibt, E. Bich, E. Vogel, E. Hassel, Viscosity measurements on gaseous sulfur hexafluoride. J. Chem. Eng. Data **50**, 896–906 (2005). https://doi.org/10.1021/je049612f
13. D. Seibt, Schwingdrahtviskosimeter mit integriertem Ein-Senkkörper-Dichtemessverfahren für Untersuchungen an Gasen in größeren Temperatur- und Druckbereichen. Fortschr.-Ber. VDI, Reihe 6, Nr. 571 (2008)
14. D. Seibt, S. Herrmann, E. Vogel, E. Bich, E. Hassel, Simultaneous measurements on helium and nitrogen with a newly designed viscometer-densimeter over a wide range of temperature and pressure. J. Chem. Eng. Data **54**, 2626–2637 (2009). https://doi.org/10.1021/je900131q
15. D. Seibt, K. Voß, S. Herrmann, E. Vogel, E. Hassel, Simultaneous viscosity-density measurements on ethane and propane over a wide range of temperature and pressure including the near-critical region. J. Chem. Eng. Data **56**, 1476–1493 (2011). https://doi.org/10.1021/je101178u
16. S. Herrmann, Viskositäts- und Dichtemessungen an *n*-Butan und Isobutan in größeren Temperatur- und Druckbereichen. Fortschr.-Ber. VDI, Reihe 6, Nr. 615 (2015)
17. S. Herrmann, E. Vogel, Viscosity and density of normal butane simultaneously measured at temperatures from (298 to 448) K and at pressures up to 30 MPa incorporating the near-critical region. J. Chem. Eng. Data **60**, 3703–3720 (2015). https://doi.org/10.1021/acs.jced.5b00654
18. S. Herrmann, E. Hassel, E. Vogel, Viscosity and density of isobutane measured in wide ranges of temperature and pressure including the near-critical region. AIChE J. **61**, 3116–3137 (2015). https://doi.org/10.1002/aic.14759
19. T. Retsina, S.M. Richardson, W.A. Wakeham, The theory of a vibrating-rod densimeter. Appl. Sci. Res. **43**, 127–158 (1986). https://doi.org/10.1007/BF00386040
20. T. Retsina, S.M. Richardson, W.A. Wakeham, The theory of a vibrating-rod viscometer. Appl. Sci. Res. **43**, 325–346 (1987). https://doi.org/10.1007/BF00540567
21. K. Brachthäuser, R. Kleinrahm, H.W. Lösch, W. Wagner, Entwicklung eines neuen Dichtemeßverfahrens und Aufbau einer Hochtemperatur-Hochdruck-Dichtemeßanlage, Fortschr.-Ber. VDI, Reihe 8, Nr. 371 (1993)
22. H. Watanabe, N. Yamada, M. Okaji, Linear thermal expansion coefficient of silicon from 293 to 1000 K. Int. J. Thermophys. **25**, 221–236 (2004). https://doi.org/10.1023/B:IJOT.0000022336.83719.43
23. J.J. Hall, Electronic effects in the elastic constants of *n*-type silicon. Phys. Rev. **161**, 756–761 (1967). https://doi.org/10.1103/PhysRev.161.756
24. G. Schilling, Vermessung der thermischen Zustandsgrößen von *n*-Heptan, *n*-Nonan, 2,4-Dichlortoluol und Brombenzol im Flüssigkeitsgebiet bei Temperaturen von 233,15 K bis 473,15 K und Drücken bis 30 MPa zum Einsatz als Referenzflüssigkeiten für Biegeschwinger-Dichtemessgeräte. Dissertation, Ruhr-Universität Bochum, Bochum, Germany (2006)
25. Deutsches Institut für Normung e.V., DIN EN 10088-1 Nichtrostende Stähle – Teil 1: Verzeichnis der nichtrostenden Stähle; Deutsche Fassung EN 10088-1:2005 (Beuth Verlag, Berlin, 2005). https://www.dinmedia.de/de/norm/din-en-10088-1/65991201
26. Gruppo Lucefin, Technical card, material X6CrNiTi18-10. Gruppo Lucefin, Esine, Italy, 2015. https://www.lucefin.com/wp-content/files_mf/1.4541en.pdf
27. W. Cencek, M. Przybytek, J. Komasa, J.B. Mehl, B. Jeziorski, K. Szalewicz, Effects of adiabatic, relativistic, and quantum electrodynamics interactions on the pair potential and thermophysical properties of helium. J. Chem. Phys. **136**, 224303 (2012). https://doi.org/10.1063/1.4712218
28. D.O. Ortiz Vega, K.R. Hall, J.C. Holste, A.H. Harvey, E.W. Lemmon, An equation of state for the thermodynamic properties of helium. NIST Internal Report 8474. U.S. Department of Commerce, National Institute of Standards and Technology (Gaithersburg, 2023). https://doi.org/10.6028/NIST.IR.8474
29. V.D. Arp, R.D. McCarty, D.G. Friend, Thermophysical properties of helium-4 from 0.8 to 1500 K with pressures to 2000 MPa. NIST Technical Note 1334 (revised). U.S. Department of Commerce, National Institute of Standards and Technology (Washington, DC, 1998). https://doi.org/10.6028/nist.tn.1334
30. J.C. Rainwater, On the phase space subdivision of the second virial coefficient and its consequences for kinetic theory. J. Chem. Phys. **81**, 495–510 (1984). https://doi.org/10.1063/1.447332
31. D.G. Friend, J.C. Rainwater, Transport properties of a moderately dense gas. Chem. Phys. Lett. **107**, 590–594 (1984). https://doi.org/10.1016/S0009-2614(84)85163-5
32. J.C. Rainwater, D.G. Friend, Second viscosity and thermal-conductivity virial coefficients of gases: extension to low reduced temperature. Phys. Rev. A **36**, 4062–4066 (1987). https://doi.org/10.1103/PhysRevA.36.4062

33. E. Bich, E. Vogel, The initial density dependence of transport properties: noble gases. Int. J. Thermophys. **12**, 27–42 (1991). https://doi.org/10.1007/BF00506120
34. BIPM, IEC, IFCC, ILAC, ISO, IUPAC, IUPAP, OIML, Evaluation of measurement data—Supplement 1 to the guide to the expression of uncertainty in measurement—Propagation of distributions using a Monte Carlo method," Technical Report No. JCGM 101:2008, Joint Committee for Guides in Metrology, Sèvres, France, (2008). https://doi.org/10.59161/JCGM101-2008
35. M.L. Huber, R.A. Perkins, E.W. Lemmon, Reference correlation for the viscosity of nitrogen from the triple point to 1000 K and pressures up to 2200 MPa. Int. J. Thermophys. **45**, 146 (2024). https://doi.org/10.1007/s10765-024-03440-1
36. M.L. Huber, Models for the viscosity, thermal conductivity, and surface tension of selected pure fluids as implemented in REFPROP v10.0, NISTIR 8209, U.S. Department of Commerce, National Institute of Standards and Technology (2018). https://doi.org/10.6028/NIST.IR.8209
37. A. Docter, H.W. Lösch, W. Wagner, Entwicklung und Aufbau einer Anlage zur simultanen Messung der Viskosität und der Dichte fluider Stoffe, Fortschr.-Ber. VDI, Reihe 3, Nr. 494 (1997)
38. M.O. McLinden, C. Lösch-Will, Apparatus for wide-ranging, high-accuracy fluid (p,ρ,T) measurements based on a compact two-sinker densimeter. J. Chem. Thermodyn. **39**, 507–530 (2007). https://doi.org/10.1016/j.jct.2006.09.012
39. R. Kleinrahm, X. Yang, M.O. McLinden, M. Richter, Analysis of the systematic force-transmission error of the magnetic-suspension coupling in single-sinker densimeters and commercial gravimetric sorption analyzers. Adsorption **25**, 717–735 (2019). https://doi.org/10.1007/s10450-019-00071-z
40. R. Span, E.W. Lemmon, R.T. Jacobsen, W. Wagner, A. Yokozeki, A reference equation of state for the thermodynamic properties of nitrogen for temperatures from 63.151 to 1000 K and pressures to 2200 MPa. J. Phys. Chem. Ref. Data **29**, 1361–1433 (2000). https://doi.org/10.1063/1.1349047
41. M. Thol, R. Beckmüller, R. Weiss, A.H. Harvey, E.W. Lemmon, R.T. Jacobsen, R. Span, Thermodynamic properties for neon for temperatures from the triple point to 700 K at pressures to 700 MPa, implemented in the NIST Standard Reference Database 23, Reference Fluid Thermodynamic and Transport Properties Database (2018), (REFPROP Version 10.0))
42. E.W. Lemmon, I.H. Bell, M.L. Huber, M.O. McLinden, NIST Standard Reference Database 23: Reference Fluid Thermodynamic and Transport Properties Database (REFPROP Version 10.0), Standard Reference Data Program, National Institute of Standards and Technology, Gaithersburg, 2018. https://doi.org/10.18434/T4/1502528
43. C. Evers, H.W. Lösch, W. Wagner, An absolute viscometer-densimeter and measurements of the viscosity of nitrogen, methane, helium, neon, argon, and krypton over a wide range of density and temperature. Int. J. Thermophys. **23**, 1411–1439 (2002). https://doi.org/10.1023/A:1020784330515
44. T. El Hawary, Messung der Dichte und Viskosität in der Gasphase von Methan, Stickstoff und Methan-Stickstoff-Gemischen mit einer weiterentwickelten kombinierten Viskositäts-Dichte-Messanlage und einer neuen Viskositätsmessanlage für geringe Gasdichten.Dissertation, Ruhr-Universität Bochum, Bochum (2009). https://nbn-resolving.org/urn:nbn:de:hbz:294-26662
45. N. Pieperbeck, R. Kleinrahm, W. Wagner, M. Jaeschke, Results of (pressure, density, temperature) measurements on methane and on nitrogen in the temperature range from 273.15 K to 323.15 K at pressures up to 12 MPa using a new apparatus for accurate gas-density measurements. J. Chem. Thermodyn. **23**, 175–194 (1991). https://doi.org/10.1016/S0021-9614(05)80295-2
46. W. Duschek, R. Kleinrahm, W. Wagner, M. Jaeschke, Measurement and correlation of the (pressure, density, temperature) relation of nitrogen in the temperature range from 273.15 K to 323.15 K at pressures up to 8 MPa. J. Chem. Thermodyn. **20**, 1069–1077 (1988). https://doi.org/10.1016/0021-9614(88)90113-9
47. D. Seibt, E. Vogel, E. Bich, D. Buttig, E. Hassel, Viscosity measurements on nitrogen. J. Chem. Eng. Data **51**, 526–533 (2006). https://doi.org/10.1021/je050399c
48. J.A. Gracki, G.P. Flynn, J. Ross, Viscosity of nitrogen, helium, hydrogen, and argon from −100 to 25° C up to 150–250 atm. J. Chem. Phys. **51**, 3856–3863 (1969). https://doi.org/10.1063/1.1672602
49. J. Kestin, W. Leidenfrost, An absolute determination of the viscosity of eleven gases over a range of pressures. Physica **25**, 1033–1062 (1959). https://doi.org/10.1016/0031-8914(59)90024-2
50. R.F. Berg, M.R. Moldover, Recommended viscosities of 11 dilute gases at 25 °C. J. Phys. Chem. Ref. Data **41**, 043104 (2012). https://doi.org/10.1063/1.4765368
51. R. Hellmann, E. Bich, E. Vogel, V. Vesovic, Intermolecular potential energy surface and thermophysical properties of the CH_4-N_2 system. J. Chem. Phys. **141**, 224301 (2014). https://doi.org/10.1063/1.4902807

52. A.O. Rankine, On the viscosities of the gases of the argon group. Proc. R. Soc. A **83**, 516–525 (1910). https://doi.org/10.1098/rspa.1910.0040
53. R.S. Edwards, The effect of temperature on the viscosity of neon. Proc. R. Soc. A **119**, 578–590 (1928). https://doi.org/10.1098/rspa.1928.0115
54. M. Trautz, K.F. Kipphan, Die Reibung, Wärmeleitung und Diffusion in Gasmischungen. IV. Die Reibung binärer und ternärer Edelgasgemische. Ann. Phys **394**, 743–748 (1929). https://doi.org/10.1002/andp.19293940610
55. M. Trautz, R. Zink, Die Reibung, Wärmeleitung und Diffusion in Gasmischungen. XII. Gasreibung bei höheren Temperaturen. Ann. Phys **399**, 427–452 (1930). https://doi.org/10.1002/andp.19303990405
56. M. Trautz, H.E. Binkele, Die Reibung, Wärmeleitung und Diffusion in Gasmischungen. VIII. Die Reibung des H_2, He, Ne, Ar und ihrer binären Gemische. Ann. Phys **397**, 561–580 (1930). https://doi.org/10.1002/andp.19303970503
57. M. Trautz, H. Zimmermann, Die Reibung, Wärmeleitung und Diffusion in Gasmischungen. XXX. Die innere Reibung bei tiefen Temperaturen von Wasserstoff, Helium und Neon und binären Gemischen davon bis 90,0° abs. herab. Ann. Phys. **414**, 189–194 (1935). https://doi.org/10.1002/andp.19354140206
58. A. van Itterbeek, O. van Paemel, Measurements on the viscosity of neon, hydrogen, deuterium and helium as a function of the temperature, between room temperature and liquid hydrogen temperatures. Physica **7**, 265–272 (1940). https://doi.org/10.1016/S0031-8914(40)90115-X
59. R. Wobser, F. Müller, Die innere Reibung von Gasen und Dämpfen und ihre Messung im Höppler-Viskosimeter. Kolloid-Beihefte **52**, 165–276 (1941). https://doi.org/10.1007/BF02564872
60. H.L. Johnston, E.R. Grilly, Viscosities of carbon monoxide, helium, neon, and argon between 80° and 300°K. Coefficients of viscosity. J. Phys. Chem. **46**, 948–963 (1942). https://doi.org/10.1021/j150422a019
61. J.M.J. Coremans, A. van Itterbeek, J.J.M. Beenakker, H.F.P. Knaap, P. Zandbergen, The viscosity of gaseous He, Ne, H_2 and D_2 below 80°K. Physica **24**, 557–576 (1958). https://doi.org/10.1016/S0031-8914(58)80070-1
62. E. Thornton, Viscosity and thermal conductivity of binary gas mixtures: krypton-argon, krypton-neon, and krypton-helium. Proc. Phys. Soc. **77**, 1166–1169 (1961). https://doi.org/10.1088/0370-1328/77/6/309
63. R. DiPippo, J. Kestin, K. Oguchi, Viscosity of three binary gaseous mixtures. J. Chem. Phys. **46**, 4758–4764 (1967). https://doi.org/10.1063/1.1840632
64. R. DiPippo, J. Kestin, The viscosity of seven gases up to 500 °C and its statistical interpretation, in *Proceedings of the 4th Symposium on Thermophysical Properties*. Ed. by J.R. Moszynski (American Society of Mechanical Engineers, College Park, 1968), pp. 304–313
65. A.G. Clarke, E.B. Smith, Low-temperature viscosities and intermolecular forces of simple gases. J. Chem. Phys. **51**, 4156–4161 (1969). https://doi.org/10.1063/1.1672640
66. R.A. Dawe, E.B. Smith, Viscosities of the inert gases at high temperatures. J. Chem. Phys. **52**, 693–703 (1970). https://doi.org/10.1063/1.1673042
67. J. Kestin, W. Wakeham, K. Watanabe, Viscosity, thermal conductivity, and diffusion coefficient of Ar-Ne and Ar-Kr gaseous mixtures in the temperature range 25–700° C. J. Chem. Phys. **53**, 3773–3780 (1970). https://doi.org/10.1063/1.1673840
68. S.F. Borisov, B.A. Kalinin, P.E. Suetin, Measuring the viscosity of gases by the transient-flow method. J. Eng. Phys. **24**, 49–51 (1973). https://doi.org/10.1007/BF00827333
69. J. Kestin, H.E. Khalifa, S.T. Ro, W.A. Wakeham, The viscosity and diffusion coefficient of eighteen binary gaseous systems. Physica A **88**, 242–260 (1977). https://doi.org/10.1016/0378-4371(77)90003-6
70. F.A. Guevara, G. Stensland, High temperature viscosity ratios for neon. Phys. Fluids **14**, 746–748 (1971). https://doi.org/10.1063/1.1693497
71. J. Kestin, S.T. Ro, W.A. Wakeham, Viscosity of the binary gaseous mixtures He-Ne and Ne-N_2 in the temperature range 25–700° C. J. Chem. Phys. **56**, 5837–5842 (1972). https://doi.org/10.1063/1.1677125
72. N.J. Trappeniers, A. Botzen, H.R. van den Berg, A. van Oosten, The viscosity of neon between 25°C and 75°C at pressures up to 1800 atmospheres. Corresponding states for the viscosity of the noble gases up to high densities. Physica **30**, 985–996 (1964). https://doi.org/10.1016/0031-8914(64)90231-9

73. E.G. Reynes, G. Thodos, Viscosity of helium, neon, and nitrogen in the dense gaseous region. J. Chem. Eng. Data **11**, 137–140 (1966). https://doi.org/10.1021/je60029a001
74. J. Kestin, J.H. Whitelaw, A relative determination of the viscosity of several gases by the oscillating disc method. Physica **29**, 335–356 (1963). https://doi.org/10.1016/S0031-8914(63)80294-3
75. K. Humberg, M. Richter, Viscosity measurements of krypton at temperatures from (253.15 to 473.15) K with pressures up to 2 MPa. Ind. Eng. Chem. Res **58**, 8878–8885 (2019). https://doi.org/10.1021/acs.iecr.9b01533
76. K. Humberg, Viscosity measurements of binary gas mixtures and analysis of approaches for the modeling of mixture viscosities. Dissertation, Fakultät für Maschinenbau, Ruhr-Universität Bochum, Bochum (2020). https://doi.org/10.13154/294-7710
77. V.P. Slusar, N.S. Rudenko, V.M. Tret'yakov, Experimental study of the viscosity of simple substances along the saturation line and under pressure. III. Neon. Ukr. Fiz. Zh. **18**, 190–194 (1973)
78. W. Herreman, W. Grevendonk, An experimental study on the shear viscosity of liquid neon. Cryogenics **14**, 395–398 (1974). https://doi.org/10.1016/0011-2275(74)90081-2
79. F. Huth, The viscosity of liquid neon. Cryogenics **2**, 368 (1962). https://doi.org/10.1016/0011-2275(62)90085-1
80. S. Förster, Viscosity measurements in liquid neon, argon, and nitrogen. Cryogenics **3**, 176–177 (1963). https://doi.org/10.1016/0011-2275(63)90012-2
81. L. Bewilogua, A. Handstein, H. Hoeger, Measurements on liquid neon. Cryogenics **6**, 21–24 (1966). https://doi.org/10.1016/S0011-2275(96)90057-0
82. P.A.W. Bratby, E.A. Harris, The viscosity of liquid neon isotopes. Phys. Lett. A **40**, 25–26 (1972). https://doi.org/10.1016/0375-9601(72)90182-X
83. G.P. Flynn, R.V. Hanks, N.A. Lemaire, J. Ross, Viscosity of nitrogen, helium, neon, and argon from −78.5° to 100° C below 200 atmospheres. J. Chem. Phys. **38**, 154–162 (1963). https://doi.org/10.1063/1.1733455
84. J. Kestin, A. Nagashima, Viscosity of neon-helium and neon-argon mixtures at 20° and 30°C. J. Chem. Phys. **40**, 3648–3654 (1964). https://doi.org/10.1063/1.1725066
85. A. Michels, R.O. Gibson, Isothermenmessungen bei höheren Drücken. Ann. Phys. **392**, 850–876 (1928). https://doi.org/10.1002/andp.19283922205
86. A. Michels, T. Wassenaar, P. Louwerse, Isotherms of neon at temperatures between 0° C and 150° C and at densities up to 1100 amagat (pressures up to 2900 atmospheres). Physica **26**, 539–543 (1960). https://doi.org/10.1016/0031-8914(60)90106-3
87. V.A. Rabinovich, L.A. Tokina, V.M. Berezin, Experimental determination of the compressibility of neon and argon at 300 to 720 °K for pressures up to 500 bar. Teplofiz. Vys. Temp. **8**, 745–749 (1970)
88. W.F. Vogl, K.R. Hall, Compressibility data and virial coefficients for helium, neon and one mixture. Physica **59**, 529–535 (1972). https://doi.org/10.1016/0031-8914(72)90204-2
89. C. Gladun, Some thermodynamic investigations into liquid neon isotope mixtures. Cryogenics **7**, 78–80 (1967). https://doi.org/10.1016/S0011-2275(67)80032-8
90. L.R. Scott, Density measurements for neon at low temperatures. Ph.D. Thesis, Univesity of Michigan, Ann Arbor (1967)
91. R.M. Gibbons, The equation of state of neon between 27 and 70 K. Cryogenics **9**, 251–260 (1969). https://doi.org/10.1016/0011-2275(69)90231-8
92. H. Lippold, Isothermal compressibility and density of liquid argon and neon up to pressures of 1000 kg/cm^2. Cryogenics **9**, 112–114 (1969). https://doi.org/10.1016/0011-2275(69)90189-1
93. E.V. Onosovskii, Investigation of compressibility of neon in the near-critical region. Teplofiz. Svoistva Vesh. Mater. **3**, 31–34 (1971)
94. W. Ramsay, M.W. Travers, II. Argon and its companions. Phil. Trans. Roy. Soc. A **197**, 47–89 (1901). https://doi.org/10.1098/rsta.1901.0014
95. C.A. Crommelin, H. Kamerlingh Onnes, Isothermals of monatomic gases and of their binary mixtures. XVII. Isothermals of neon and preliminary determinations concerning the liquid condition of neon, Proc. KNAW 18 I, 515–520 (1915)
96. C.A. Crommelin, H. Kamerlingh-Onnes, J.P. Martinez, Isothermals of monatomic substances and their binary mixtures. XX. Isothermals of neon from +20° C to −217° C. Proc. KNAW **22 I**, 108–118 (1919)
97. L. Holborn, J. Otto, Über die Isothermen einiger Gase zwischen +400° und −183°. Z. Phys. **33**, 1–11 (1925). https://doi.org/10.1007/BF01328287

98. G.P. Baxter, H.W. Starkweather, The density, compressibility and atomic weight of neon. Proc. Natl. Acad. Sci. USA **14**, 50–57 (1928). https://doi.org/10.1073/pnas.14.1.50
99. J.A. Sullivan, R.E. Sonntag, *P-V-T* behavior of neon at temperatures from 70° to 120°K and pressures to 300 atm. Adv. Cryog. Eng. **12**, 706–713 (1967)
100. W.B. Streett, Density and phase equilibria in the system neon-nitrogen at high pressure. Cryogenics **8**, 88–93 (1968). https://doi.org/10.1016/0011-2275(68)90048-9
101. E.V. Onosovskii, A.I. Moroz, Experimental *p-v-T* data for neon in the temperature range of 65–273°K and pressures up to 250 bars. Teplofiz. Svoistva Vesh. Mater. **2**, 95–102 (1970)
102. W.B. Streett, Pressure-volume-temperature data for neon from 80–130°K and pressures to 2000 atmospheres. J. Chem. Eng. Data **16**, 289–292 (1971). https://doi.org/10.1021/je60050a007
103. D. Vidal, M. Lallemand, Provisional density data for helium and neon up to 12 kbar at the temperature of 25°C. C. R. Acad. Sci. Ser. B **281**, 381–383 (1975)
104. V.Y. Maslennikova, A.N. Egorov, D.S. Tsiklis, Molar volumes and thermodynamic properties of neon at temperatures 25–150 ° C and pressures up to 7 kbar. Sov. Phys. Dokl. **21**, 440–441 (1976)
105. M. Kimura, Y. Hanayama, T. Nishitake, Measurement of ultrasound velocity in gases under high pressures up to 3.5 GPa. Jpn. J. Appl. Phys **26**, 1366–1377 (1987). https://doi.org/10.1143/JJAP.26.1366
106. M.O. McLinden, Densimetry for primary temperature metrology and a method for the in situ determination of densimeter sinker volumes. Meas. Sci. Technol. **17**, 2597–2612 (2006). https://doi.org/10.1088/0957-0233/17/10/011
107. N. von Preetzmann, R. Span, Measurement of the (p,ρ,T) behavior of helium, neon, and their mixtures at temperatures from (100 to 283.15) K and pressures up to 10.0 MPa. Cryogenics **137**, 103765 (2024). https://doi.org/10.1016/j.cryogenics.2023.103765
108. G.F. Newell, Theory of oscillation type viscometers V: disk oscillating between fixed plates. Z. Angew. Math. Phys. **10**, 160–174 (1959). https://doi.org/10.1007/BF01600523
109. E. Vogel, Reference viscosity of argon at low density in the temperature range from 290 K to 680 K. Int. J. Thermophys. **31**, 447–461 (2010). https://doi.org/10.1007/s10765-010-0760-6
110. R. Hellmann, E. Vogel, The viscosity of dilute water vapor revisited: new reference values from experiment and theory for temperatures between (250 and 2500) K. J. Chem. Eng. Data **60**, 3600–3605 (2015). https://doi.org/10.1021/acs.jced.5b00599
111. E. Vogel, The viscosities of dilute Kr, Xe, and CO_2 revisited: new experimental reference data at temperatures from 295 K to 690 K. Int. J. Thermophys. **37**, 63 (2016). https://doi.org/10.1007/s10765-016-2068-7
112. E. Vogel, Recommended values for the viscosity in the limit of zero density and its initial density dependence for twelve gases and vapors: revisited from experiment between 297 K and 691 K. J. Phys. Chem. Ref. Data **49**, 043102 (2020). https://doi.org/10.1063/5.0023688
113. E. Vogel, E. Bastubbe, S. Rhode, Kalibrierung eines Quarzglas-Schwingscheibenviskosimeters für Präzisionsmessungen an Gasen und organischen Dämpfen. Wiss. Z. W.-Pieck-Univ. Rostock **33**, 34–42 (1984)
114. J. Kestin, S.T. Ro, W.A. Wakeham, Reference values of the viscosity of twelve gases at 25° C. Trans. Faraday Soc. **67**, 2308–2313 (1971). https://doi.org/10.1039/TF9716702308
115. J. Kestin, S.T. Ro, W.A. Wakeham, Viscosity of the noble gases in the temperature range 25–700° C. J. Chem. Phys. **56**, 4119–4124 (1972). https://doi.org/10.1063/1.1677824
116. E. Bich, R. Hellmann, E. Vogel, Ab initio potential energy curve for the helium atom pair and thermophysical properties of the dilute helium gas. II. Thermophysical standard values for low-density helium. Mol. Phys **105**, 3035–3049 (2007). https://doi.org/10.1080/00268970701744584
117. T. Strehlow, Opto-elektronische Meßeinrichtung für ein Schwingscheibenviskosimeter zur Untersuchung der Temperatur- und Anfangsdichteabhängigkeit des Viskositätskoeffizienten von Gasen und organischen Dämpfen. Dr. rer. nat. Thesis, W.-Pieck-Universität Rostock, Rostock, Germany (1987)
118. R.F. Berg, W.C. Burton, Noble gas viscosities at 25 ° C. Mol. Phys. **111**, 195–199 (2013). https://doi.org/10.1080/00268976.2012.713132
119. E. Bich, E. Vogel, Initial density dependence, In: J. Millat, J.H. Dymond, C.A. Nieto de Castro (eds.), Transport properties of fluids. Their correlation, prediction and estimation (Cambridge University Press, Cambridge, 1996), pp. 72–82
120. E. Bich, R. Hellmann, E. Vogel, Ab initio potential energy curve for the neon atom pair and thermophysical properties for the dilute neon gas. II. Thermophysical properties for low-density neon. Mol. Phys **106**, 1107–1122 (2008). https://doi.org/10.1080/00268970802302662

121. W. Wagner, A mathematical-statistical method for establishing thermodynamic equations—demonstrated using the vapor pressure curve of pure fluid substances as an example. Fortschr.-Ber. VDI-Z., Reihe 3, Nr. 39 (1974)
122. J.O. Hirschfelder, C.F. Curtiss, R.B. Bird, *Molecular theory of gases and liquids* (Wiley, New York, 1954)
123. A. Laesecke, C.D. Muzny, Ab initio calculated results require new formulations for properties in the limit of zero density: the viscosity of methane (CH_4). Int. J. Thermophys. **38**, 182 (2017). https://doi.org/10.1007/s10765-017-2305-8
124. X. Xiao, D. Rowland, S.Z.S. Al Ghafri, E.F. May, Wide-ranging reference correlations for dilute gas transport properties based on *ab initio* calculations and viscosity ratio measurements. J. Phys. Chem. Ref. Data **49**, 013101 (2020). https://doi.org/10.1063/1.5125100
125. P.D. Neufeld, A.R. Janzen, R.A. Aziz, Empirical equations to calculate 16 of the transport collision integrals $\Omega^{(l,s)*}$ for the Lennard-Jones (12,6) potential. J. Chem. Phys. **57**, 1100–1102 (1972). https://doi.org/10.1063/1.1678363
126. S. Sotiriadou, K.D. Antoniadis, M.J. Assael, V. Martinek, M. Thol, M.L. Huber, Reference correlation of the viscosity of neon. Int. J. Thermophys. **47**, 77 (2026). https://doi.org/10.1007/s10765-026-03745-3
127. T. Dietl, A. El Hawary, R.M. Gavioso, R. Hellmann, K. Meier, Speed of sound measurements and derived third and fourth acoustic virial coefficients of supercritical neon. Metrologia **61**, 045007 (2024). https://doi.org/10.1088/1681-7575/ad58e6

Publisher's Note Springer Nature remains neutral with regard to jurisdictional claims in published maps and institutional affiliations.

Authors and Affiliations

Ulrike Kochan-Eilers[1] · Ruben Harten[1] · Eckhard Vogel[2] · Karsten Meier[1]

✉ Karsten Meier
karsten.meier@hsu-hh.de

[1] Institut für Thermodynamik, Helmut-Schmidt-Universität/Universität der Bundeswehr Hamburg, Holstenhofweg 85, 22043 Hamburg, Germany

[2] Institut für Chemie, Universität Rostock, 18059 Rostock, Germany